THE EFFECT OF BASIN EDGE SLOPE ON THE DYNAMIC RESPONSE OF SOIL DEPOSITS

A THESIS SUBMITTED TO
THE GRADUATE SCHOOL OF NATURAL AND APPLIED SCIENCES
OF
MIDDLE EAST TECHNICAL UNIVERSITY

BY

SERAP CILIZ

IN PARTIAL FULFILLMENT OF THE REQUIREMENTS
FOR
THE DEGREE OF DOCTOR OF PHILOSOPHY
IN
CIVIL ENGINEERING

FEBRUARY 2007

Approval of the Graduate School of Natural and Applied Sciences.

_____

Prof. Dr. Canan ÖZGEN

Director

I certify that this thesis satisfies all the requirements as a thesis for the degree of Doctor of Philosophy.

_____

Prof. Dr. Güney ÖZCEBE

Head of Department

This is to certify that we have read this thesis and that in our opinion it is fully adequate, in scope and quality, as a thesis for the degree of Doctor of Philosophy.

_____

Prof. Dr. M. Yener ÖZKAN

Supervisor

Examining Committee Members:

Prof. Dr. Orhan EROL	(METU, CE)	_____
Prof. Dr. M. Yener ÖZKAN	(METU, CE)	_____
Prof. Dr. Celal KARPUZ	(METU, MINE)	_____
Assoc. Prof. Dr. K. Önder ÇETİN	(METU, CE)	_____
Prof. Dr. Murat MOLLAMAHMUTOĞLU	(GAZİ, CE)	_____

I hereby declare that all information in this document has been obtained and presented in accordance with academic rules and ethical conduct. I also declare that, as required by these rules and conduct, I have fully cited and referenced all material and results that are not original to this work.

Name, Last name : Serap CILIZ

Signature :

ABSTRACT

THE EFFECT OF BASIN EDGE SLOPE

ON THE DYNAMIC RESPONSE OF SOIL DEPOSITS

Cılız, Serap

Ph.D., Department of Civil Engineering

Supervisor: Prof. Dr. M. Yener Özkan

February 2007, 133 pages

The effects of basin edge slope on the dynamic response of soil deposits are assessed by using one-dimensional and two-dimensional numerical analyses. 24 basin models having trapezoidal cross section are generated to represent different geometries (basin depth, basin edge slope) and soil type. Harmonic base motions with different predominant periods (T_p) are used in the analyses.

The results indicate that, for a constant basin edge slope and a constant ratio of fundamental period of site to the predominant period of base motion (T_n/T_p), the response is almost the same for different soil types, basin depths and base motions.

In the sloping edge region, one-dimensional response analysis predictions are found to be conservative compared to two-dimensional analysis predictions; however beyond this region they are unconservatively biased by a factor as high as 1.5. The sloping edge region and the horizontal region of the basin are denoted by normalized distance (ND) values varying from 0 to 1 and 1 to 2 respectively. The critical region where maximum amplification observed falls in the range of ND=1.0 to ND=1.5 for basins having slopes greater than 30^o. The lower boundary of the critical region is shifted towards as low as ND=0.2 for basins having slopes less than 30^o.

For a constant value of T_n/T_p, the increase in the amplification is smooth for basins with gentle slopes as compared to basins with steep slopes for the region where ND~1. For a basin and earthquake couple approaching to resonance state (T_n/T_p=1), the amplification for the region where ND is greater than 1 is found to be as high as 100% of that is found for the region where ND~1.

Keywords: Basin Edge Effect; Harmonic Base Motion; Dynamic Soil Response; Two-dimensional Analysis; One-Dimensional Analysis

ÖZ

HAVZA KENAR EĞİMİNİN

ZEMİN TABAKALARININ DİNAMİK TEPKİSİNE ETKİSİ

Cılız, Serap

Doktora, İnşaat Mühendisliği Bölümü

Tez Yöneticisi: Prof. Dr. M. Yener Özkan

Şubat 2007, 133 Sayfa

Havza kenar eğiminin zemin tabakalarının dinamik tepkisi üzerine etkisi bir boyutlu ve iki boyutlu sayısal analizler kullanılarak değerlendirilmiştir. Farklı geometrileri (havza derinliği, havza kenar eğimi) ve zemin tipini temsil eden yamuk en kesite sahip 24 havza modeli oluşturulmuştur. Farklı hâkim periyotlara (T_p) sahip harmonik zemin hareketleri analizlerde kullanılmıştır.

Sonuçlar göstermiştir ki, sabit bir havza kenar eğimi ve sabit bir zemin hâkim periyodunun depremin hâkim periyoduna oranı (T_n/T_p) için, farklı zemin tipleri, havza derinlikleri ve zemin hareketleri ile elde edilen dinamik tepki oldukça benzerdir.

Eğimli bölgede, bir boyutlu tepki analiz sonuçlarının, iki boyutlu analiz sonuçlarına göre konservatif olduğu tespit edilmiştir, fakat bu bölgenin ötesinde bir boyutlu tepki analiz sonuçları konservatif değildir, 1.5'lere varan oranlarda sapma göstermiştir. Havzanın eğimli ve düz bölgeleri sırasıyla normalize edilmiş mesafe (ND) cinsinden 0 ile 1 ve 1 ile 2 aralığında değişen değerler ile gösterilmiştir. En yüksek zemin büyütme değerinin elde edildiği kritik bölge, 30^o den büyük kenar eğimine sahip havzalar için ND=1.0 ile ND=1.5 aralığına denk gelmektedir. 30^o den küçük kenar eğimine sahip havzalar için kritik bölgenin alt sınırı ND=0.2 değerine doğru kaymaktadır.

Sabit bir T_n/T_p oranı için, ND=1 değeri civarında zemin büyütmesindeki artış, hafif eğimli havzalarda dik eğimli havzalara göre daha yumuşaktır. Rezonans haline (T_n/T_p=1) yaklaşan havza ve deprem çifti için, ND değeri 1 den büyük olan bölgedeki zemin büyütmesinin, ND değeri 1 civarındakine göre %100'e varan oranda daha yüksek olduğu tespit edilmiştir.

Anahtar Kelimeler: Havza Kenar Eğiminin Etkisi; Harmonik Zemin Hareketi; Dinamik Saha Tepkisi; İki Boyutlu Analiz; Bir Boyutlu Analiz

To My Son, Onur CILIZ

ACKNOWLEDGMENTS

The author wishes to express her eternal gratitude to her supervisor Prof. Dr. M. Yener Özkan for his assistance, guidance, advices, encouragements, patience and sincere cooperation throughout this research. He is highly appreciated for advising such an interesting and challenging subject that is really worthy to study extensively with curiosity and great concern.

The author also wishes to express her gratitude to Assoc. Prof. Dr. K. Önder Çetin for his valuable support and positive attitude during this study.

Finally, the author is indebted to her husband Mustafa Cılız for his patience, support and encouragement.

TABLE OF CONTENTS

PLAGIARISM iii
ABSTRACT iv
ÖZ vi
DEDICATION viii
ACKNOWLEDGMENTS ix
TABLE OF CONTENTS x
LIST OF TABLES xiii
LIST OF FIGURES xiv
CHAPTER 1: INTRODUCTION 1
1.1. GENERAL INFORMATION 1
1.2. OBJECTIVES OF THE STUDY 2
CHAPTER 2: LITERATURE REVIEW 3
2.1. SURFACE TOPOGRAPHY 3
2.1.1. TOPOGRAPHIC EFFECTS 3
2.1.1.1. RIDGES 4
2.1.1.2. CANYONS 15
2.1.1.3. SLOPES 17
2.1.2. TOPOGRAPHIC EFFECTS ON CODES 21
2.2. BASIN GEOMETRY 23
2.2.1. BASIN-EDGE EFFECTS 24
2.3. FREQUENCY CONTENT OF GROUND MOTIONS 40
2.4. EFFECT OF THE NATURAL PERIOD OF SITE ON THE SOIL AMPLIFICATION 41
CHAPTER 3: DYNAMIC RESPONSE ANALYSIS OF SOIL DEPOSITS 44
3.1. INTRODUCTION 44
3.2. DYNAMIC SOIL PROPERTIES 44
3.2.1. DYNAMIC STRESS-STRAIN BEHAVIOR OF SOILS 44
3.2.2. ASSESSMENT OF SHEAR MODULUS 45

3.2.3. ASSESSMENT OF DAMPING RATIOS 54
3.2.4. DYNAMIC SOIL MODELS.....55
3.3. GROUND RESPONSE ANALYSIS 56
3.3.1. ONE DIMENSIONAL GROUND RESPONSE ANALYSES 58
3.3.1.1. LINEAR GROUND RESPONSE ANALYSIS 61
3.3.1.2. EQUIVALENT LINEAR GROUND RESPONSE ANALYSIS 61
3.3.1.3. NONLINEAR (ELASTO-PLASTIC) GROUND RESPONSE ANALYSIS.....62
3.3.1.4. COMPARISON OF EQUIVALENT LINEAR AND NON-LINEAR SITE RESPONSE ANALYSES: 63
3.3.2. TWO-DIMENSIONAL GROUND RESPONSE ANALYSIS 64
3.3.2.1. DYNAMIC FINITE ELEMENT ANALYSIS 64
3.3.2.2. EQUIVALENT LINEAR APPROACH.....68
3.3.2.3. NONLINEAR APPROACH 69
3.3.2.4. OTHER APPROACHES TO TWO-DIMENSIONAL DYNAMIC RESPONSE PROBLEMS 70
3.3.3. THREE-DIMENSIONAL DYNAMIC RESPONSE ANALYSIS 70
3.3.3.1. EQUIVALENT LINEAR FINITE ELEMENT APPROACH 70
3.3.3.2. NON-LINEAR FINITE ELEMENT APPROACH 71
3.3.3.3. SHEAR BEAM APPROACH.....71
3.3.4. SHAKE91 72
3.3.5. QUAD4M 74
CHAPTER 4: A STUDY ON THE EFFECT OF THE RESPONSE OF SOIL DEPOSITS.....77
4.1. INTRODUCTION 77
4.2. OVERVIEW OF BASIN EDGE MODELS 77
4.2.1 GEOMETRY OF THE MODEL 78
4.2.2 INPUT SOIL PROPERTIES 80
4.2.3 SELECTED INPUT MOTIONS 82
4.2.3.1 HARMONIC BASE MOTION 82

4.2.3.2 RECORDED STRONG MOTION 83
4.3. SEISMIC RESPONSE ANALYSES OF SELECTED SOIL PROFILES.....86
4.4. FINITE ELEMENT MODEL.....87
4.5. DISCUSSION OF RESULTS.....94
4.5.1 EFFECT OF SOIL NONLINEARITY ON THE BEHAVIOUR OF ONE-DIMENSIONAL SOIL MODEL 94
4.5.2 RESPONSE OF SELECTED SOIL PROFILES UNDER HARMONIC AND RECORDED MOTIONS.....98
4.5.3 EFFECT OF EQ DURATION ON SOIL RESPONSE 101
4.5.4 EFFECTS OF BASIN EDGE SLOPE ON SOIL RESPONSE.....104
CHAPTER 5: CONCLUSIONS.....112
REFERENCES 116
APPENDIX A: SAMPLE INPUT DATA FOR QUAD4M.....130
CIRRICULUM VITAE.....132

LIST OF TABLES

Table 2.1: Observations of horizontal ground motion amplification transverse to predominant ridge line; Stewart et. al. (2001).....14
Table 2.2: Dimensional geologic structural effects; Silva (1988).....29
Table 3.1: Evaluation of G_{max}.....48
Table 4.1: Geometric dimensions of models.....79
Table 4.2: Characteristic information for base motions.....82
Table 4.3: Basic parameters of the base motions.....99

LIST OF FIGURES

Figure 2.1: Generalized 2D geometries of irregular surface topography; Stewart (2001)..... 4
Figure 2.2: (a) Approximating a ridge formation by a triangular wedge; Aki (1988) (b) Infinite wedge excited by plane SH waves; Faccioli (1991)..... 6
Figure 2.3: Amplification as a function of normalized frequency across ridge subjected to vertically incident SH wave; Geli et. al. (1988)..... 7
Figure 2.4: Relative distributions of peak horizontal accelerations along a ridge from Matsuzaki area in Japan; Jibson R. (1987)..... 9
Figure 2.5: Effect of surface topography on damage distribution in the Irpinia (Italy) 1980 earthquake; Castellani et al. (1982).....10
Figure 2.6: Amplitude spectral ratio-frequency graph for the Cedar Hill; USGS report (1996) 11
Figure 2.7: Amplification as a function of normalized frequency across canyon subjected to vertically incident SH waves; Trifunac (1973).....16
Figure 2.8.a: Horizontal amplification at slope crest for a vertically incident SV wave; Ashford et al. (1997) 18
Figure 2.8.b: Horizontal amplification at the crest of a vertical slope for inclined SV wave incident from -30 deg to +30 deg; Ashford and Sitar (1997) 19
Figure 2.9: Amplification at crest of a 21m tall, 3H:1V cut slope for vertically incident waves; Stewart and Sholtis (1999).....20
Figure 2.10: τ site response factor according to PS-92.....23
Figure 2.11: Basin edge effects in the 1995 Kobe earthquake, Pitarka et al. (1998).....26

Figure 2.12.a: Smoothed SH transfer functions to homogeneous half space outcrop motions for a wide, shallow alluvial valley with shape ratio of 0.1; Bard and Gariel (1986) 27
Figure 2.12.b: Smoothed SH transfer functions to homogeneous half space outcrop motions for a valley with shape ratio of 0.4; Bard and Gariel (1986) 28
Figure 2.13: Reflection of seismic waves; Graves (1993) 31
Figure 2.14: The Valley Geometry; Rassem et al. (1997) 33
Figure 2.15: Basin depth amplification factors implied by the attenuation relationships by Lee and Anderson (2000) and Field (2000) for sites along cross section through Los Angeles basin; Field et al. (2000) 36
Figure 2.16: Soil-rock profile; Heymsfield (2000) 37
Figure 2.17: Three possible 2D models for Euroseis test valley; Makra et al. (2005) 38
Figure 2.18: Geotechnical models of the Volvi basin; Semblat et al. (2005) 39
Figure 2.19: Vertically exaggerated cross-sectional view of a basin-edge model with seven soil layers; Narayan (2006) 40
Figure 2.20: Uniform soil layer on elastic rock subjected to vertical shear waves, Roesset (1977) 42
Figure 2.21: Amplification ratio soil/rock for h=100ft, V_s=1.88cps and IR=6.7; Roesset (1977) 43
Figure 3.1: Tangent shear modulus 46
Figure 3.2: Secant shear modulus 46
Figure 3.3: Modulus reduction curve 46
Figure 3.4: Typical G/G_{max} versus cyclic shear strain relationships for sands by Seed and Idriss (1970) and for gravels by Seed et. al. (1986) 51
Figure 3.5: Data points G/G_{max} versus cyclic shear strain relationship for gravely soils base on testing by all 15 investigators along with best fit curve and ± one standard deviation; Rollins et all. (1998) 52

Figure 3.6: Modulus reduction curve for fine-grained soils of different plasticity; Vucetic and Dobry (1991) 54
Figure 3.7: Site-specific ground response analyses; Govinda Raju et al. (2004) 57
Figure 3.8: Refraction processes that produce nearly vertical wave propagation near the ground surface; Kramer S.L. (1996) 59
Figure 3.9: Mapping of quadrilateral element from irregular shape in x-y coordinate system to square shape in s-t coordinate system; Kramer S.L. (1996) 65
Figure 3.10: One-dimensional idealization of a horizontally layered soil deposit over a uniform half-space; Idriss and Sun (1992) 73
Figure 3.11: Finite models for dooting on half space; Lysmer and Kuhlemeyer (1969) 75
Figure 4.1: Geometric parameters of the trapezoidal models 78
Figure 4.2: Shear wave velocity versus depth for relatively soft and stiff soil profile 80
Figure 4.3: G_{max} versus depth for relatively soft and stiff soil profile 81
Figure 4.4: Modulus reduction and damping ratio curves 81
Figure 4.5: Harmonic base motion characteristics 83
Figure 4.6: Characteristics of Dinar Earthquake 84
Figure 4.7: Characteristics of Coalinga Earthquake 86
Figure 4.8: Strain Elements 87
Figure 4.9: Model 24 geometry 88
Figure 4.10: Effect of mesh size on the results 89
Figure 4.11: The details of the mesh for each model 93
Figure 4.12: Input soil parameter for one-dimensional analyses 95
Figure 4.13: Common soil column used in one-dimensional model 95
Figure 4.14: Variation of PGA_{1D}/PGA_{rock} with T_{after} 96
Figure 4.15: Variation of PGA_{1D}/PGA_{rock} with T_{before} 97
Figure 4.16: The comparison between T_{after} and T_{before} 97
Figure 4.17: Effect of PGA of motion on amplification 98
Figure 4.18: Variation of $PGA_{(2D)}/PGA_{(Rock)}$ with normalized distance for constant amplitude, variable periods 100

Figure 4.19: Variation of $PGA_{(2D)}/PGA_{(Rock)}$ with normalized distance for constant period, variable amplitudes 100
Figure 4.20: Cycle definition and characteristics of harmonic base motions 101
Figure 4.21.a: Effect of duration on amplification for Model 8 102
Figure 4.21.b: Effect of duration on T_{after} for Model 8 102
Figure 4.22.a: Effect of duration on amplification for Model 19 103
Figure 4.22.b: Effect of duration on T_{after} for Model 19 103
Figure 4.23: Variation of $PGA_{(2D)}/PGA_{(1D)}$ with normalized distance 106
Figure 4.24: Variation of $PGA_{(2D)}/PGA_{(Rock)}$ with normalized distance 106
Figure 4.25: Variation of $PGA_{(2D)}/PGA_{(1D)}$ with normalized distance for constant Tn/Tp=1.35 107
Figure 4.26: Variation of $PGA_{(2D)}/PGA_{(rock)}$ with normalized distance for constant Tn/Tp=1.35 108
Figure 4.27: Critical region where max amplification due to basin edge effect is observed for T_n/T_p =1.35 109
Figure 4.28: Critical region where max amplification due to basin edge effect is observed for T_n/T_p =1.70 109
Figure 4.29: Variation of $PGA_{(2D)}/PGA_{(1D)}$ with normalized distance for constant $\alpha=34^0$ 110
Figure 4.30: Variation of $PGA_{(2D)}/PGA_{(Rock)}$ with normalized distance for constant $\alpha=34^0$ 111
Figure 4.31: Variation of $PGA_{(2D)}/PGA_{(Rock)}$ with T_n/T_p for constant $\alpha=34^0$ 111

CHAPTER 1

INTRODUCTION

1.1. GENERAL INFORMATION

The characteristics of base motion at a given site depend on number of factors such as: source mechanism, the distance of the rock from source to site, wave interference and local site conditions of the site. The local site condition includes the depth of soil layers, variation of soil type and properties, lateral irregularity and the surface/subsurface topography of the site. Local site effects can cause amplification and/or de-amplification of seismic motion at the surface. Therefore, the effect of surface topography and/or basin geometry on base motion is very important for reducing the earthquake risk to the general population in earthquake-prone regions.

Site conditions affect base motion in distinct ways. The lower impedance of surface layers relative to bedrock result in amplification of incoming waves. Geologic structure as reflected in surface and buried topography can significantly alter the characteristics of base motions. Surface topography changes both the intensity and frequency content of ground motions. Buried topography such as alluvial basins often increases the duration of shaking and also affects both the frequency and intensity.

Surface waves generated at the basin borders propagate into the plain and are effective in a finite distance from the borders before they are totally damped out. In the case of deep, narrow valleys, in addition to the surface waves, body waves are reflected from the rock boundaries and trapped in the valley resulting in the further aggravations in three-dimensional effects. Such

geological structure results in stronger and prolonged earthquake base motions. These effects can not be evaluated by the typical one-dimensional site response analyses. Two and in some cases three-dimensional analyses are required.

1.2. OBJECTIVES OF THE STUDY

The aim of this study is to assess the effects of the basin edge slope on the dynamic response of horizontal soil deposits by using one-dimensional and two-dimensional numerical models capable of incorporating the non linear stress strain behavior of soils through utilizing equivalent linear method. One-dimensional approach is based on the assumption that the main response in soil is due to vertical propagation of shear waves from the underlying bedrock. In this study, SHAKE91 software is used to calculate one-dimensional response and a finite-element computer code QUAD4M is employed for two-dimensional response evaluation. For the analyses, 24 models are developed to represent different geometries (i.e. depth of basin, slope of basin edge) and soil type. Harmonic base excitations with different periods are used in the analyses, with a maximum acceleration of 0.15g. Effect of basin topography is investigated by the amplification ratio, $PGA_{(2D)}/PGA_{(Rock)}$, defined as the ratio of PGA_{soil} estimated by two-dimensional analysis to PGA_{rock}. In order to make a comparison between the results of one-dimensional and two-dimensional analyses, $PGA_{(2D)}/PGA_{(1D)}$ is defined as a dimensionless ratio. Using the results of these analyses, the main parameters governing the variations of seismic motions in alluvial valley are investigated.

The detailed descriptions of these analyses are presented in the following chapters.

CHAPTER 2

LITERATURE REVIEW

2.1. SURFACE TOPOGRAPHY

The effects of topographic irregularities on base motion play an important role on its characteristics, especially the amplitude and frequency content. Previous studies indicated that, buildings located at the tops of hills, ridges and canyons suffered more intensive damage than those located at the base: the San Fernando Earthquake (1971), the Fruili Earthquake (Italy, 1976), the Irpinia Earthquake (Italy, 1980), the Chile Earthquake (1985), the Athens Earthquake (Greece, 1999) and Bingöl Earthquake (Turkiye, 2003) are some of the examples during which severe structural damage has been reported on hill or close to steep slope. In the following sections details are given in order to have a better understanding regarding these effects.

2.1.1. TOPOGRAPHIC EFFECTS

In this section, variations in seismic ground response between level sites and areas with irregular surface topography are presented. The presentation here is limited principally to two-dimensional geometries which were categorized by Stewart (2001) as ridges, canyons, or slopes as shown in Figure 2.1. Numerous studies have investigated topographic effects for an isolated, two-dimensional, homogeneous ridge, canyon and slope on the surface of a homogeneous half space. In the following sections, amplification

factors predicted by models for these geometries and available observational studies used for model calibration is reviewed briefly.

.

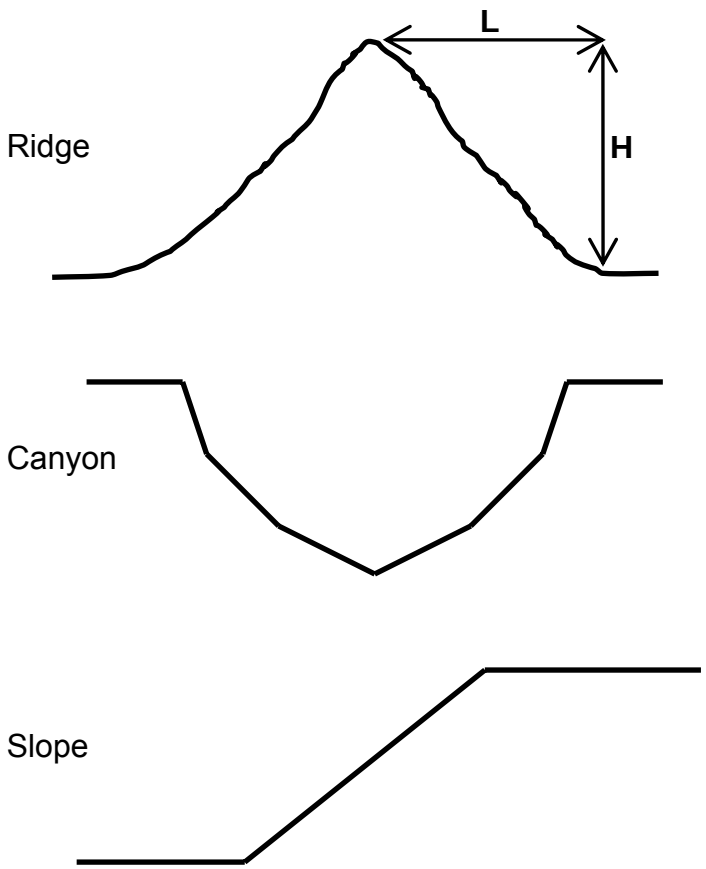

Figure 2.1: Generalized 2D geometries of irregular surface topography; Stewart (2001)

2.1.1.1. RIDGES

The effect of surface topography to the seismic ground response has been the subject of numerous studies during the last 25 years. Previous research on topographic effects generally focused on either (1) numerical studies or (2) empirical studies employing sufficient instrumentation to directly quantify crest/base amplification. These studies have examined the cases of ridge or valley type surface irregularities in a two-dimensional form

whereas only a limited number of results are available for three-dimensional configurations (Sanchez-Sesma et al., 1994). Pioneering work on the subject was accomplished by Aki and Larner in 1970 who introduced a numerical method based on a discrete superposition of plane waves. This method was later extended by other investigators such as Boore (1972), Bouchon (1973), Bard (1982) and Geli et. al. (1988). Useful results were also reported by Wong and Trifunac (1974), Wong (1982) and Sanchez-Sesma et al. (1985).

Bouchon (1973) studied the effect of topography on surface motion in the cases of incident SH, P and SV waves by using the Aki and Larner method (1970). Several types of topography ranging from a ridge to a valley were used. Different incidence angles were considered for a wavelength interval extending from 2h to 20h, where h is the vertical dimension of the anomaly. Residual stresses were added to the methodology. Bouchon (1973) found that, the surface displacement appears to be very much influenced by surface irregularities. He also stated that, in the case of a ridge, a zone of amplification took place near the top, whereas, a zone of attenuation occurred near the bottom.

According to Aki (1988), the topographic effects caused by simple irregularities can be estimated from exact solutions to idealize problems. In his study it is stated that, apex displacements are amplified by a factor $2\pi/\phi$, where ϕ is the vertex angle of the wedge for a triangular infinite wedge subjected to vertically propagating SH-waves (with particle motion parallel to its axis) as illustrated in Figure 2.2 (a). For certain cases of ridge-valley terrain shown in Figure 2.2 (b), this approach can be used to approximate the topographic effects. Faccioli (1991) used this triangular wedge structure to model approximately ridge valley topography, as shown in Figure 2.2 (b). This simple model predicted amplification at crest relative to base equal to $\nu 1/\nu 2$ and may be used for rough numerical estimates of amplifications at the crest of ridges or de-amplifications at the bottom of valleys or canyons.

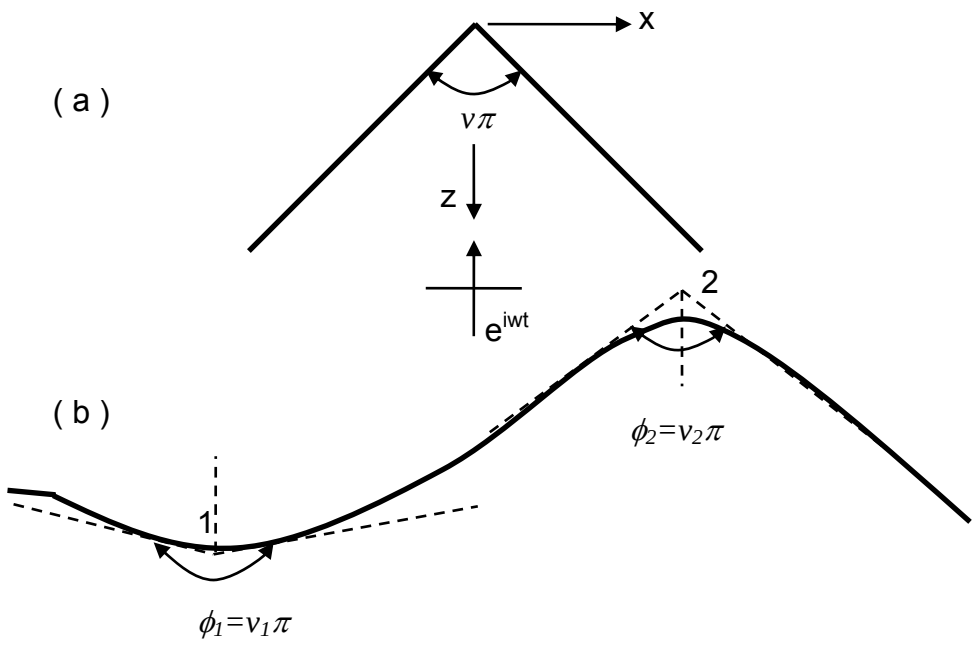

Figure 2.2: (a) Approximating a ridge formation by a triangular wedge; Aki (1988) (b) Infinite wedge excited by plane SH waves; Faccioli (1991)

Geli et al. (1988) and Bard (1995) from 11 analytical studies found that, levels of crest-to-base time-domain amplification (i.e. ratios of peak motions) vary between 1 and 2 (average ≈ 1.5) for shape ratios H/L ≈ 0.4 subjected to vertically incident SH waves as illustrated in Figure 2.3. Broadband crest amplification is maximized at dimensionless frequency η = $2L/\lambda$ = 2, which corresponds to a wavelength (λ) equal to the ridge half-width. The maximum spectral acceleration is about 1.6 for this case. Geli et al. (1988) found that amplification is generally lower for incident P waves than S waves, and the amplification is slightly greater for horizontal motion in the plane of the models than for out-of-plane motions. According to Pedersen et al. (1994) although simple and repeatable trends in the results could not be identified, amplification is also sensitive to the vertical angle of incident wave field.

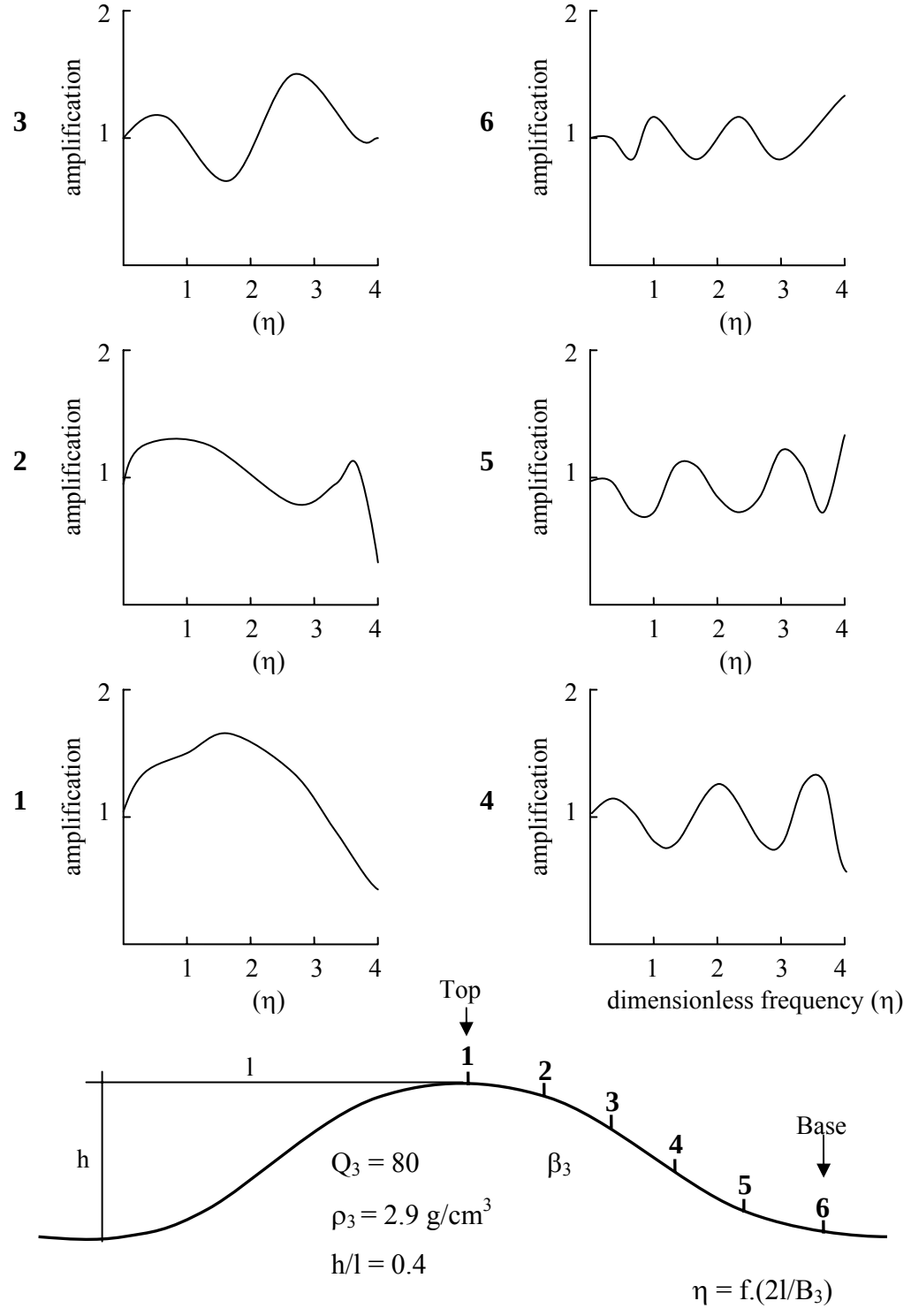

Figure 2.3: Amplification as a function of normalized frequency across ridge subjected to vertically incident SH wave; Geli et. al. (1988)

Besides these theoretical predictions, instrumental data also show the effect of surface topography on ground motion. Davis and West (1973) performed field experiments in order to obtain data needed for studying the effects of topography on seismic motion. The data recorded during San Fernando earthquake Feb. 9, 1971, from the instruments deployed at the crest and base of Kagel Mountain and Josephine Peak, California and at the crest, middle and base of Butler Mountain near Tonopah were studied. Although the three mountains are similar in shape, their sizes are different. They found that, the smallest mountain amplified the motion in a narrow range of periods (peaking around 0.3 to 0.5 sec), the medium-size mountain showed amplification over a slightly broader range (peaking at periods of 0.4 to 0.5 sec), whereas the largest mountain showed less amplification, but it occurred over a broader range of periods. It was concluded by Davis and West that topography plays a significant role and was an important consideration in determining the seismic motion that a particular site received.

The amplification of surface motion in ridge or steep slope type topography has also been verified by Jibson (1987) from measurements during five earthquakes in Matsuzaki, Japan. Increased amplification near the crest of a ridge was the outcome of these measurements. The graph in Figure 2.4 shows the variation of normalized peak recorded horizontal accelerations from five earthquakes as a function of elevation across a ridge. This graph was normalized by the mean value of the crest's peak horizontal accelerations and the standard error bars were also included. It is seen that the average peak crest acceleration was about 2.5 times the average base acceleration.

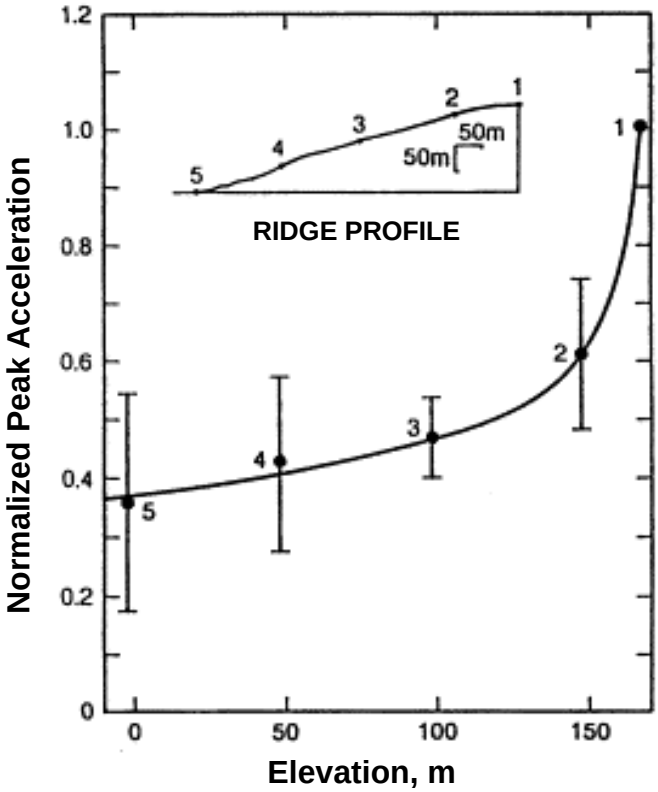

Figure 2.4: Relative distributions of peak horizontal accelerations along a ridge from Matsuzaki area in Japan; Jibson R. (1987)

Amplification of motions at the crest of a ridge relative to the base is also supported by the study of Brambati et al. (1980) in which the damage patterns during 1980 Friuli earthquakes in Italy were presented. Similarly increased earthquake damages close to the crest of a step like topography has been reported by Castellani et al. (1982) for the Irpinia 1980 earthquake which is illustrated in Figure 2.5. In this figure it is shown that, an Italian village is sitting at the top of a hill and the damage was concentrated close to the crest of a steep slope whereas it was insignificant in the locations away from the crest.

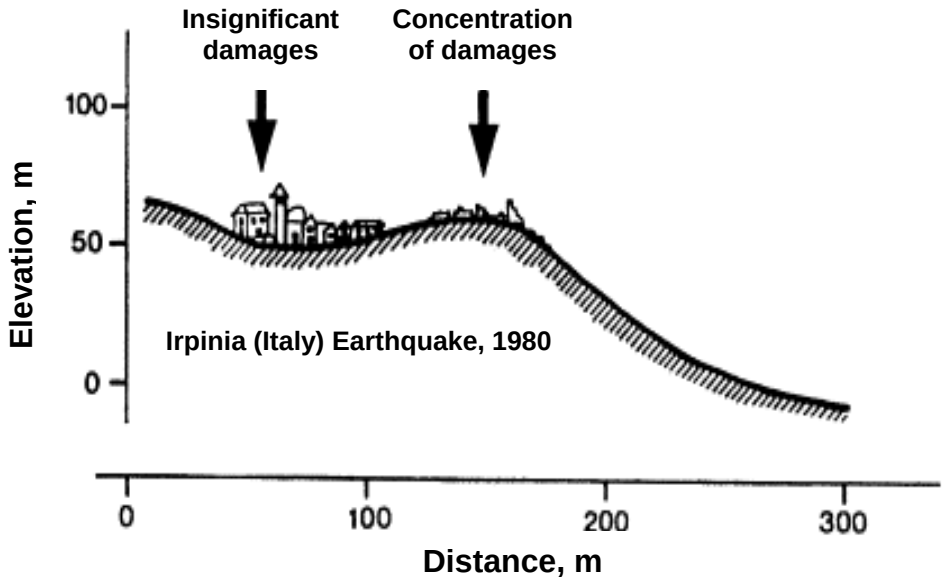

Figure 2.5: Effect of surface topography on damage distribution in the Irpinia (Italy) 1980 earthquake; Castellani et al. (1982)

For the Northridge earthquake (1994), temporary stations were established around the Tarzana site to investigate topographic effects using data from aftershocks of earthquake by Spudich et al. (1994). The preliminary findings from the Wennerberg and Spudich studies were in compliance with the previous theoretical and field data on the effect of topography. One of the highest accelerations ever recorded during an earthquake occurred at the Cedar Hill Nursery in Tarzana located about 6 kilometers south of the epicenter. The strong-motion record showed a peak acceleration of 1.78g and sustained large amplitudes near 1g for about 7-8 seconds. However, much smaller ground accelerations were observed at Encino Reservoir and on Ventura Blvd., each less than 2 kilometers from the Cedar Hill Nursery site. The USGS (U.S. Geological Survey) deployed an array of 21 seismographs to record aftershocks at the site to identify the factors that caused the large motions and to identify reasons for the large differences in ground motions at these three closely spaced sites (USGS report, 1996).

The Cedar Hill Nursery main-shock recording was made at top of a hill about 15 meters high, 500 meters long, and 130 meters wide. By comparing aftershock ground motions recorded at the top and base of the hill, USGS scientists observed that the top of the hill was shaked more strongly than the base. Specifically, the top to base amplification ratio was about 2 for motions parallel to the hill (approximately east-west, which is the direction of the 1.78g main-shock peak acceleration). For motions perpendicular to the long axis of the hill, the top to base amplification ratio was as large as 4.5 for 3.2 hertz motions (Figure 2.6). Assuming that the hill soils responded linearly during the main shock, the large east-west main-shock motion was amplified by about a factor of 2 due to the topography (USGS report, 1996).

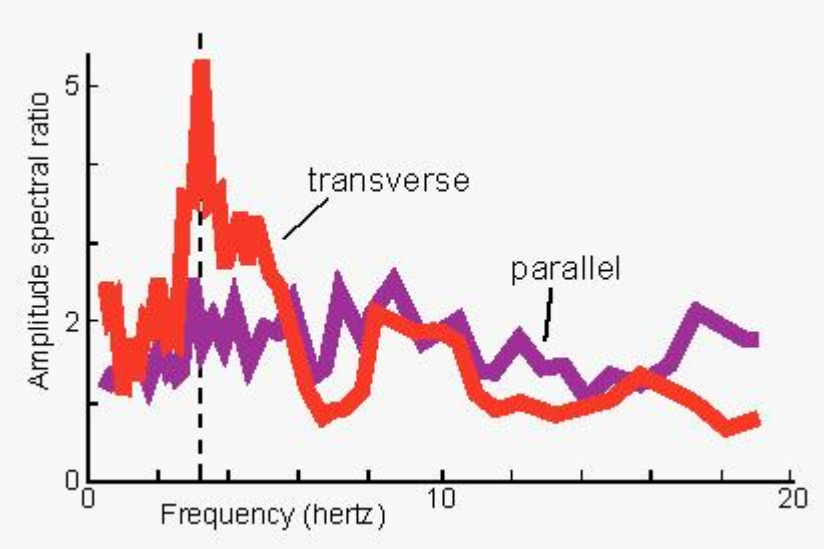

Figure 2.6: Amplitude spectral ratio-frequency graph for the Cedar Hill; USGS report (1996)

Instruments at the Cedar Hill Nursery in Tarzana recorded significant amplifications of seismic energy that were far greater than those of nearby sites. The amplifications, partly related to the local topography, are about twice what would be expected for similar sites in the Los Angeles region.

Tarzana also had an isolated very high peak during the Whittier 1987 earthquake. At that time the peak horizontal acceleration at Tarzana was 0.62g while at Arleta, closer to the epicenter, was only 0.09g. It is stated by Finn (1995) that these high amplifications are due to the effects of topography on the incoming waves.

Response of the Tarzana strong motion site during the 1994 Northridge earthquake was investigated by Vahdani et al. (2002). In their study, one-dimensional (SHAKE), two-dimensional (TELDYN and SASSI), and three-dimensional (SASSI) analyses were conducted using both recorded aftershock data and an estimated ground acceleration time histories at a 100m depth. The results of the analyses of Vahdani et al. (2002) indicate that (1) local geology and topography could only partially account for the observed ground motion amplification, and (2) the PGA and response spectra at a point near the edge of the ridge (the location of the instrument at the time of the main shock) is in good agreement with recorded values when the angle of incident of shear waves (SV waves) at 100 m depth is assumed at 30° from vertical.

There are also many researches related with low amplitudes recordings of aftershock sequences or micro tremors (Çelebi, 1987; Pederson et al., 1994). By using the spectral ratios of motions obtained from aftershocks recorded at ridge and sites of differing geology, Çelebi (1987) found that amplification did take place during occurrence of aftershocks as well as during the main shock.

Despite the fact that most observational studies of topographic effects were performed on ridge geometries, verification studies for topographic effects across ridges are limited. These studies were generally based on interpretations of weak motion data from arrays across two or three dimensional surface geometries. Table 1.1 summarizes several such studies in which amplification effects were evaluated in the frequency domain from direct interpretation of surface recording. Unfortunately, ground motion variations identified in these studies generally result from a combination of

ground response variability (due to non-identical soil-rock conditions underlying the seismograph sites) and topographic effects. Subsurface characterization was not performed at the seismometers at all the sites listed on Table 2.1 and in most cases no attempt was made to remove potential prejudice in identified amplification factors associated with ground response variability. Therefore, the results may not be so useful for engineering application (Stewart et. al., 2001).

A direct boundary element method for calculating the three-dimensional scattering of seismic waves from irregular topographies and buried valleys due to incident P, S and Rayleigh waves was investigated by Reinoso et al. (1998). In this study, the behavior of two types of mountains for different incidences was shown. For some incidences, factors of vertical amplification reached up to 20 times the incident motion and factors of horizontal amplification were found to be as high as four times the free field motion. The largest amplifications have been found in mountains with vertical walls while mountains with smooth slopes exhibited little amplification with factors smaller than four. Results in the time domain showed how the duration of motion could be incremented compared with the free-field motion and illustrated the great amplification of the incident wavelength at some sites of the mountains.

Table 2.1: Observations of horizontal ground motion amplification transverse to predominant ridge line; Stewart et. al. (2001)

Site	Earthquake	Slope Faces[1]	Approx. Slope Angle (deg.)	Slope Height (m)	Peak Crest Motion	Max Spectral Amp.	Approx. Freq. of Max. Amp.[2]	Crest/Base Geology	Reference
Kagel Mountain, CA	1971 San Fernando AS	3-D	28	430	na	10-30[a]	1.0	similar	Davis and West, 1973
Josephine Peak, CA	1971 San Fernando AS	3-D	17	910	na	3[a]	0.9	similar	Davis and West, 1973
Butler Mountain, NV	Explosions	ridge	36	150-180	na	5-7[a]	0.8	similar	Davis and West, 1973
Tien Shan Mtns., USSR	Microtremors	ridge	na	na	na	8[b]	na	loess/bsmt	Tucker et al., 1984
W. Nag. Prefec., Japan	1984 W. Nagana Prefec. AS	ridge	46	50-100	na	10	na	andesite/ash	Umeda et al. 1986
Canal Beagle, Chile	1985 Chilean AS	ridge	14	20	0.01 cm/s	5-10[b]	na	similar	Celebi, 1987
Coalinga Anticline, CA	1983 Coalinga AS	ridge	10-15	30	0.05 g	4-8[b]	na	similar	Celebi, 1991
Superstition Mtn., CA	1987 Sprstn. Hills AS	na	4	na	0.04 cm/s	20	na	similar	Celebi, 1991
Robinwood Ridge, CA	1989 Loma Prieta AS	ridge	25	100	0.02 cm/s	1.5-4[b]	0.8-2	similar[3]	Hartzell et al., 1994
Sourpi, Central Greece	Microtremors	ridge	30	300	na	3[b]	broad	similar	Pedersen et al., 1994
Mont St. Eynard, France	Microtremors	ridge	65	350	na	3.5[b]	na	similar	Pedersen et al., 1994
Nice, France	Microtremors	ridges	35-40	80-120	na	7-9[b]	na	similar	Nechtschein et al., 1995
Tarzana, CA	1994 Northridge AS	ridge	14	15	na	4.5b	1.1	similar[3]	Spudich et al., 1996
Epire, Greece	Microtremors	ridge	23-26	90	na	2[c]	broad	na	Chavez-Garcia et al. 1996

na = not available

[1]Slope face descriptions: 3-D = three-dimensional geometry; ridge = approximate 2-D geometry with two slope faces

[2]Normalized frequency equivalent to ridge half width (W) normalized by wavelength, not available if V_S not reported

[3]Potential for geologic amplification noted by authors

[a] pseudo relative velocity response spectra

[b] Fourier amplitude ratio

[c] Based on Horizontal to vertical spectral ratio (HVSR)

2.1.1.2. CANYONS

The effect of surface topography on the ground motions was observed on many earthquakes in the past such as 1971 San Fernando, 1985 Central Chilean, 1989 Loma Prieta and 1994 Northridge earthquakes.

During 1971 San Fernando earthquake, relatively high accelerations were measured above the south abutment of Pacoima Dam (1.25g horizontal and 0.70g vertical) and these were attributed to topographic amplification (Kramer, S.L., 1996). After this event, an accelerograph array with 17 channels was installed. In order to capture the spatially non-uniform features of earthquake ground motions, nine channels were placed along the dam-rock interface. This system was in operation during the 1994 Northridge earthquake, but unluckily the middle portion of most of the recorded accelerograms contained off-scale motions which could not be digitized. Accelerograph arrays across dam sites provided good candidate data sets for verifying analytical models (Stewart et. al., 2001).

After 1971 San Fernando earthquake, Trifunac (1973) and Wong and Trifunac (1974) studied the effect of canyon geometry on ground motion assuming linear-elastic medium and simple canyon geometry such as semi-cylinder or semi-ellipse. A general overview of ground motion variations across simplified canyon geometry was provided by Trifunac (1973) as shown in figure 2.7. Trifunac (1973) indicated the ground motion amplitude at various locations across a canyon as a function of normalized frequency $\eta = 2a / \lambda$ for vertically incident SH waves (where λ=wavelength). He found that, amplification is strongly frequency dependent and becomes significant when wavelengths are similar to or smaller than the canyon dimension. Maximum amplification was stated as 1.4 and occurred near the canyon edge and remained approximately constant for $\eta > 0.5$, while the maximum base de-amplification was reported as 0.5. He also found that, if the same canyon geometry is subjected to an inclined SH wave arriving from the left, wave trapping on the left canyon wall would cause higher amplification levels than

on the right side, with amplification levels as high as two being possible for horizontally propagating waves. Similar studies for P and SV waves were performed by Wong (1982) and Lee and Cao (1989), and indicated amplification levels generally smaller than those for SH waves. According to Wong and Trifunac (1974), canyon geometry is also significant. They stated that, for shallow canyons (ratio of depth to width < 0.05) amplification is being negligible and for deep canyons, edge amplification is not significantly different than that, but more base amplification occurs.

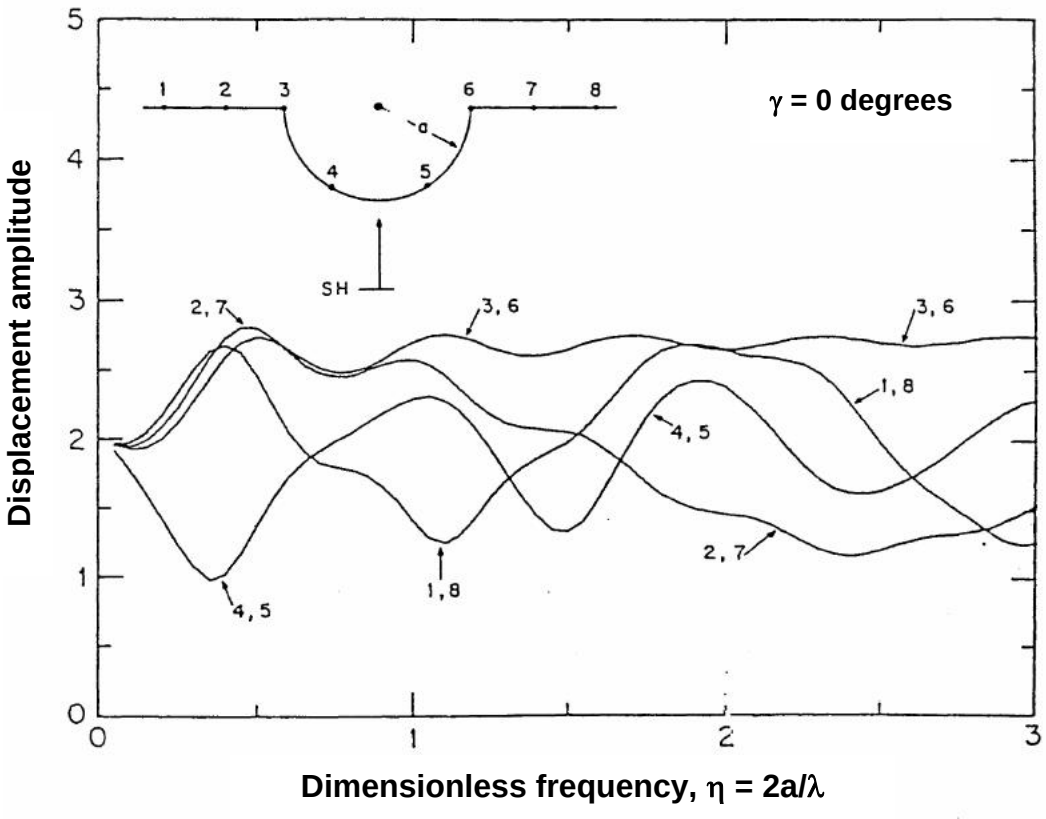

Figure 2.7: Amplification as a function of normalized frequency across canyon subjected to vertically incident SH waves; Trifunac (1973)

Topographic and soil effects were investigated by Bouckovalas et al. (2001) in the 1999 Athens (Greece) earthquake. The evidence of the topographic effect was based on the systematic concentration of severely

damaged reinforced concrete buildings along the crest of Kifissos river canyon. Two-dimensional seismic ground response analyses were undertaken for two locations along the canyon; (1) the site of Hotel Dekelia and (2) the site of Adames. At Dekelia Hotel, the canyon was V-shaped with an approximate depth of 40m and 15^{o} inclination of the cliffs relative to the horizontal. At Adames, the riverbed was wider, and the east bank was considerably lower than the west bank. The maximum depth of the canyon was also 40m, but the cliff was twice as steep. Comparison of the results for two different locations showed the significance of the cliff inclination. In the case of Adames with 30^{o} angle of inclination, the average topographic amplification was about 50% for a wide range of period, whereas at Hotel Dekelia similar values of amplification were computed for the period range 0.3 to 0.5 sec. These results supported the significant contribution of local topography conditions to the distribution of damage.

Another case-study from the Athens 1999 earthquake was done by Assimaki et al. (2005). They illustrated the effect of local stratigraphy, material heterogeneity and soil–structure interaction in altering the energy focusing mechanism at the vertex of convex topographies. Elastic two-dimensional wave propagation analyses were performed by using available geotechnical and seismological data of the Kifissos river canyon. According to the results of this study, cliff geometry alone could not predict the high level of experienced damage. Stiff soil sites amplified seismic motions also. Soil–structure interaction on stiff soil deposits filtered the high frequencies of the horizontal motions.

2.1.1.3. SLOPES

Single slope faces geometries have been investigated by Sitar and Clough (1983) and Ashford et al. (1997). The later study analyzed a stepped half space subjected to plane SH waves and SV/P waves at various incidence angles. It was found that amplification generally increases with

slope angle and proximity to crest, and is maximized for slope height (H) to wavelength (λ) ratios H/ λ = 0.2. Results by Ashford et al. (1997) for vertically incident SV waves are summarized in Figure 2.8(a). Ashford et al. (1997) studied stepped half spaces with vertical slope faces and found that the amplification increased significantly if the incident waves are inclined such that they travel into the slope face. According to this result presented in Figure 2.8(b), 10 degrees change in the vertical incidence angle yields 50% increase in amplification.

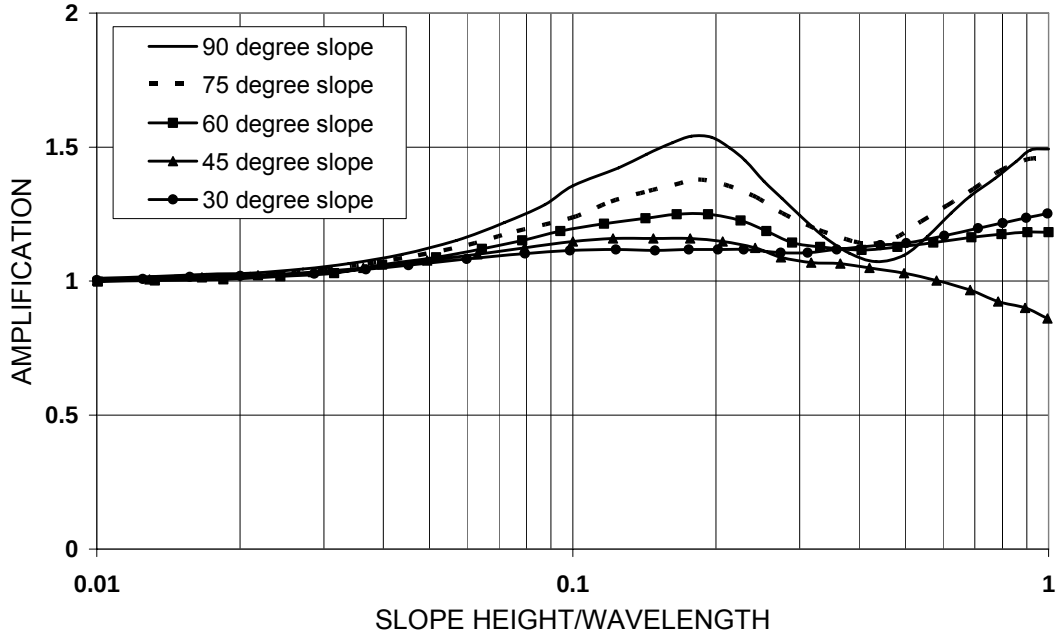

Figure 2.8.a: Horizontal amplification at slope crest for a vertically incident SV wave; Ashford et al. (1997)

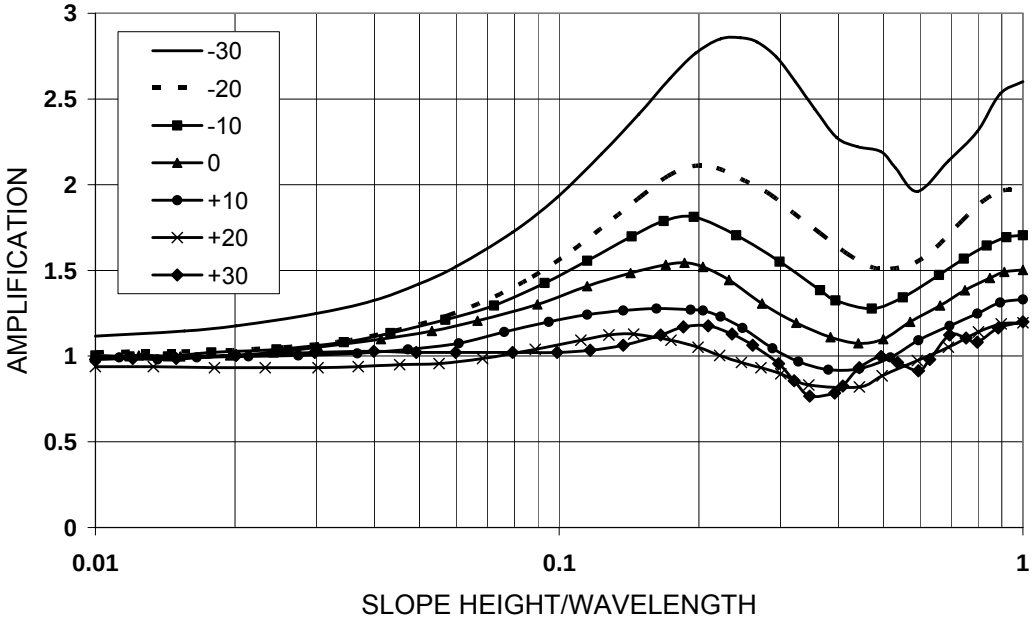

Figure 2.8.b: Horizontal amplification at the crest of a vertical slope for inclined SV wave incident from -30 deg to +30 deg; Ashford and Sitar (1997)

Similarly, Stewart and Sholtis (1999) evaluated topographic effects across a slope face from strong motion data, with appropriate corrections for ground response variability. In their study the data obtained from the 1983 Coalinga main shock and two aftershocks (M=6.4) was used. The investigated site is water pumping plant for which recordings above and below a 21 m high cut slope was available. Crest amplification of 5% damped acceleration response spectra identified from the three recordings are presented in Figure 2.9. The maximum crest amplification is about 1.2, which is reasonably consistent with the results obtained by Ashford and Sitar (1997) and Ashford et al. (1997).

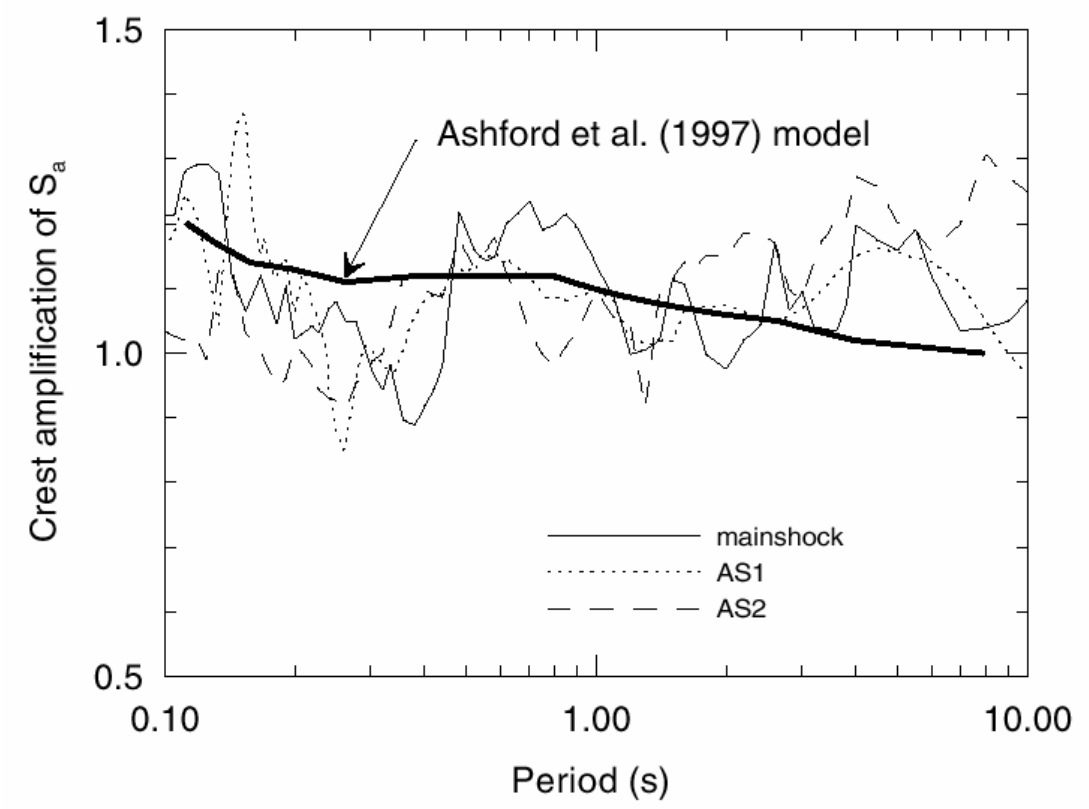

Figure 2.9: Amplification at crest of a 21m tall, 3H:1V cut slope for vertically incident waves; Stewart and Sholtis (1999)

The effects of surface topography on the seismic ground response during 1995 Egion earthquake in Greece was studied by Athanasopoulos GA et al. (1999). The ground motion was analyzed by using 2-D finite element code capable of modeling the surface relief and the stratigraphy of the area with the aim of explaining the contrast in earthquake damages between the central elevated part of town and the low and flat waterfront area. It was found that the base motion was greatly amplified (290%) at the elevated region whereas at sites close to fringe of the slope the amplification was even greater (460 %).

Seismic response of step-like slope topography has been analyzed with the finite difference method for visco-elastic soil under vertically propagating SV seismic waves by Bouckovalas et al. (2004). Canyon topography was used for analytical verification of numerical scheme. The

effect of slope inclination, normalized height, significant cycle and soil damping on seismic ground motion was analyzed in a parametric manner. According to results, step-like topography may lead to intense amplification or de-amplification variability at neighboring (within a few tens of meters) points behind and front of the crest and also produce a parasitic vertical acceleration.

2.1.2. TOPOGRAPHIC EFFECTS ON CODES

In recent years, topographic effects have been integrated into building codes. The French PS-92 seismic code and the Euro Code 8 (EC-8) (draft 2003) contain provisions for topographic amplification factors.

According to EC-8, for important structures (importance factor>1.0) topographic amplification effects should be taken into account. Some simplified amplification factors for the seismic action should be used in the stability verification of ground slopes. Such factors, denoted ST, are in first approximation considered independent of the fundamental period of vibration and, hence, should multiply as a constant scaling factor the ordinates of the elastic design response spectrum given in EN1998-1. These amplification factors should in preference be applied when the slopes belongs to two-dimensional topographic irregularities, such as long ridges and cliffs with height greater than about 30 m (EN1998-1 Annex A).

The topography effects may be neglected for average slope angles less than about 15°, while a specific study is recommended in the case of strongly irregular local topography. For greater angles the followings are recommended:

a. Isolated cliffs and slopes: ST > 1.2 should be used for sites near the top edge.

b. Ridges with crest width significantly less than the base width: ST > 1.4 should be used near the top of the slopes for average slope angles >30° and ST > 1.2 for smaller slope angles.

c. Presence of a looser surface layer: In the presence of a looser surface layer, the smallest ST value given in (a) and (b) should be increased by at least 20%, in accordance with 3.2.2.1(4) of EN1998-1.

d. Spatial variation of amplification factor: The value of ST may be assumed to decrease as a linear function of height above the base of the cliff or ridge, and to become unity at the base.

According to French code (PS-92), except if the effect of topography on the seismic motion is directly taken into account using a dynamic calculation based on a proper idealization of the relief, a multiplying coefficient T called site response factor or topography factor should be used.

$$T=1+0.8(I-i-0.4) \qquad 1 \leq T \leq 1.4$$

Where; I and i are the gradients of the lower and upper slopes respectively.

It is noteworthy that the French (PS-92) and the European (EC-8) seismic codes provide similar lower limits for topography effects on seismic ground motion, with the difference that the criteria for slope height H are given in nominal rather than in normalized values. More specifically, the PS-92 requires that H>10 m and i>22°, while the EC-8 requires that H>30 m and i>15°.

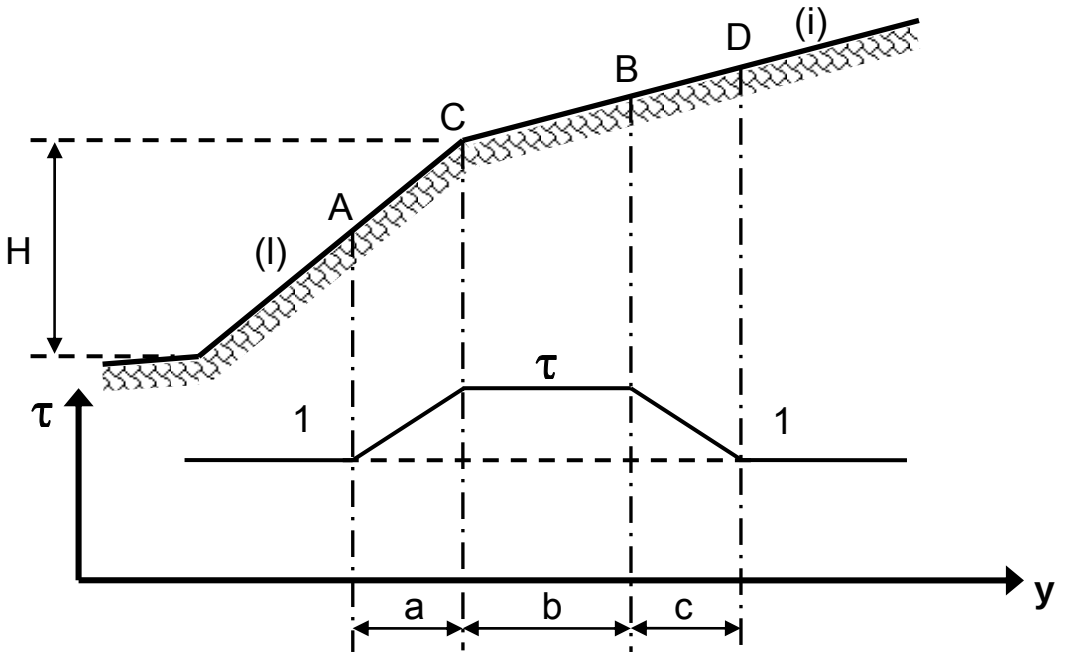

Figure 2.10: τ site response factor according to PS-92

2.2. BASIN GEOMETRY

The effect of basin geometry on ground motion is an important case in geotechnical earthquake engineering, since many large cities are located on or near alluvial valleys. A basin is formed by alluvial deposits and sedimentary rocks. These sedimentary rocks are geologically younger and have lower seismic wave velocities than the underlying rocks upon which they have been deposited. The thickness of the basin can vary between 100 m and 10 km. According to Graves et al. (1998), waves that become trapped in deep sedimentary basins can produce up to 50% stronger amplitudes at intermediate and low frequencies (f<1Hz) than those recorded on comparable surface materials outside basins. Additionally, their durations, measured using the Husid plot, can be twice as long.

Past studies of basin response have typically been limited to ground motions with frequencies less than about 1 Hz. Davis et al. (2000) showed

that basin response effects are also important at higher frequencies, or can affect structures having higher fundamental mode frequencies.

2.2.1. BASIN-EDGE EFFECTS

The importance of basin effects on strong ground motion was first recognized after 1971 San Fernando Earthquake. Hanks (1975) and Liu and Heaton (1984) made detailed analyses of wave propagation effects along various profiles which traversed the basins with the help of the availability of high-quality ground motion recordings throughout the San Fernando and Los Angeles basins during this earthquake. These data clearly showed the development of basin-generated surface waves, which lead to amplified ground motions and extended durations of shaking within the sedimentary basins but in 1975, this effect could not be recognized due to the lack of understanding. On the other hand, Toriumi et al. (1984) confirmed that the observed surface waves in Osaka basin were developed near the basin edge after analyzing the records of 27 earthquakes, which occurred between 1970 and 1982. Further confirmation of these ideas was provided by Vidale and Helmberger (1988), who successfully modeled these data using two-dimensional finite difference calculations.

Vidale and Hermberger (1988) found that the curvature of a basin in which softer alluvial soils have been deposited can trap body waves and cause some incident body waves to propagate through the alluvium as surface waves. These waves can produce stronger shaking and longer duration than would be predicted by one-dimensional analyses that consider only vertically propagating S-waves.

Damage patterns during 1994 Northridge earthquake have also demonstrated the importance of basin effects. Studies showed that, the distribution of some of the major damage centers during the earthquake coincided roughly with alluvial basins such as the Los Angeles Basin and San Fernando Basin. The strong correlation of ground motion amplification

pattern with the fault location stated that the underlying basin-edge structure strongly affects the site response. One-dimensional and two-dimensional modeling studies were done in order to understand the mechanism by which this geologic structure could affect amplification levels. Chang et al. (1996) attempted to simplify two-dimensional seismic basin response by series of one-dimensional ground response analyses and concluded that one-dimensional simplifications don't produce consistent predictions. Graves et al. (1998) numerically studied basin edge problem and found large amplifications, consistent with field observations.

By means of wave propagation modeling using basin edge structures, 1995 Kobe earthquake provided further evidence from recorded strong motion data that ground motions may be particularly large at the edges of fault-controlled basins. Severe damage to buildings due to the Kobe earthquake was observed in a zone about 30 km long and 1 km wide, and offset about 1km southeast of the fault on which the earthquake occurred as shown in Figure 2.11. The Kobe region is very heavily populated with dense urbanization extending up into the foothills north of the surface fault trace. Since the density and type of construction is similar throughout the urban region, zones of concentrated damage reflect locally amplified ground motion levels rather than spatial variations in the built environment. Numerical simulations stated that near fault ground motions in the Kobe earthquake were amplified by the basin edge effect. According to Kawase, (1996) and Pitarka et al. (1998), this effect is caused by the constructive interference between direct seismic waves that propagated vertically upward through the basin sediments from below, and seismic waves that diffracted at the basin edge and proceeded laterally into the basin.

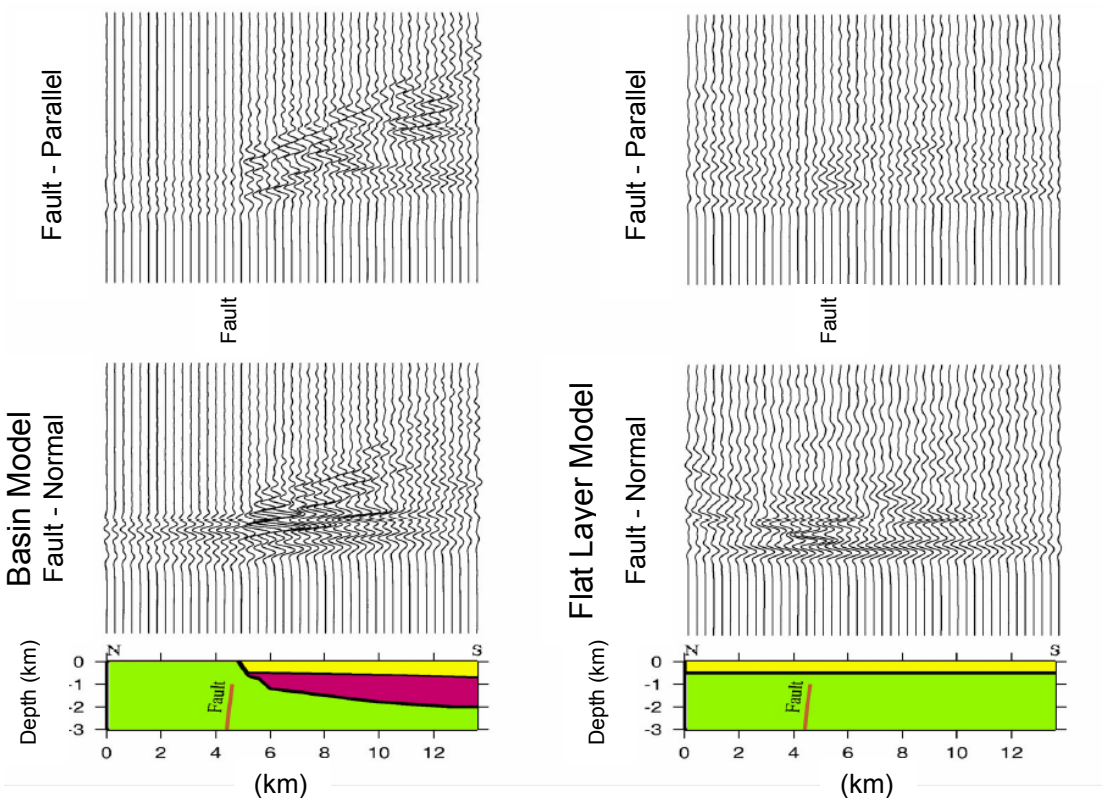

Figure 2.11: Basin edge effects in the 1995 Kobe earthquake, Pitarka et al. (1998)

King and Tucker (1984) measured ground motions along transverse and longitudinal profiles across the Chusal Valley near the Afghanistan border of the former Soviet Union. Interpretation of the response in a series of small (ML≤4.0) earthquakes suggested that one-dimensional ground response analyses could predict the average response of sediments near the center of the valley but not at the edges. Significant differences between the amplification functions at the center and edges of the valley were observed, explaining why the motions at those locations were considerably different. Similar effects have been observed for other valleys in different earthquakes such as Caracas in 1967, San Fernando in 1971, and Leninakan, Armenia in 1988.

Bard and Gariel (1986) used an analytical approach to study the two-dimensional response of shallow and deep alluvial basins. According to the results illustrated in Figure 2.12 (a) and (b), one-dimensional and two-

dimensional amplification functions at the center of the shallow, flat valley (station 8) were quite similar, which indicates that one-dimensional analyses would be appropriate for that region. However, closer to the edge of the valley (station 4), the amplification functions were found to be considerably different. For the deep valley, the agreement between one-dimensional and two-dimensional amplification functions was much better at the center of the valley than by the edges. A similar trend was not reported for the shallow valley case.

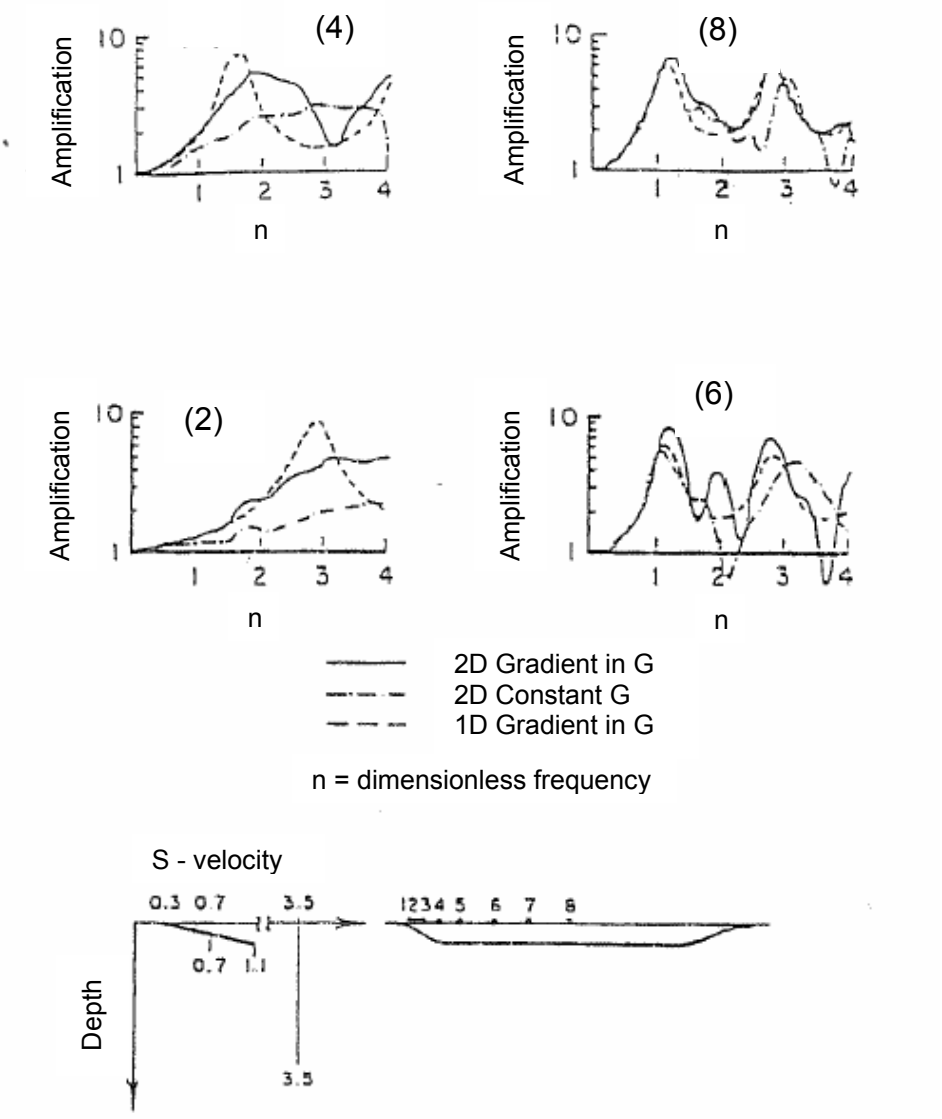

Figure 2.12.a: Smoothed SH transfer functions to homogeneous half space outcrop motions for a wide, shallow alluvial valley with shape ratio of 0.1; Bard and Gariel (1986)

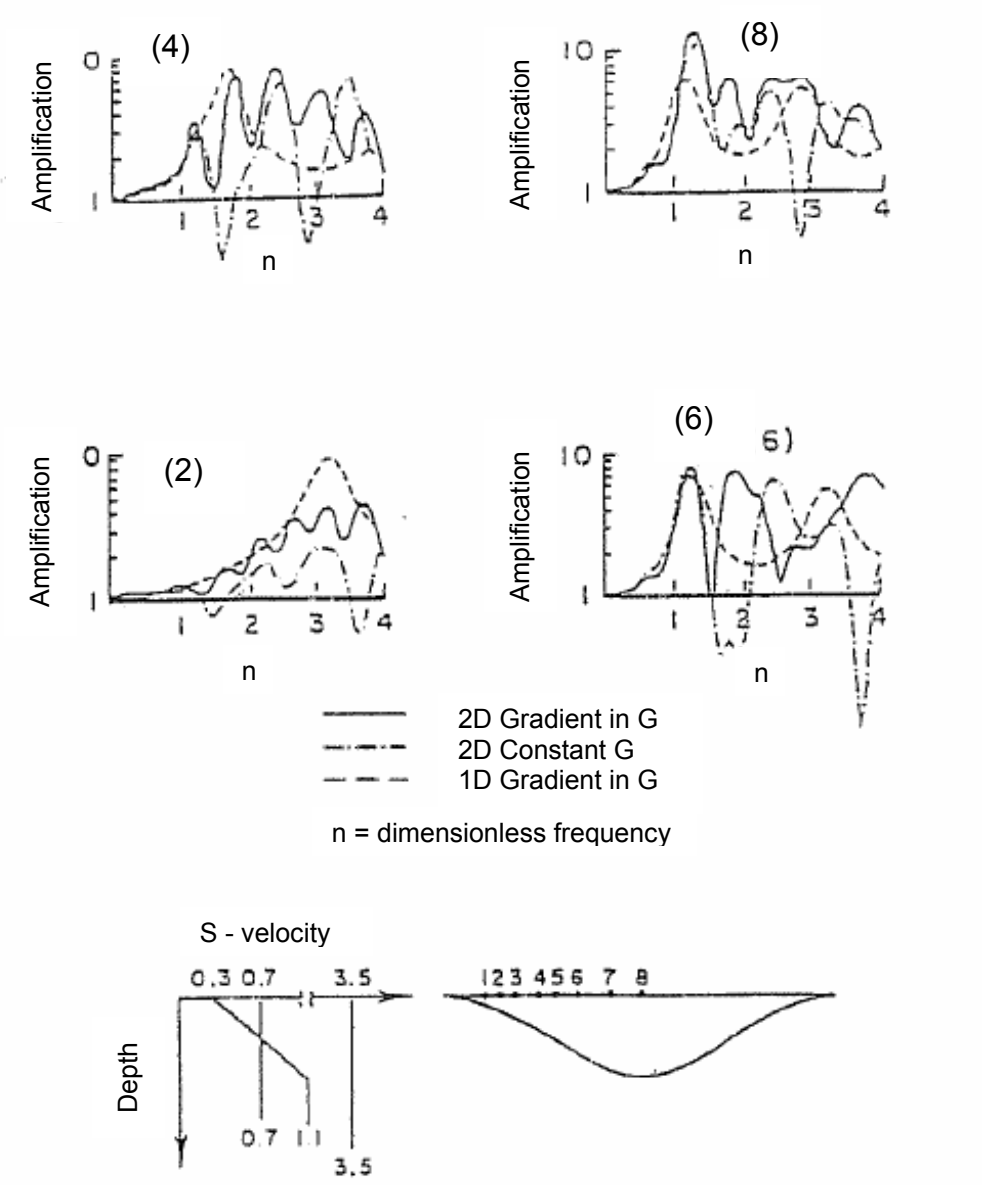

Figure 2.12.b: Smoothed SH transfer functions to homogeneous half space outcrop motions for a valley with shape ratio of 0.4; Bard and Gariel (1986)

In fact, evaluation of the effects of topographic and subsurface irregularities requires at least two, in some cases three-dimensional analyses. Such analyses are often complicated and time consuming and may require more detailed site characterization which may not be so feasible. Although it may be difficult to predict, there is little doubt that such effects

exist. Silva (1988) summarized the effects of topographic and subsurface irregularities, with comments on their quantitative predictability as shown in Table 2.2.

Table 2.2: Dimensional geologic structural effects; Silva (1988)

Structure	**Condition**	**Type**	**Size**	**Quantitative Predictability**
Surface Topography	Sensitive to shape ratio, largest for ratio between 0.2 and 0.6;most pronounced when λ=mountain width	Amplification at top of structure, amplification and deamplification at base, rapid changes in amplitude phase along slopes	Ranges up to a factor 30 but generally from about 2 to 10	Poor: generally under predict size; may be due to ridge-ridge interaction and 3D effects
Sediment-Filled Valley	Local changes in shallow sediment thickness	Increased duration	Duration of significant motions can be doubled	Fair
	Generation of long period surface waves from body waves at shallow incidence angles	Increased amplification and duration due to trapped surface waves	Duration and amplification of significant motions may be increased over 1D projections	Good at periods exceeding 1 sec
Shallow and wide (depth/width <0.25) sediment-filled valleys	Effects most pronounced near edges; largely vertically propagating shear waves away from edges	Broadband amplification near edges due to generation of surface waves	1D models may under predict at higher frequencies by about 2 near edges	Good: away from edges 1D works well' near edges extend 1D to higher frequencies
Deep and narrow (depth/width >0.25) sediment-filled valley	Effects throughout valley width	Broadband amplification across valley due to whole valley modes	1D models may under predict for a wide bandwidth by about 2 to 4; resonant frequencies shifted from 1D	Fair: given detailed description of vertical and lateral changes in material properties

Graves (1993) modeled successfully the characteristics in the Marina District of San Francisco during the 1989 Loma Prieta earthquake that the usual one-dimensional analysis was unable to model the motions. Graves (1993) gave an example study to explain the basin effect in this region. He stated that, the wave that enters the layer may resonate in the layer, but cannot become trapped for the case of one-dimensional wave propagation as shown in the Figure 2.13. In the two-dimensional case, Graves (1993) found that, if the wave is propagating in the direction in which the basin is thickening and enters the basin through its edge, it can become trapped within the basin if post-critical incidence angles develop. The resulting total internal reflection at the base of the layer is illustrated at the top right of Figure 2.13. In the lower part of Figure 2.13, simple calculations of the basin response are compared with those for the simple horizontal layered model. In each case, a plane wave is incident at an inclined angle from below. The left side of the figure shows the amplification due to impedance contrast effects that occurs on a flat soil layer overlying rock (bottom) relative to the rock response (top). A similar amplification effect is shown for the basin case on the right side of the Figure 2.13. However, in addition to this amplification, the body wave entering the edge of the basin becomes trapped, generating a surface wave that propagates across the basin.

Recent weak motion studies by Hartzell et al. (2000) have shown that in some cases, one-dimensional modeling is capable of accounting for observed amplification at intermediate to low frequencies ($f<2Hz$), whereas in other cases two-dimensional and three-dimensional models are necessary to explain observed amplification levels, particularly when the measure of amplification is sensitive to duration. Hartzell et al. (2000) suggested that use of the two-dimensional and three-dimensional models is necessary for locations near a steeply sloping basin edge.

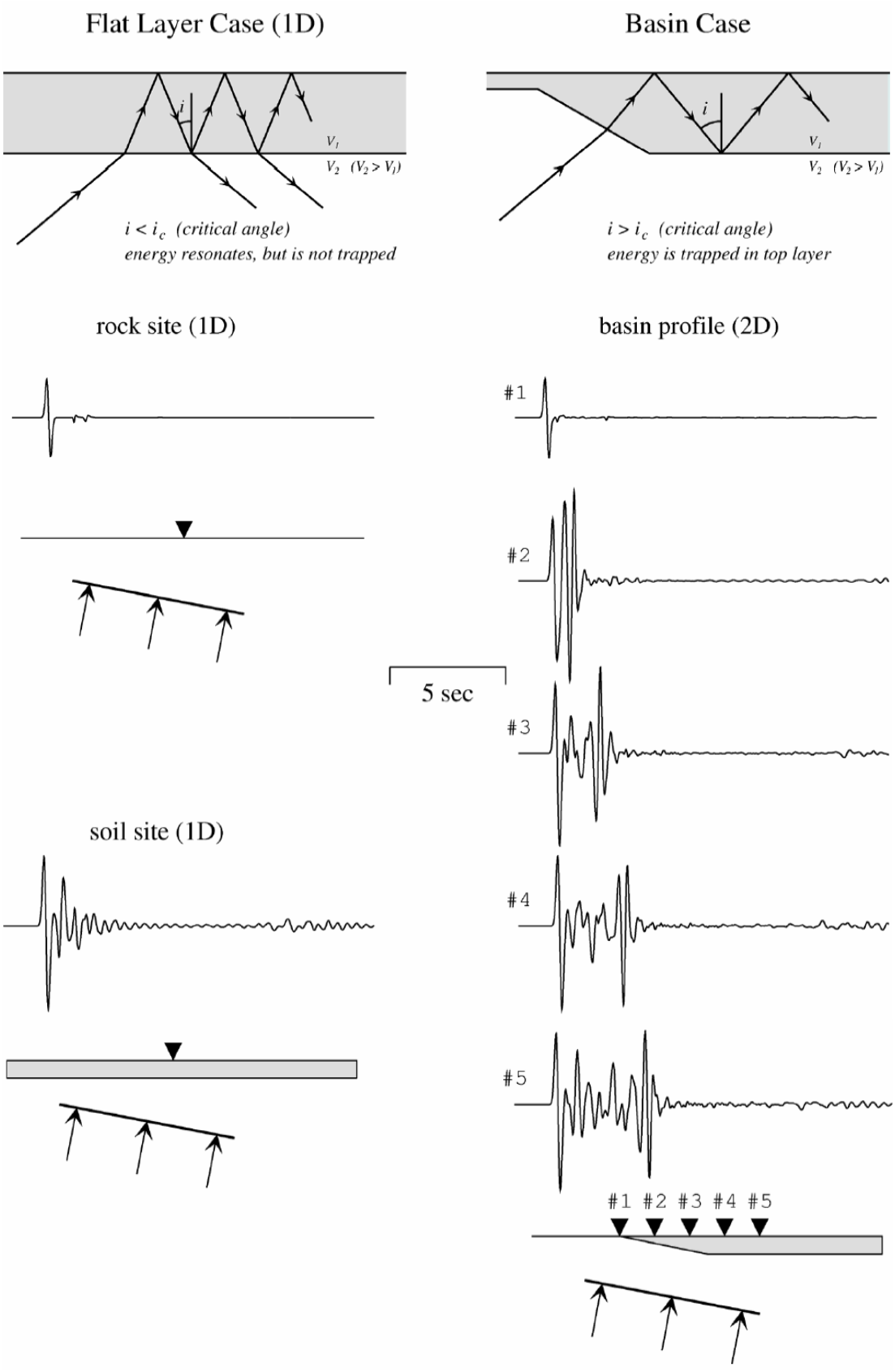

Figure 2.13: Reflection of seismic waves; Graves (1993)

The results of the analyses of Stewart et al., (2001) indicate that, current empirical ground motion attenuation relations do not distinguish between sites located on shallow alluvium and those in deep sedimentary basins, and therefore might be expected to underestimate the ground motions recorded in basins. Similar amplification effects are shown for the one-dimensional and two-dimensional cases; however, the trapping of body waves in the two-dimensional case generates surface waves that propagate across the basin. These trapped waves have been observed in recordings from the 1971 San Fernando earthquake, the 1994 Northridge earthquake, and the 1995 Kobe earthquake.

The seismic response of alluvial valleys was studied by Rassem et al. (1997). Three engineering models were developed as part of their analyses. The models were based on one-dimensional, two-dimensional and frame model approaches. Significant vibration modes and their variation in the horizontal and vertical directions were identified by the frame model. Sensitivity analyses were performed on the valley response to evaluate the effect of the uncertainty in establishing the dynamic soil properties. The parameters for which the response is investigated include the valley dimensions and geometry, site location, soil type and input rock motion. The geometric parameters are shown in Figure 2.14. Results indicate that these parameters may have significant effects on soil response. For narrow and deep valleys (B/D<10), the response approximation provided by one-dimensional analysis underestimates the response predictions in the middle of the deep valley. The only sites, where one-dimensional analysis succeeds in approximating the response of the two-dimensional model are those located near or at the center of wide or shallow valleys (B/D $\geq$10).

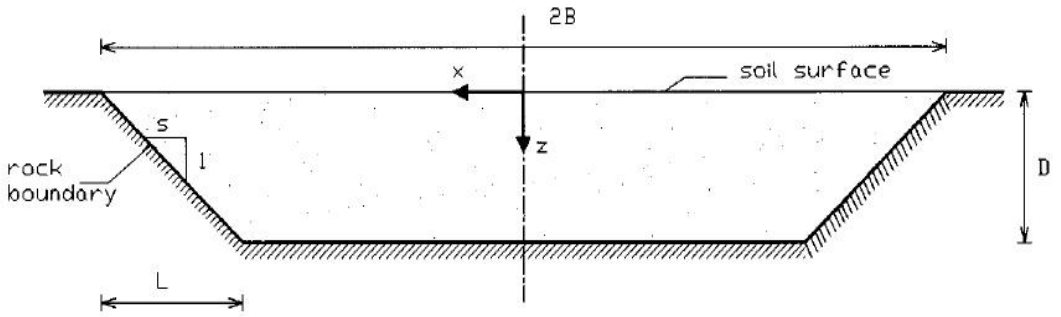

Figure 2.14: The Valley Geometry; Rassem et al. (1997)

The magnitude M=6.8 earthquake occurred in Northern Armenia on 7 December 1988 and caused destruction and fatalities within the epicentral region. The city of Leninakan located 25 km from the ruptured fault, suffered heavier damage than the city of Kirovakan, only 10 km from the fault. The city of Leninakan is in the centre of the Shirak Valley, which was formed by volcanic and tectonic activity. The city is founded on 300-400m thick lake and river deposits underlain by basalts and Neocene rocks. Damage distribution was uniform across the entire city. In contrast to Leninakan, Kirovakan is located in a mountainous region in the narrow Pambak River Valley. Soil conditions in Kirovakan vary significantly place to place. Collapse and heavy damage was confined in a small region where up to 150 m of stiff sandy clays fills a very narrow valley. Despite the fact that the rock motion in Kirovakan was smaller, damage in this region was significantly high. To explain the striking contrast in distribution of damage in Kirovakan, one-dimensional wave propagation analysis was performed by Yegian et al. (1994). These one-dimensional simulations were based on the usual assumption of flat horizontal layers. However, by comparing the results of one-dimensional analyses with observed damage, they found that such analyses underpredicted the ground surface motion in one region in Kirovakan in which the soil profile constitutes a triangular sedimentary basin whose width is only about five times its depth. A more realistic two-dimensional finite element analysis was later performed by Bielak et al.

(1999). Results of this two-dimensional simulation indicate the striking difference from one-dimensional analyses and predict maximum ground and structural response in the frequency range of 2.5 to 4.5 Hz, which corresponds to natural frequencies of the four and the five story structures, which are heavily damaged during the earthquakes.

The effect of basin edge on the distribution of damage in 1995 Dinar earthquake was investigated by Bakır et al. (2002). The town is located at the edge of an alluvial basin in Southeast Anatolia, Turkey. Inflicted structural damage was highly concentrated in a region located on the alluvium and adjacent to the rock outcrop. Possible effects of the edge of basin on which the town is located were investigated through one-dimensional and two-dimensional response analyses. They found that one-dimensional analyses considerably underpredict the spectral response in the heavily damage zone and differences between the spectral responses obtained from the two approaches diminish with increasing distance from the rock outcrop. They concluded that the two-dimensional amplification was significant over a distance from the edge of the basin.

The analyses of seismic site effects in various alluvial basins were investigated by Semblat et al. (2002). The amplification of seismic motion was analyzed in terms of level, occurring frequency and location for a shallow deposit in the center of Nice (France) and deep irregular basin in Cracas (Venezuela). Site effects were investigated by using the boundary element method and compared with the experimental results in the centre of Nice basin previously obtained by Semblat et al. (2000). The experimental results were obtained to real earthquakes (weak motion) and micro tremor measurements. One-dimensional analytical analysis of amplification didn't give a satisfactory estimation of the maximum reached level. A boundary element model was then proposed considering different wave types. The influence of frequency and incidence was analyzed. For real earthquakes, the numerical results are in good agreement with experimental measurements for each motion component. As a result, two-dimensional basin effects were found to be very strong by Semblat et al. (2002).

Deep alluvial valley in Caracas was analyzed considering the boundary element method in the frequency domain by Semblat et al, (2002). A numerical model for the nearest mountain including a part of the local topography was considered. They found that, site effects occur in the thickest part of the basin for low frequencies and in the two intermediate thinner areas for frequencies above 1.0 Hz. The influence of both incidence and shear wave velocities was also investigated and comparison was done with micro tremor recordings.

The results of the analyses of Semblat et al. (2002) indicate that, for deep alluvial valley in Caracas and shallow basin in Nice, the amplification factor reach maximum values of 20. Site effects nevertheless have very different features concerning the frequency dependence and the location of maximum amplification. For shallow alluvial valley, the amplification factor is very small for low frequencies and increases with increasing frequency and also the maximum amplification is located on the surface. On the other hand, for the deep alluvial valley, different amplification values are found for various frequencies and strong amplification areas appear inside the basin.

The results obtained by Field et al. (2000), Lee and Anderson (2000), and Steidl (2000) for sites in the Los Angeles basin stated that amplification increase significantly with basin depth, with representative results shown in Figure 2.15. The amplification factors in Figure 2.15 are defined relative to the prediction appropriate to each site class (i.e., not relative to a particular geologic formation).

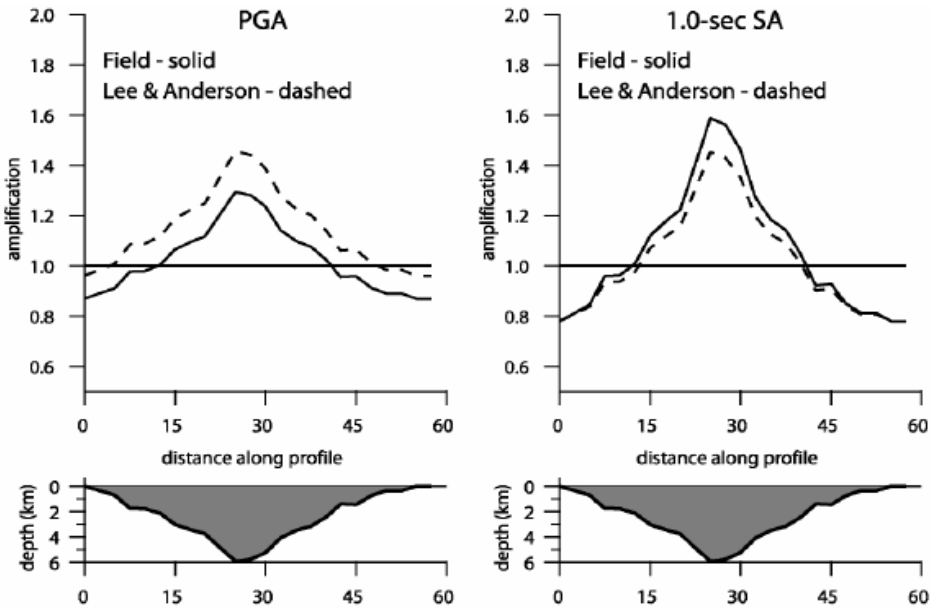

Figure 2.15: Basin depth amplification factors implied by the attenuation relationships by Lee and Anderson (2000) and Field (2000) for sites along cross section through Los Angeles basin; Field et al. (2000)

A parametric study was done by Heymsfield (2000) to show the significance of a sloping rock half-space on surface response. Slope-rock boundary, the incidence angle and frequency of SH wave was used as parameters. The soil profile is shown in Figure 2.16. Four rock slopes were examined with two-dimensional analysis. According to this dimensionless study, the following results were obtained:

- Surface displacements show higher values than those from a one-dimensional analyses solution.
- Maximum surface response shifts towards the crest of the rock slope as frequency increases.
- A reduction in the incidence angle slightly shifts surface displacement away from the rock slope crest.

- For vertical incidence, the region that encompasses scattering due to the rock slope anomaly increases as the rock slope decreases.

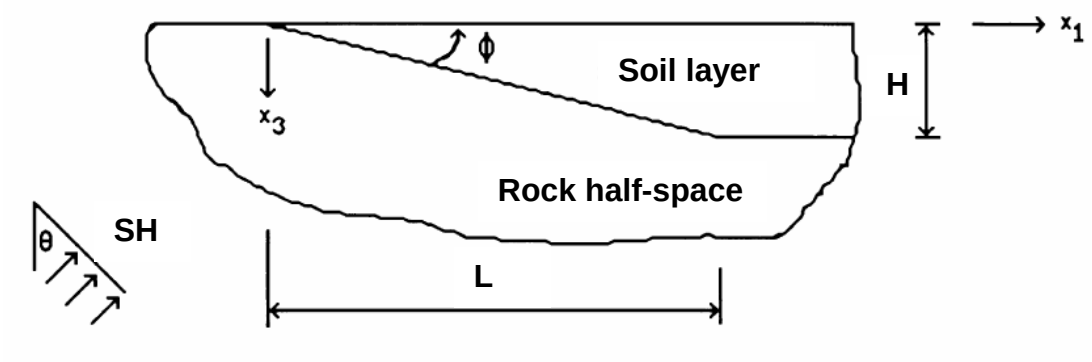

Figure 2.16: Soil-rock profile; Heymsfield (2000)

Parametric study was done at Euroseistest valley in northern Greece to show the necessary parameters to correctly characterize the site response of a two dimensional sedimentary valley by Makra et al. (2005). In this study, eight different soil layers and four faults were identified as seen in Figure 2.17. Variations in the velocity structure in the sediments and variations of the shape between sediments and bedrocks were considered. To determine the site response, results from different one-dimensional model were compared with two-dimensional ones. In this study 'aggravation factor' defined by Cha´vez-Garcia et al. (2000) was used in order to take into account the effects of lateral heterogeneity. This factor was defined as the average ratio between response spectra computed at the surface of the two-dimensional model and the response spectra computed at the surface of the equivalent one-dimensional model. According to results obtained by Makra et al. (2005), in terms of predicting site response, a rough idea of its shape ratio and the average mechanical properties of the sediments are better than a very detailed one-dimensional profile at the central site.

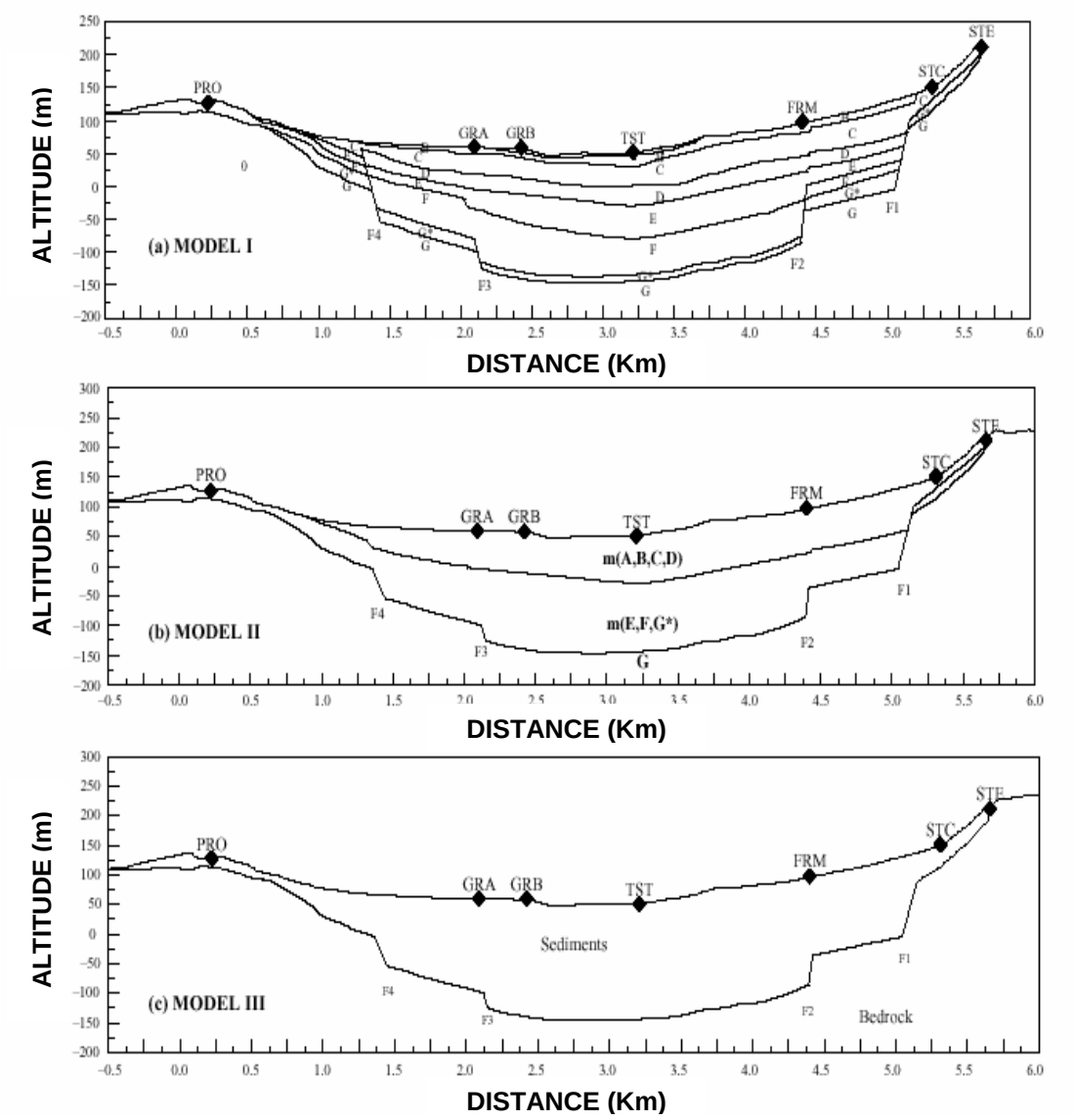

Figure 2.17: Three possible 2D models for Euroseis test valley; Makra et al. (2005)

Soil layering on site effects in both time domain and frequency domain was analyzed with boundary element method by Semblat et al. (2005). The European test site of Volvi (Greece) was considered and two-dimensional amplification in the basin was investigated for various soil models. Two numerical models were selected for this study. One of them is with only two soil layers and other one is complete one with six soil layers as shown in Figure 2.18. According to this study, the geometry of the basin has a very

strong influence on seismic wave amplification in terms of both amplification level and time duration lengthening in the central part of the basin.

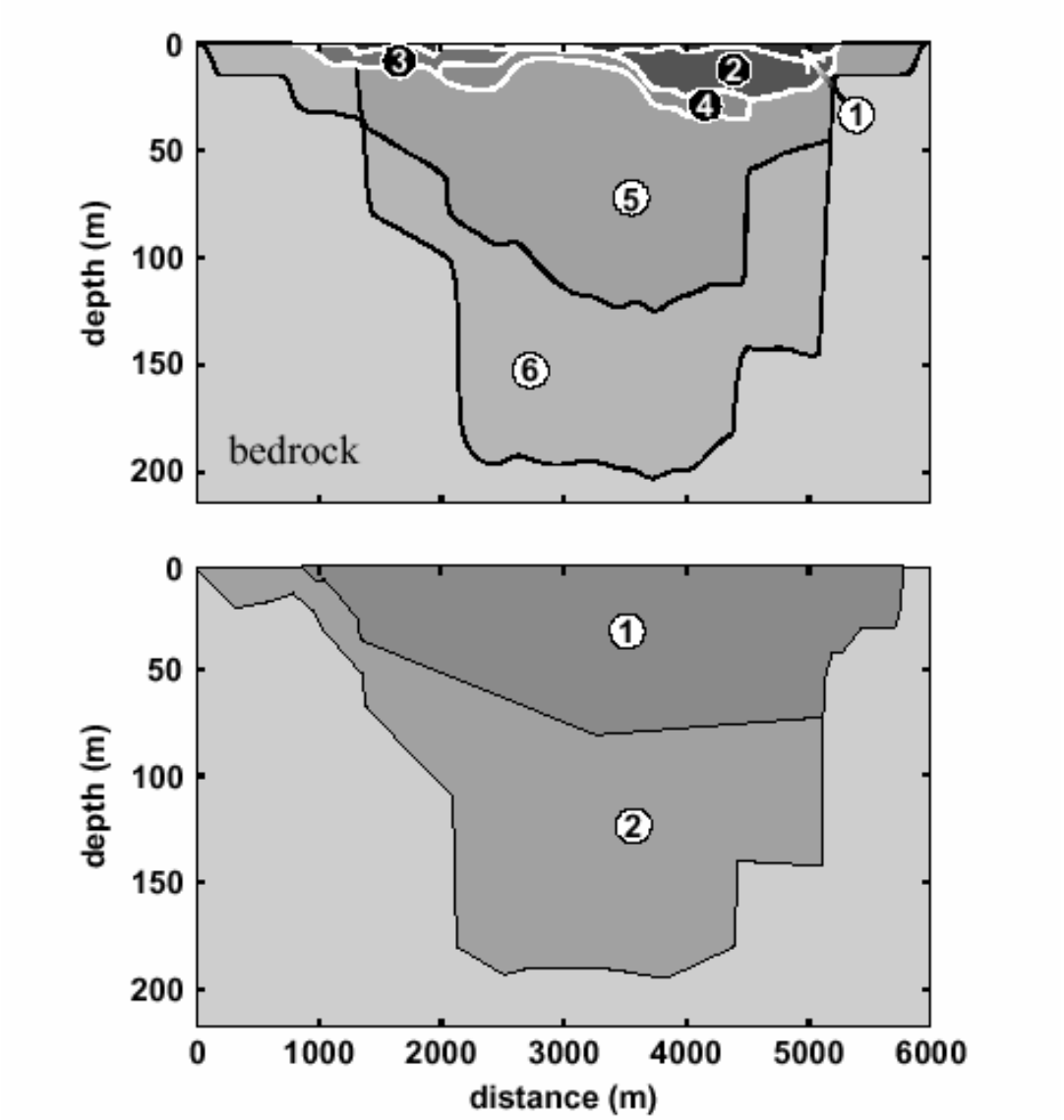

Figure 2.18: Geotechnical models of the Volvi basin; Semblat et al. (2005)

The effects of soil layering in the basin on the characteristics of basin edge induced surface waves and associated differential ground motion has been investigated using 2.5D elastodynamic wave equation by Narayan (2006). Six models were conceived with different number of soil layers one of

which is shown in Figure 2.19. Total thickness of soil layer (400m), the fundamental frequency of soil deposits (0.6 Hz) and impedance constant with respect to the bedrock was kept constant. The result of basin model was compared with flat layer basin model. Decrease of amplitudes of basin-edge induced surface waves with increase of layers in the basin was found. Shifting of dominant frequency towards the higher value was obtained with increase of soil layers in the basin. Effect of soil layering was more on Rayleigh wave as compared with the Love wave. According to Narayan (2006), the level of strain developed by induced surface waves, particularly Love wave, reveals that differential ground motion may play an important role in damage near the basin-edge to the large span structures.

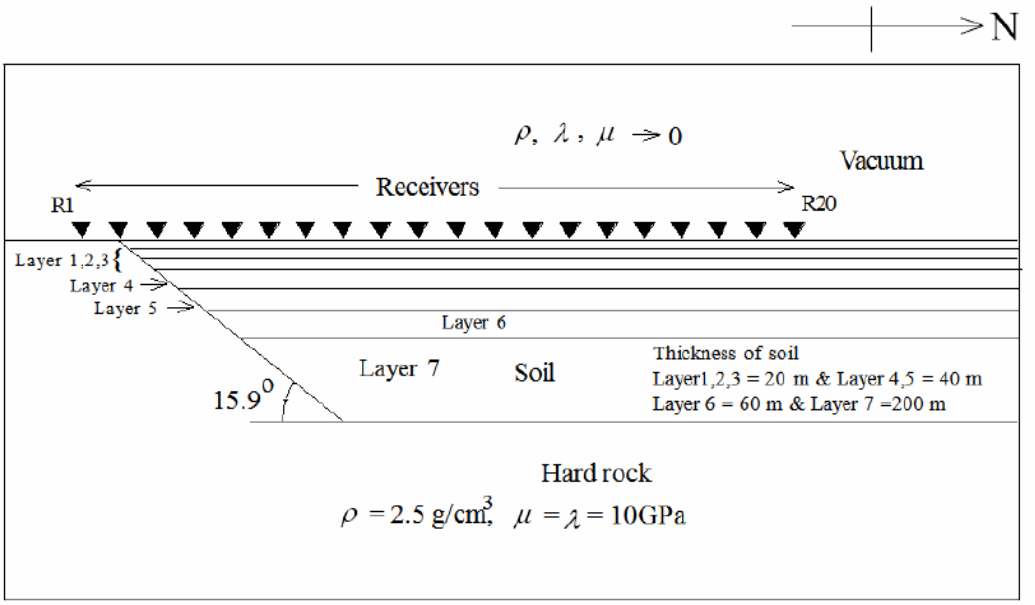

Figure 2.19: Vertically exaggerated cross-sectional view of a basin-edge model with seven soil layers; Narayan (2006)

2.3. FREQUENCY CONTENT OF GROUND MOTIONS

The influence of frequency content of ground motions on site amplification was investigated by modeling and a procedure for quantifying the characteristic period of the ground motion is needed. Various approaches

proposed in literature were reviewed by Green, R.A. et al. (2003) such as Gutenberg and Richter (1956), Figueroa (1960), Seed et al. (1969), and Rathje et al. (1998), with the most recent and extensive study being that by Rathje et al. (1998).

Rathje et al. (1998) explored three approaches to quantifying the characteristic period of the ground motion which are (1) mean period (T_m), (2) predominant period (T_p), and (3) smoothed spectral predominant period (T_o). Since T_m and T_o are not related to NEHRP Provisions' design spectrum, alternative T V/A is proposed for use in quantifying the characteristic period of ground motion. T V/A is the period corresponding to the intersection of the constant spectral acceleration and velocity regions of a 5% damped Newmark-Hall type spectrum constructed using the actual PGA and PGV values of a given ground motion. T V/A is computed by:

$$\text{T V/A} = \frac{\text{pgv}}{\text{pga}} \times 2\pi \times \frac{\alpha_v(\xi = 5\%)}{\alpha_A(\xi = 5\%)} \qquad (2.1)$$

2.4. EFFECT OF THE NATURAL PERIOD OF SITE ON THE SOIL AMPLIFICATION

In the analyses of Roesset (1977), the soil layer was assumed to behave linearly and it has a thickness h, total (saturated) unit weight γ_s, shear wave velocity V_s, and internal damping ratio β_s. The rock has total unit weight γ_r, shear wave velocity V_r, and zero damping. The uniform layer on elastic rock used by Roesset was shown in Figure 2.20.

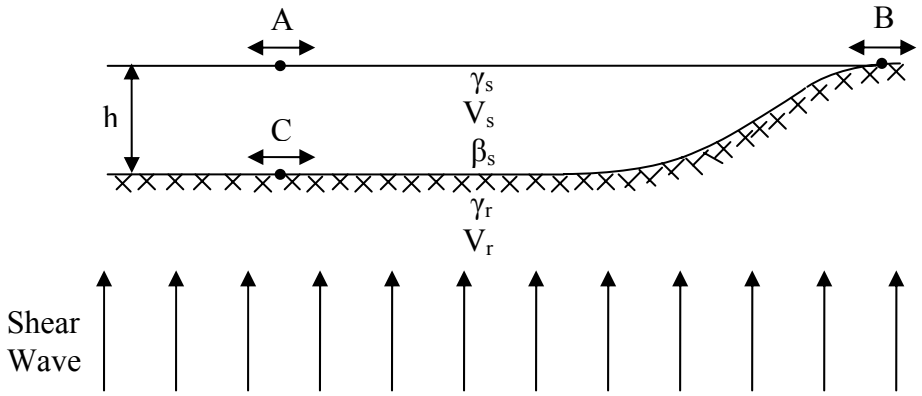

Figure 2.20: Uniform soil layer on elastic rock subjected to vertical shear waves, Roesset (1977)

Roesset (1977) investigated the ratio between the motions on top of the soil (point A) and on the rock outcrop (point B) and found that, when the acceleration at B is a harmonic motion of frequency f and amplitude a_B, the acceleration at A is also harmonic of the same frequency and amplitude a_A. He stated that, the amplification ratio a_A/a_B, is a function of (1) the ratio of frequencies $f/(V_s/4h)$, (2) the soil damping β_s, and (3) the rock/soil impedance ratio which is equal to $(\gamma_r.V_r)/(\gamma_s.V_s)$. Figure 2.21 presents a_A/a_B calculated for a layer with h=100ft (30.5m), $V_s/4h$=1.88 cps, and IR= 6.7. According to Roesset (1977);

> The maximum amplification occurs essentially at the natural frequency of the layer where $f_{soil}=V_s/4h$, and it is approximately equal to :

$$\left(\frac{a_A}{a_B}\right)\max = \left(\frac{I}{\left(\frac{I}{IR}\right)+\left(\frac{\pi}{2}\right)}\right)\beta_S \qquad (2.2)$$

> That is, the maximum soil/rock amplification for steady-state harmonic motion in these simple models depends on two factors which are β_s and IR. When IR=rigid rock, the only way the system can dissipate

energy is in the soil and $(a_A/a_B)_{max}$=16. If IR decreases, the amplification $(a_A/a_B)_{max}$ also decreases.

Another way of expressing the contribution of the impedance ratio IR in Equation 2.2 is an "additional equivalent soil damping" with a total damping β_{tot} in the system at its natural frequency:

$$\beta tot = \beta s + \left(\frac{2}{\pi IR}\right) \tag{2.3}$$

Equation 2.3 is very important since the maximum amplification $(a_A/a_B)_{max}$ is always inversely proportional to β_{tot} not only for the case of the uniform layer but also for other soil profiles on rock. β_{tot} always includes an internal damping contribution (β_s) and a second term reflecting the rock-soil impedance contrast IR although the specific definition of IR and the numerical factor $2/\pi$ generally will change depending on the profile.

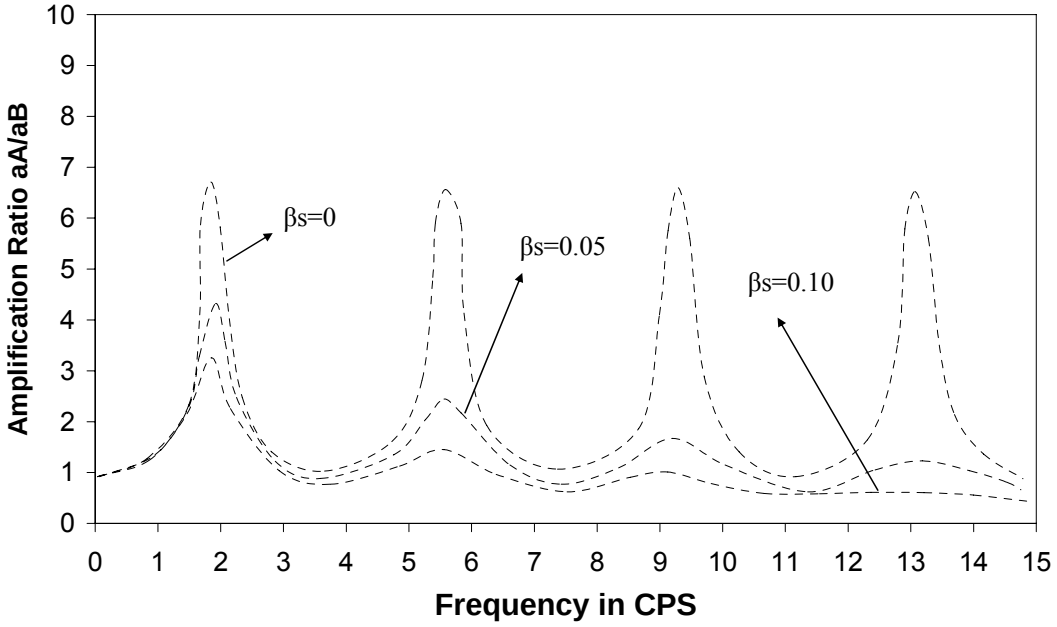

Figure 2.21: Amplification ratio soil/rock for h=100ft, V_s=1.88cps and IR=6.7; Roesset (1977)

CHAPTER 3

DYNAMIC RESPONSE ANALYSIS OF SOIL DEPOSITS

3.1. INTRODUCTION

One of the important problems in geotechnical earthquake engineering is the evaluation of ground response. There are many parameters used for this evaluation; among those the majors are the behavior of soil under dynamic loading and the ground response analysis. In the following sections, the dynamic response of soil and the most commonly used methods for ground response analyses are given.

3.2. DYNAMIC SOIL PROPERTIES

Dynamic properties of soils are dependent on so many different parameters. For a given problem, these parameters may vary by a factor of ten in a soil deposit that appears to be relatively homogeneous, because of their dependence on such parameters as strain amplitude, state of effective stress and number of cycles of loading. For many problems the shear stress-strain relation is very important (Hardin and Drnevich, 1972b).

3.2.1. DYNAMIC STRESS-STRAIN BEHAVIOR OF SOILS

In general, the cyclic simple shear stress and strain during an earthquake can be characterized by varying amplitude and frequency. To

obtain complete stress reversal, the simple shear stress cycled between positive and negative values equal in magnitude. Resulting simple shear stress-strain relation is a loop. This loop can be described in two ways: first, by the actual path of the loop itself, and second, by parameters that describe its general shape as the slope of a line through its end points, the shear modulus G, the breath of the loop and damping ratio D. The breath of the loop is related to the area, which is a measure of energy dissipation.

3.2.2. ASSESSMENT OF SHEAR MODULUS

Shear modulus is the inclination of a hysteresis loop and depends on the stiffness of the soil. It can be described at any point during the loading process by the tangent shear modulus, G_{tan} as shown in Figure 3.1. Since G_{tan} varies throughout a cycle of loading, its average value over the entire loop can be approximated by the secant shear modulus, G_{sec}, as shown in Figure 3.2. The secant shear modulus of an element of soil varies with cyclic shear strain amplitude. At low strain amplitudes, it is high, but decreases as the strain amplitudes increases. The locus of points corresponding to the tips of loops of various cyclic strain amplitudes is called a backbone curve. The slope of the curve represents the largest value of the shear modulus, G_{max}. At greater strain amplitudes, the modulus ratio G_{sec}/G_{max} drops to values of less than 1. Characterization of the stiffness of an element of soil requires consideration of both G_{max} and the manner in which the modulus ratio G/G_{max} varies with cyclic strain amplitude and other parameters. The variation of the modulus ratio with shear strain is described graphically by a modulus reduction curve shown in Figure 3.3.

Maximum shear modulus, G_{max}, can be measured directly in the laboratory using the resonant column vibration test or in the field using seismic techniques to measure shear or Rayleigh wave velocities. The measured shear wave velocities can be used to compute G_{max} as;

$$G_{\max} = \rho V_s^{\,2} \tag{3.1}$$

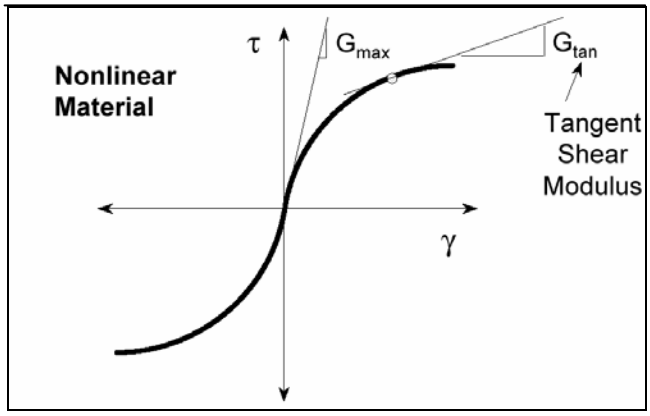

Figure 3.1: Tangent shear modulus

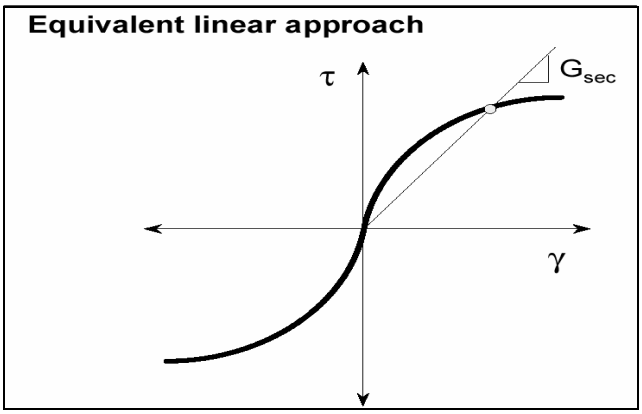

Figure 3.2: Secant shear modulus

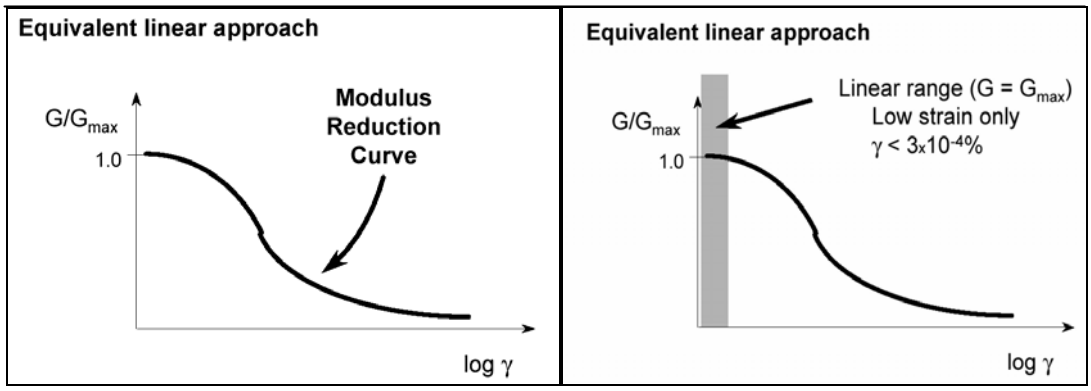

Figure 3.3: Modulus reduction curve

Hardin and Black (1969) have shown that for many undisturbed cohesive soils, as well as sands, G_{max} can be calculated from

$$G_{\max} = 1230\left(\frac{(2.973-e)^2}{1+e}\right)(OCR)^K \bar{\sigma}_o^{1/2} \qquad (3.2)$$

in which,

e = Void ratio

OCR = Over consolidation ratio

K = Over consolidation ratio exponent

$\bar{\sigma}_o$ = Mean principal effective stress, psi

G_{max} = Shear Modulus at low strain (γ<0.25x10-4), in (psi)

Following relationship between the shear modulus and the confining pressure is suggested by Seed and Idriss (1970) for sands;

$$G_{\max} = 1000K_{2\max}(\sigma'_m)^{0.5} \qquad (3.3)$$

in which,

K_{2max} = Shear modulus coefficient

σ'_m = Effective mean principal stress (lb/ft2)

For fine-grained soils, preliminary estimates of the maximum shear modulus can be obtained from plasticity index, over consolidation ratio and undrained strength. Table 3.1 shows the evaluation of G_{max}.

Table 3.1: Evaluation of G_{max}

Formula	Where	Reference
$G_{\max} = 1000 K_{2\max} (\sigma_m)^{1/2}$	G_{max} = maximum shear modulus K_{2max} = maximum soil modulus coefficient σ_m = effective mean principal stress $\sigma_m = \left(\frac{1+2K_o}{3}\right)\sigma_v'$ K_o = at-rest earth pressure coefficient σ_v' = effective vertical stress	Seed, H.B.; Wong, R.T.; Idriss, I.M. and Tokimatsu, K. (1986)
$G_{\max} = 325(N_{60})^{0.68}$	G_{max} = maximum shear modulus N_{60} = measured N-value corrected for hammer efficiency of 60%	Imai, T. and Tonouchi, K. (1982)
$G_{\max} = \left[\frac{G_e(\gamma_e = 0.5\%)}{\sigma}\right]\sigma_v$	$\left[\frac{G_e(\gamma_e = 0.5\%)}{\sigma}\right]$ is equivalent shear moduli for geomembrane HDPE/clay (dry) 47 HDPE/clay (wet) 63 Textured HDPE/clay (dry) 58 HDPE/georid 43 HDPE/Gundseal 35 HDPE/geotextile 36 HDPE/Ottowa sand 52 PVC/Gundseal 58 PVC/geotextile 57 σ_v = overburden pressure at the elevation of the liner	Yegian, M.K.; Harb, J.N. and Kadakal, U. (1998)

Table 3.1: (continued)

Formula	Where	Reference
$G_{\max} = \left(\frac{\gamma}{g}\right)(V_s)^2$	G_{max} = maximum shear modulus γ = soil unit weight g = acceleration of gravity V_s = shear wave velocity	Seed, H.B.; Wong, R.T.; Idriss, I.M. and Tokimatsu, K. (1986)
$G_{\max} = 65N$	G_{max} = maximum shear modulus N = N-value measured in SPT test	Seed, H.B.; Idriss, I.M. and Arango, I. (1983)
$G_{\max} = 2000S_u$	G_{max} = maximum shear modulus S_u = undrained shear strength	Seed, H.B. and Idriss, I.M. (1970); Egan, J.A. and Ebeling, R.M. (1985)
$G_{\max} = 1000\left[35(N_{60})^{0.34}\right](\sigma_V')^{0.4}$	G_{max} = maximum shear modulus N_{60} = N-value measured in SPT test delivering %60 of the theoretical free fall energy of the drill rod σ_v' = effective vertical stress	Seed, H.B.; Wong, R.T.; Idriss, I.M. and Tokimatsu, K. (1986)
$G_{\max} = 1000\left[20(N_{1,60})^{1/3}\right](\sigma_m)^{1/2}$	G_{max} = maximum shear modulus $N_{1.60}$ = N-value measured in SPT test delivering %60 of the theoretical free fall energy of the drill rod and corrected for an effective overburden pressure of 1ton/square foot σ_m = effective mean principal stress $\sigma_m = \left(\frac{1+2K_o}{3}\right)\sigma_v'$ K_o = at-rest earth pressure coefficient σ_v' = effective vertical stress	Seed, H.B.; Wong, R.T.; Idriss, I.M. and Tokimatsu, K. (1986)
$G_{\max} = 1634(q_c)^{0.25}(\sigma_v')^{0.375}$	G_{max} = maximum shear modulus for quartz sands q_c = CPT tip resistance σ_v' = effective vertical stress	Kramer, S.L. (1996)

Table 3.1: (continued)

Formula	Where	Reference
$G_{\max} = 406(q_c)^{0.695} e^{-1.13}$	G_{max} = maximum shear modulus for clay q_c = CPT tip resistance e = void ration	Kramer, S.L. (1996)
$G_{\max} = \left[\frac{1230}{1+e}\right](2.97-e)^2 (OCR)^k (\sigma_m)^{1/2}$	G_{max} = maximum shear modulus for clays of moderate sensitivity e = void ration OCR = over consolidation ratio k = a parameter related to the plasticity index (PI) PI(%) k 0 0 20 0.18 40 0.30 60 0.41 80 0.48 100 0.5 σ_m = average effective confining pressure $\sigma_m = \left(\frac{1+2K_o}{3}\right)\sigma_v'$ K_o = at-rest earth pressure coefficient σ_v' = effective vertical stress	Das, B.M. (1993)
$G_{\max} = \left[\frac{2630}{1+e}\right](2.17-e)^2 (\sigma_m)^{1/2}$	G_{max} = maximum shear modulus for round grained sands e = void ration σ_m = average effective confining pressure $\sigma_m = \left(\frac{1+2K_o}{3}\right)\sigma_v'$ K_o = at-rest earth pressure coefficient σ_v' = effective vertical stress	Das, B.M. (1993)

Table 3.1: (continued)

Formula	Where	Reference
$G_{\max} = \left[\frac{1230}{1+e}\right](2.97-e)^2(\sigma_m)^{1/2}$	G_{max} = maximum shear modulus for angular grained sands e = void ration σ_m = average effective confining pressure $\sigma_m = \left(\frac{1+2K_o}{3}\right)\sigma_v'$ K_o = at-rest earth pressure coefficient σ_v' = effective vertical stress	Das, B.M. (1993)

Seed and Idriss (1970) developed the first widely used modulus reduction and damping curves for sand. Their curves showed a range of modulus reduction behavior shown in Figure 3.4.

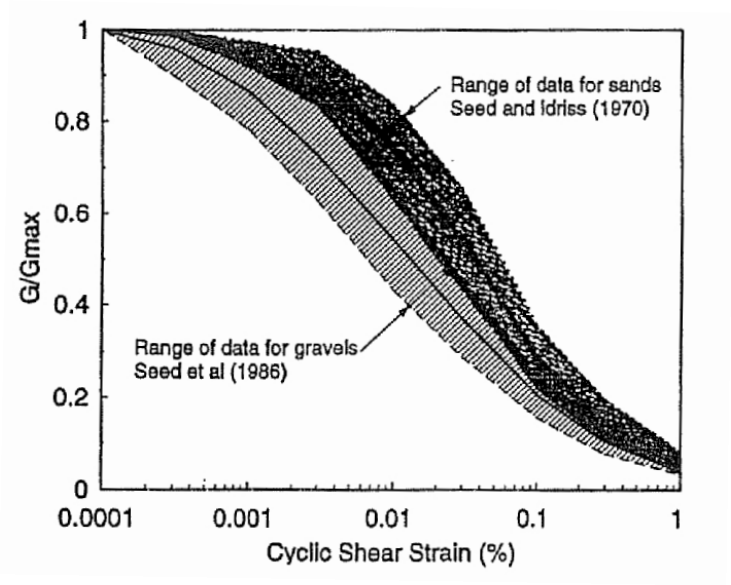

Figure 3.4: Typical G/G_{max} versus cyclic shear strain relationships for sands by Seed and Idriss (1970) and for gravels by Seed et. al. (1986)

Seed at al. (1986) developed modulus reduction and damping curves for gravel. These curves were based on the average behavior of 12-inch diameter cyclic tri-axial tests on four different gravels. Modulus attenuation with strain for gravels was quite similar to that of sands, as illustrated by the normalized modulus versus strain plot as shown in Figure 3.4 (Seed et al., 1986). The G/G_{max} versus γ data points compiled for gravel is presented in Figure 3.5. These data, representing 980 data points, were compiled from the 15 investigations listed in the Figure 3.5. Rollins et all. (1998) noted that a large percentage of data points fall within the range of data for sands proposed by Seed and Idriss (1970).

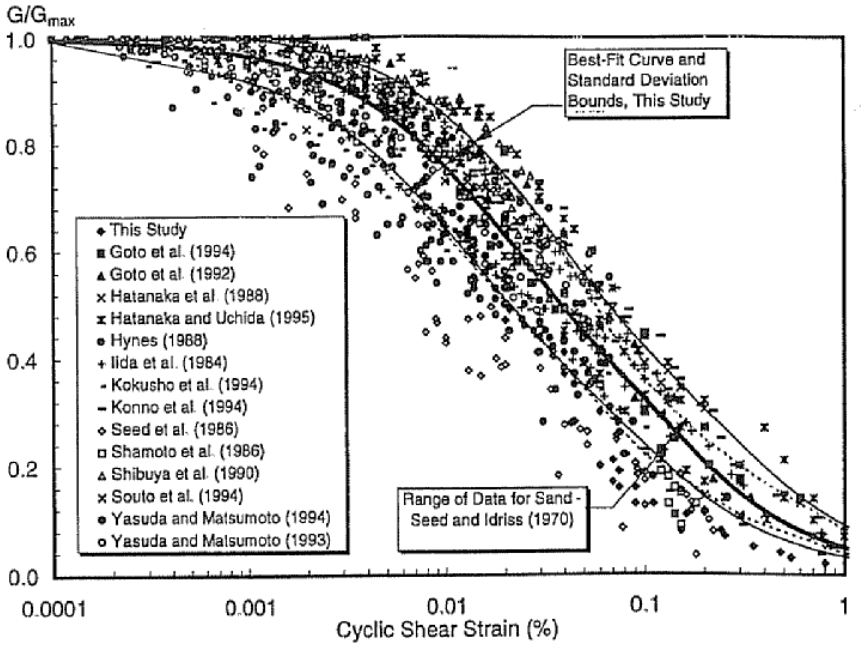

Figure 3.5: Data points G/G_{max} versus cyclic shear strain relationship for gravely soils base on testing by all 15 investigators along with best fit curve and ± one standard deviation; Rollins et all. (1998)

In the early years, the modulus reduction behaviors of coarse and fine grained soils were treated separately. Recent research, however, has

revealed a gradual transition between the modulus reduction behavior of non-plastic coarse-grained soil and plastic fine-grained soil.

The shape of the modulus reduction curves for fine-grained soils affected soil plasticity (Zen et al., 1978 and Kokushu et al., 1982). The shear modulus of highly plastic soils was observed to degrade more slowly with shear strain compared to low-plasticity soils. Vucetic and Dobry (1991), building on the work of Kokoshu (1980) in an investigation motivated by the performance of Mexico City clay in the 1985 Michoacan earthquake, showed clearly how modulus and damping behavior are influenced by soil plasticity. Dobry and Vucetic (1987) and Sun et al. (1988) concluded that the plasticity index influenced the shape of the modulus reduction curve as shown in Figure 3.6. The PI=0 modulus reduction curve is very similar to the average modulus reduction curve that was commonly used for sands. This similarity suggests that the modulus reduction curves in Figure 3.6 may be applicable to both fine- and coarse-grained soils.

Sun, Golesorkhi, and Seed (1988) developed a series of modulus reduction and damping curves for different ranges of plasticity index. Separate curves for $5 < PI < 10$, $10 < PI < 20$, $20 < PI < 40$, $40 < PI < 80$, and $PI > 80$ were developed.

Modulus reduction and damping characteristics, particularly for low-plasticity soils, are also influenced by effective confining pressure. Ishibashi and Zhang (1993) proposed expressions for shear modulus and damping ratio that accounted for plasticity index and effective confining pressure. Ishibashi and Zhang equations predict G/G_{max} values slightly greater than 1 over a range of low strains.

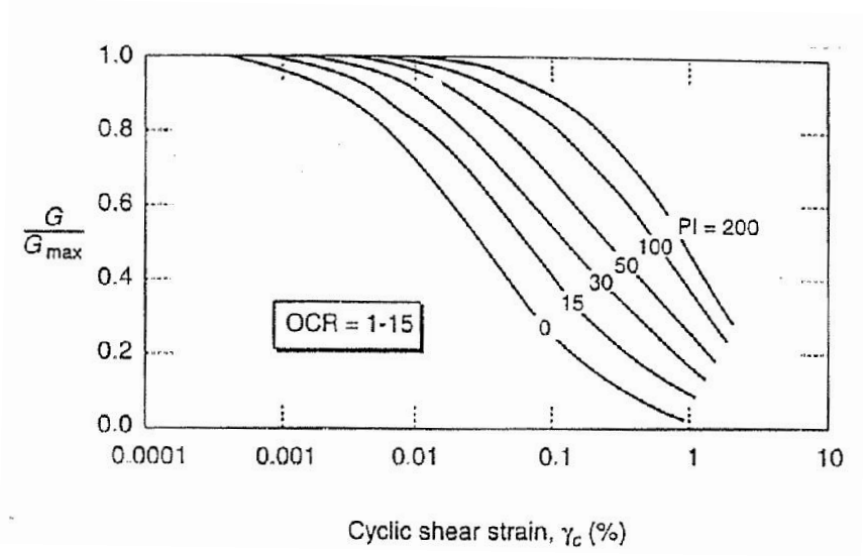

Figure 3.6: Modulus reduction curve for fine-grained soils of different plasticity; Vucetic and Dobry (1991)

3.2.3. ASSESSMENT OF DAMPING RATIOS

The damping curve describes the manner in which the damping ratio varies with shear strain amplitude. Because soils exhibit nonlinear, inelastic stress-strain behavior, their equivalent damping ratios increase with increasing strain level. Different types of soil exhibit different damping characteristics. In general, soil damping increases with decreasing plasticity index. A number of investigators have studied the damping behavior of different soils and proposed standard damping curves for those soils.

Damping behavior is influenced by plasticity characteristics according to Kokushu et al. (1982), Dobry and Vucetic (1987) and Sun et al. (1988). Damping ratios of highly plastic soils are lower than those of low plasticity soils at the same cyclic strain amplitude. The PI=0 damping curve is nearly identical to the average damping curve that was used for coarse-grained soils when they were treated separately from fine-grained soils. The damping behavior of gravel is very similar to that of sand (Seed et al., 1984).

3.2.4. DYNAMIC SOIL MODELS

There are three broad classes of dynamic soil models:

(1) Equivalent linear models,

(2) Cyclic nonlinear models,

(3) Advanced constitutive models.

Equivalent linear models treat soils as linear visco-elastic materials. Nonlinear behavior is accounted for the use of strain-dependent stiffness and damping parameters. Cyclic nonlinear models represent the nonlinear, inelastic behavior of soils using a nonlinear backbone curve and series of rules that govern unloading-reloading behavior. Advanced constitutive models use basic principles of mechanics to describe soil behavior for general initial stress conditions, a wide variety of stress paths with rotating principal stresses, cyclic or monotonic loading, high or low strain rates, and drained or undrained conditions.

Equivalent linear models are the simplest and most commonly used but have limited ability to represent many aspects of soil behavior under cyclic loading conditions. In this method, a set of shear modulus and damping values are estimated for each soil element. The low-strain values are often used for the initial estimate. The maximum shear strain time history is computed for each element of the model. From these time histories the effective shear strain amplitudes are estimated. Using appropriate material curves, it is checked whether the strain level is compatible with the values of shear strain moduli and damping values. If not, improved values of shear moduli and damping are used for the next iteration. This process is repeated until convergence is attained.

3.3. GROUND RESPONSE ANALYSIS

Site response analysis is done to predict the response of a soil deposit due to earthquake motion. Ideally, a complete ground response analysis should take into account the following factors (Govinda Raju et al., 2004):

- Rupture mechanism at source of an earthquake (source)
- Propagation of stress waves through the crust to the top of bedrock beneath the site of interest (path)
- How ground surface motion is influenced by the soils that lie above the bedrock (site)

In reality, several difficulties arise and uncertainties exist in taking account the above listed factors:

- Mechanism of fault rupture is very complicated and difficult to predict in advance
- Crustal velocity and damping characteristics are generally poorly known
- Nature of energy transmission between the source and site is uncertain.

In professional practice, the following procedures are usually adopted to make the process tractable and overcome the above difficulties:

- Seismic hazard analyses (probabilistic or deterministic) are used to predict bedrock motions at the location of the site.
- Seismic hazard analyses rely on empirical attenuation relationships to predict bedrock motion parameters.
- Ground response problem becomes one of determining responses of soil deposit to the motion of the underlying bedrock.

The sequence of steps to be followed to modify the earthquake motions in the bedrock to account for the effects of soil profile at a site is presented in Figure 3.7.

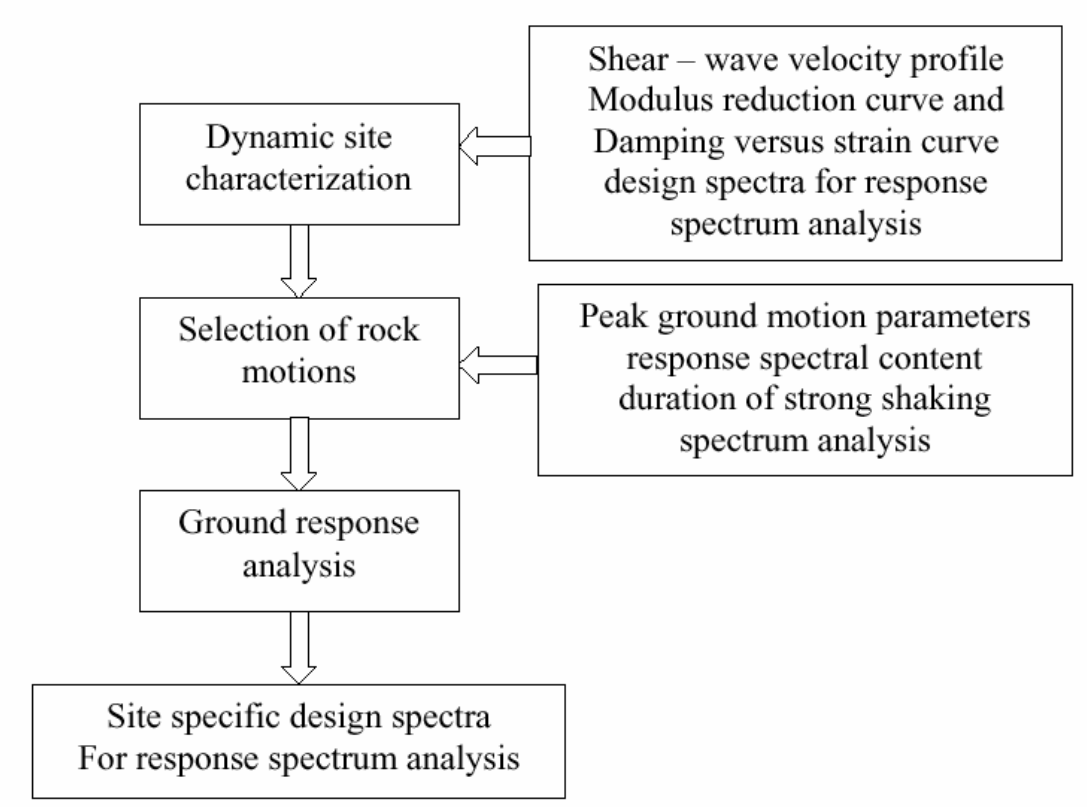

Figure 3.7: Site-specific ground response analyses; Govinda Raju et al. (2004)

As a first step, based on the results of the geophysical as well as geotechnical investigations and laboratory testing, one or more idealized soil profiles must be selected for the site of interest.

As a second step, appropriate base motions (either natural or synthetic acceleration time histories) are selected to represent the design base motion for the site. The base motion should be associated with the specific seismotectonic structures, source areas or provinces that would cause most severe vibratory ground motion or foundation dislocation capable of being produced at the site under currently known tectonic framework. Here

an interaction with a seismologist is required. If natural time histories are used, it is preferable to use a set of natural time histories that have ground motion characteristics similar to those estimated for the design base motions. That means the selected histories should have:

- Peak ground motion parameters
- Response spectral content and
- Duration of strong shaking

In the absence of natural motions, artificial motions can be generated using the concept of spectrum compatible time histories. For this problem several procedures are available such as time domain, frequency domain generation, empirical Green's function technique, etc.

As a third step, ground response analysis is used to predict ground surface motions and to evaluate dynamic stresses and strains. Ground response analysis is usually in the form of one-dimensional. The detail information is given in the following section.

3.3.1. ONE DIMENSIONAL GROUND RESPONSE ANALYSES

The wave propagates from the source in all directions after a fault ruptures. Since the wave propagation velocities of shallower materials are generally lower than the materials beneath them, refraction process produces nearly vertical wave propagation near the ground surface as shown in Figure 3.8. One-dimensional ground response analyses are based on the assumption that all boundaries are horizontal and that the response of a soil deposit is predominantly caused by SH-waves propagating vertically from the underlying rock. Soil layers and bedrock surfaces in the analysis are assumed to be parallel and exceeding infinitely in the horizontal direction. Measured response and calculated response based on these assumptions are in agreement for many cases.

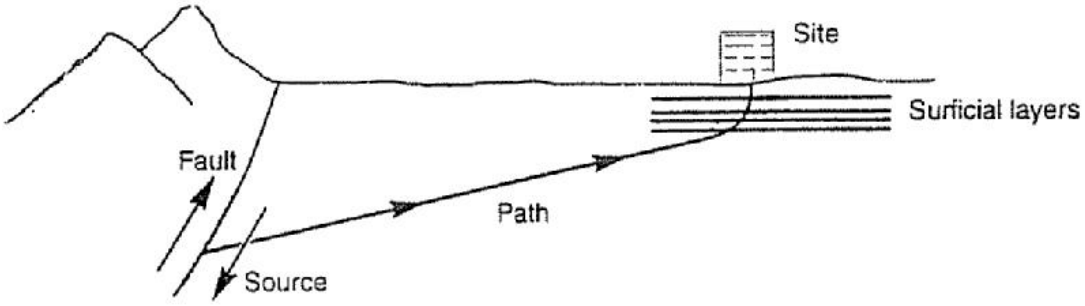

Figure 3.8: Refraction processes that produce nearly vertical wave propagation near the ground surface; Kramer S.L. (1996)

There are two ways for measurement of filtering effect of soil (Roesset, 1970);

1) By considering a steady state harmonic oscillation of the soil and the underlying rock and determining the ratio of the amplitude at bedrock or at the outcropping of rock. This ratio is the transfer Function of the soil, which is a function of the frequency of the motion, and if there is damping a complex function. Its modulus is the amplification function.

2) By considering a given earthquake record at bedrock or at the outcropping of rock and determining the corresponding accelerogram, time history of shear stresses in the soil at different depths which include the effect of the soil.

Justification for using one-dimensional analysis (Govinda Raju et al., 2004);

1) In the areas of strong earthquake motion, the stress waves, from the earthquake focus are propagating nearly vertically when they arrive at the earth's surface. Wave velocity generally decreases

from the earth's interior towards the surface, and hence stress waves from the focus are bent by successive refractions into a nearly vertical path.

2) Even if the waves within the firm ground are propagating in a shallow inclined direction, the waves set up within the soil by refraction at the interface between the firm ground and soil will propagate nearly vertically (by Snell's law of refraction).

3) Vertical ground motions are generally not as important from the standpoint of structural design as horizontal ground motions.

4) Soil properties generally vary more rapidly in the vertical direction than in the horizontal direction.

In reality, a complete ground response analysis must take into account the various factors mentioned before including the additional factors such as rupture mechanism at the origin of earthquake, propagation of seismic waves through the crust to the top of bedrock. These factors are difficult to quantify and hence a complete ground response analysis becomes highly complicated. Therefore, one-dimensional ground response analyses are used extensively due to their simplicity.

A number of techniques are available for one dimensional ground response analyses. The methods differ in the simplifying assumption that are made, in the representation of stress–strain relations of soil and in the methods used to integrate the equation of motion. The development of existing methods of dynamic response analysis has been a gradual evolutionary process stimulated by changing needs of practice and the increasing knowledge about the fundamental behavior of soils under cyclic loading derived from field observations and laboratory testing. The method can be broadly grouped into the following three categories:

- Linear analysis,
- Equivalent linear analysis,
- Nonlinear analysis.

3.3.1.1. LINEAR GROUND RESPONSE ANALYSIS

An important class of techniques for ground response analysis is based on the use of transfer functions. The key to the linear approach is the evaluation of transfer functions. The transfer function determines how each frequency in the bedrock (input) motion is amplified, or de-amplified by the soil deposit. A transfer function may be viewed as a filter that acts upon some input signal to produce an output signal. A known time history of bedrock motion is represented as a Fourier series. Each term in the Fourier series of the bedrock motion is than multiplied by the transfer function to produce the Fourier series of the ground surface motion. The ground surface motion can then be expressed in the time domain using the inverse FFT (Fast Fourier Transform). Thus the transfer function determines how each frequency in the bedrock motion is amplified, or de-amplified, by the soil deposit (Kramer, 1996).

3.3.1.2. EQUIVALENT LINEAR GROUND RESPONSE ANALYSIS

Nonlinear behavior of soil can be modeled by an equivalent-linear characterization of dynamic properties (Seed and Idriss, 1970). The most widely used computer program utilizing this model is SHAKE91 (Idriss and Sun, 1992), which is a modified version of the program SHAKE (Schnabel et al., 1972). The program uses an equivalent-linear, total stress analysis procedure to compute the response of a one-dimensional, horizontally layered visco-elastic system subjected to vertically propagating shear waves. The program uses the exact continuum solution to the wave equation adapted for use with transient motions through the Fast Fourier Transform algorithm.

The equivalent-linear method models the nonlinear variation of soil shear moduli and damping as a function of shear strain. The hysteretic

stress-strain behavior of soils under symmetrical cyclic loading is represented by an equivalent modulus G, corresponding to the secant modulus through the endpoints of the hysteresis loop and equivalent-linear damping ratio β, which is proportional to the energy loss from a single cycle of shear deformation. An iterative procedure, based on linear dynamic analysis, is performed to find the shear moduli and damping ratios corresponding to the computed shear strains. Initial estimates of the shear strains and corresponding estimates of dynamic moduli and damping ratios are provided for the first iteration. For the second and subsequent iterations, moduli and damping ratio values corresponding to an "effective" strain are determined. This "effective" strain is calculated as a fraction of the maximum strain from the previous iteration (Steward et Al., 2001).

An alternative solution to the ground response problem with equivalent-linear material characterization has been developed by Silva and Lee (1987) and Schneider et al. (1993). In this approach, control motions are represented with power spectral density functions instead of time histories. The rock power spectrum is propagated through a one-dimensional soil profile using the plane wave propagators of Silva (1976). Random vibration theory is used to compute probabilistic estimates of peak time-domain values of shear strain or acceleration from the power spectrum. This procedure is coded into the computer program RASCAL (Silva and Lee, 1987).

3.3.1.3. NONLINEAR (ELASTO-PLASTIC) GROUND RESPONSE ANALYSIS

An alternative approach is to analyze the actual nonlinear response of a soil deposit using direct numerical integration in the time domain. By integrating the equation of motion in small time steps, any linear or nonlinear stress-strain model can be used. At the beginning of each time step, the stress-strain relationship is referred to obtain the appropriate soil properties

to be used in that time step. By this method, a nonlinear inelastic stress-strain relationship can be followed in a set of small incrementally linear steps.

Most currently available nonlinear one-dimensional ground response analysis computer programs characterize the stress-strain of the soil by cyclic stress-strain models such as hyperbolic model, modified hyperbolic model, Ramberg-Osgood model, Hardin-Drenevich-Cundall-Pyke model, Martin-Davidenkov model, and Iwan model. CHARSOIL, DESRA-2, DYNAID, MASH, NONLI3, TESS1 are the most commonly used computer programs for nonlinear one-dimensional ground response analysis.

3.3.1.4. COMPARISON OF EQUIVALENT LINEAR AND NON-LINEAR SITE RESPONSE ANALYSES:

- Inherent linearity can lead to spurious resonances in equivalent linear method
- Use of effective shear strain can lead to over damped or under damped system, depending on nature of strain time history
- Equivalent linear analyses can be much more efficient. Nonlinear analyses can be formulated in terms of effective stresses
- Nonlinear analyses can predict permanent deformations
- Nonlinear analyses require reliable stress-strain or constitutive models
- Differences in computed response depend on the degree of nonlinearity in the actual soil response
- For stiff sites and weak input motions, the results of both analyses is quite similar
- For soft sites, liquefiable sites and strong input motions, nonlinear analysis is preferable.

3.3.2. TWO-DIMENSIONAL GROUND RESPONSE ANALYSIS

Two-dimensional dynamic response analyses have been developed for sloping and irregular ground surfaces. The methods of one-dimensional ground response analysis are useful for gently sloping sites with parallel material boundaries. Problems in which one dimensional is considerably greater than others can be treated as two-dimensional plane-strain problems. Frequency-domain methods and time domain methods can be used for the solutions of such problems.

3.3.2.1. DYNAMIC FINITE ELEMENT ANALYSIS

The finite element method treats a continuum as an assemblage of discrete elements whose boundaries are defined by nodal points, and assumes that the response of the continuum can be described by the response of the nodal points. Elements are composed of nodes. The displacement of the soil at any point within an element, $\{v\}^T = \{uv\}$, is expressed in terms of the nodal point displacements,

$$\{q\}^T = \{u_1 u_2 u_3 u_4 v_1 v_2 v_3 v_4\}, \text{ by } \{v\} = [N]\{q\} \tag{3.4}$$

where *[N]* is matrix of shape functions. The strain-displacement matrix, *[B]*, allows the strains to be determined from the nodal point displacements

$$\{\varepsilon\} = [B]\{q\} \tag{3.5}$$

and the stress-strain matrix, *[D]*, relates stresses to strains:

$$\{\sigma\} = [D]\{\varepsilon\} \tag{3.6}$$

Defining a local coordinate system, (s, t) that maps the quadrilateral elements into squares as shown in Figure 3.9 and using the strain-displacement and stress-strain relationship, an element stiffness matrix can be written as

$$[k_e] = \int_{-1}^{1}\int_{-1}^{1} [B]^T [D][B]|J|\,ds\,dt \tag{3.7}$$

where the Jacobian;

$$|J| = \sum_{i=1}^{4}\sum_{j=1}^{4} x_i \left(\frac{\partial N_i}{\partial s}\frac{\partial N_j}{\partial t} - \frac{\partial N_i}{\partial t}\frac{\partial N_j}{\partial s}\right) y_j \tag{3.8}$$

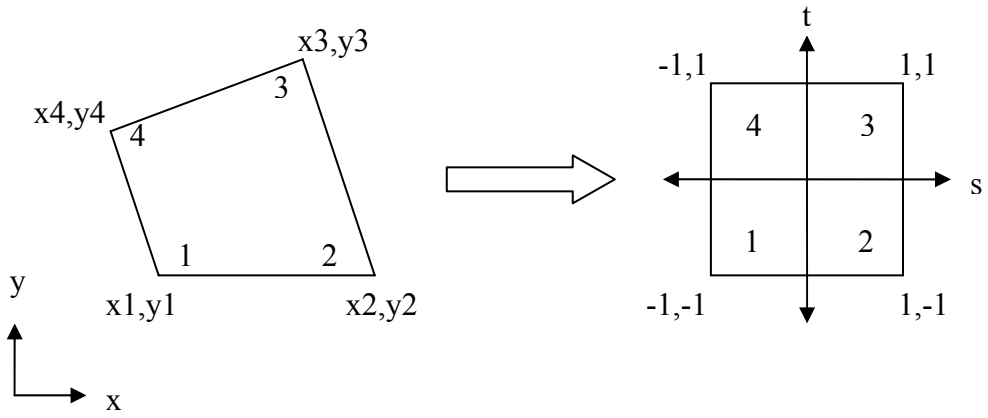

Figure 3.9: Mapping of quadrilateral element from irregular shape in x-y coordinate system to square shape in s-t coordinate system; Kramer S.L. (1996)

For mass matrix, three ways can be used for the construction of it. In a lumped-element mass matrix, the mass of the element is concentrated at the nodal points and in a consistent element mass matrix, constant density within the element is used. Experience has shown that use of the consistent element matrix tends to overestimate the natural frequencies of a system and the lumped mass matrix tends to underestimate them. Lysmer et al. (1974) suggested the use of a mixed element mass matrix, which is the average of the consistent and lumped mass matrices (Kramer S.L., 1996).

A consistent element mass matrix can be written, assuming constant density within the element as

$$[m_e] = \rho \int_{-1}^{1}\int_{-1}^{1} [N]^T [N] |J| \, ds \, dt \tag{3.9}$$

Damping matrices can be troublesome because of the implications of various formulations on the frequency dependence of damping. For nonlinear ground response analyses, however, damping results primarily from the hysteretic behavior of the soil and is therefore accounted for by variations in the stiffness matrix under cyclic loading conditions. Some small amount of viscous damping may be included in a two-dimensional ground response analysis to account for damping at very small strains and to minimize numerical problems that can arise in the complete absence of damping. A consistent damping matrix can be obtained from

$$[c_e] = \rho \int_{-1}^{1}\int_{-1}^{1} [B]^T [\eta][B] |J| ds dt \tag{3.10}$$

where $[\eta]$ is a matrix of damping terms.

The equations of motion for the element can then be written as

$$[m_e]\{\ddot{q}\} + [c_e]\{\dot{q}\} + [k_e]\{q\} = \{Q(t)\} \tag{3.11}$$

where the elementary force vector is given by

$$\{Q(t)\} = \int_{-1}^{1}\int_{-1}^{1} [N]^T \{W\}|J|dsdt + \int_{s} [N]^T \{T\}dS \tag{3.12}$$

And {*W*} is the vector of prescribed body forces and {*T*} is a vector of external tractions that may be applied to some surface, S.

Once the equations of motion for each element are obtained, they are combined in a way that satisfies compatibility of displacements to obtain the global equations of motion

$$[M]\{\ddot{u}\} + [C]\{\dot{u}\} + [K]\{u\} = \{R(t)\} \tag{3.13}$$

where;

[*M*] = Global mass matrix

[*C*] = Global damping matrix

[*K*] = Global stiffness matrix

{*u*} = Global nodal point displacement vector

[*R(t)*] = Global nodal point force vector.

For the case loading induced by base motion, the global equation of motion is;

$$[M]\{\ddot{u}\} + [C]\{\dot{u}\} + [K]\{u\} = -[M][1]\ddot{u}_b\ (t) \qquad (3.14)$$

The maximum dimensions of any element should be limited to one-eight (Kuhlemeyer and Lysmer, 1973) to one-fifth (Lysmer et al., 1975) of the shortest wavelength for the mesh size (Kramer S.L., 1996).

The most commonly used boundaries can be divided into three groups. Conditions of zero displacement or zero stress are specified at elementary boundaries. These boundaries can be used to model the ground surface accurately as a free boundary. The viscous dashpots can be used for the local boundary to simulate a semi-infinite region for the case of normally incident body waves. Boundaries that can absorb all types of body waves and surface waves at all angles of incidence and all frequencies are called consistent boundaries.

3.3.2.2. EQUIVALENT LINEAR APPROACH

A soil-structure system is represented by a two-dimensional approach. The input motion is represented by a Fourier series and the equations of motions are solved for each frequency of the series with the results summed to obtain the total response (Kramer, 1996).

For the equivalent linear approach, the mass and the stiffness matrices are assembled from the corresponding element stiffness matrices using standard finite element procedures and damping is introduced into the analysis through the use of complex shear moduli when forming the complex element stiffness matrix.

In this approach the primary computational effort is associated with the evaluation of the transfer functions. For large problems the mass and stiffness matrices are large, and evaluation of the transfer functions can be quite time consuming. For computational efficiency, the transfer functions are often evaluated at only a limited number of frequencies, with values at intermediate frequencies obtained by interpolation (Lysmer et al., 1975). Iteration toward strain compatible material properties can be incorporated on an element-by-element basis. FLUSH (Lysmer et al., 1975), QUAD4M (Hudson et al., 1994), GROUND2D (Deng et al., 1995) are the most commonly used computer programs for equivalent linear two-dimensional ground response analysis (Kramer S.L., 1996).

3.3.2.3. NONLINEAR APPROACH

Two-dimensional nonlinear dynamic response analyses are performed by writing the global equations of motion from a finite element idealization in incremental form and then integrating them in the time domain. Such analyses can be divided into two main groups according to manner in which the soil behavior is represented. One group uses cyclic nonlinear stress-strain models and the other uses advanced constitutive models. The accuracy of the analyses depends on the accuracy of the constitutive models (Kramer, 1996).

Two-dimensional nonlinear methods have the beneficial capability of computing pore pressures and permanent deformations. TARA-3 (Finn et al., 1986), DYNAFLOW (Prevost, 1981), DIANA (Kawai, 1985) are the most commonly used softwares for nonlinear two-dimensional ground response analysis (Kramer S.L., 1996).

3.3.2.4. OTHER APPROACHES TO TWO-DIMENSIONAL DYNAMIC RESPONSE PROBLEMS

One of the earliest approach to the dynamic analysis of two-dimensional systems is the shear beam analysis. The shear beam approach is based on the assumption that a dam deforms in simple shear, in other words, they restrict particle movement to the horizontal plane.

The layered inelastic shear beam (Stara-Gazetas, 1986) combines the shear beam approach with a one-dimensional nonlinear ground response analysis (Kramer S.L., 1996).

Other approach includes the simplified nonlinear method of Dakoulas (1985) and the nonlinear hysteretic method of Elgamel et al. (1985) (Kramer S.L., 1996).

3.3.3. THREE-DIMENSIONAL DYNAMIC RESPONSE ANALYSIS

When soil conditions and problem boundaries vary three-dimensionally, three-dimensional dynamic response analyses are necessary.

Three-dimensional dynamic response problems are treated in much the same way as two-dimensional problems. Dynamic finite-element analyses are available, using both equivalent linear and non-linear approaches. A number of three-dimensional analyses have been developed with an emphasis on soil-structure interaction problems (Kramer S.L., 1996).

3.3.3.1. EQUIVALENT LINEAR FINITE ELEMENT APPROACH

Three-dimensional finite elements, in general, have more nodal points, which mean more degrees of freedom than corresponding two-dimensional elements. But the basic process of element mass, damping, and stiffness

formulation, and assembly into global equations of motion, is identical. As a summary:

- Discretize domain into mesh (grid) of elements
- Assume behavior of continuum can be represented by behavior of finite number of points
- Require constitutive models
- Time-consuming analyses

TLUSH (Kawaga et al., 1981), SASSI (Lysmer et al., 1981), CLASSI (Luco and Wong, 1982), and HASSI (Katayama et al., 1991) are the most commonly used computer programs for equivalent linear three-dimensional ground response analysis (Kramer S.L., 1996).

3.3.3.2. NON-LINEAR FINITE ELEMENT APPROACH

Three dimensional nonlinear ground response analyses are extensions of their two dimensional counterparts. DYNAFLOW (Prevost, 1981), TRANL (Baylor et al., 1974), FLEX (Vaughan, 1983) are some of the programs that can be used in non-linear finite element approach (Kramer S.L., 1996).

3.3.3.3. SHEAR BEAM APPROACH

Shear Beam type solution is used especially for earth dams and embankments. There are some assumptions related with this approach:

- Assume lateral deformations due to shearing only
- Assume linear stress-strain behavior
- No strain on horizontal planes

Hatanaka (1952) and Ambraseys (1960) developed shear-beam type solutions for earth dams in rectangular canyons of different width/height ratios. Dakoulas and Gazetas (1986) developed a closed-form solution for a homogeneous earth dam (Kramer S.L., 1996).

3.3.4. SHAKE91

SHAKE91 is a computer program for conducting equivalent linear seismic response analyses of horizontally layered soil deposits. The analysis is done in the frequency domain, and therefore, for any set of properties it is a linear analysis.

The object motion can be specified at the top of any sub layer within the soil profile or at the corresponding outcrop.

An equivalent linear procedure (Idriss and Seed, 1968; Seed and Idriss, 1970) is used to account for the nonlinearity of the soil using an iterative procedure to obtain values for modulus and damping that are compatible with the equivalent uniform strain induced in each sub layer.

The soil profile is idealized as a system of homogeneous, visco-elastic sub layers of infinite horizontal extent as shown in Figure 3.10. The response of this system is calculated considering vertically propagating shear waves.

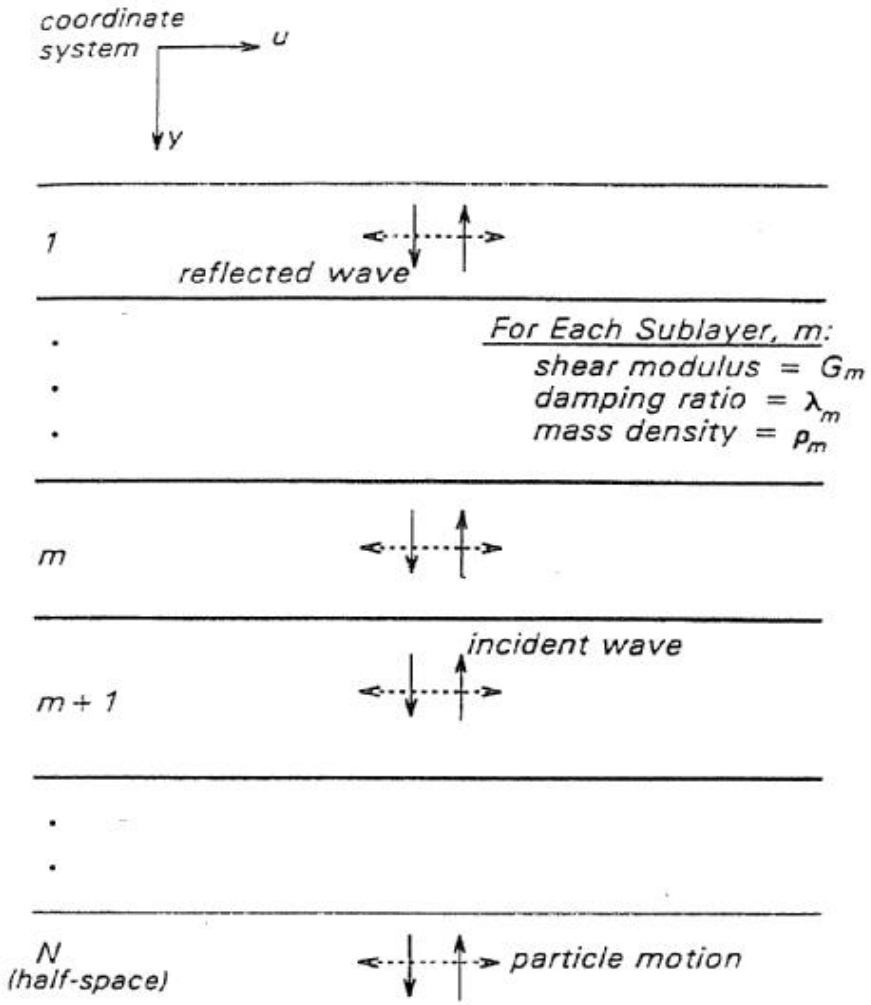

Figure 3.10: One-dimensional idealization of a horizontally layered soil deposit over a uniform half-space; Idriss and Sun (1992)

The following assumptions are incorporated in the analysis (Schnabel et al, 1972):

(1) Each sub layer, m, is completely defined by its shear modulus, G_m, damping ratio, λ_m, total unit weight, γ_{tm} (or corresponding mass density) and thickness, h_m; these properties are independent of frequency.

(2) The responses in the soil profile are caused by the upward propagation of shear waves from the underlying rock half-space.

(3) The shear waves are specified as acceleration ordinates at equally spaced time intervals.

(4) The strain dependence of the shear modulus and damping in each sub layer is accounted for by an equivalent linear procedure based on an equivalent uniform strain computed in that sub layer. The ratio of this uniform shear strain divided by the calculated maximum strain is specified by the user; the same value of this ratio is used for all sub layers.

3.3.5. QUAD4M

QUAD4M is a computer program to evaluate the seismic response of soil structures using finite element procedures and incorporating a compliant base. It was written as a modification of QUAD4.

QUAD4 was written by Idriss, Lysmer, Hwang and Seed (1973) as two-dimensional time domain solution to dynamic soil response. It incorporated for the first time independent damping in each element in the continuum.

QUAD4M incorporates into QUAD4 a transmitting base so that the half-space beneath a mesh can be modeled and the need to assume a rigid foundation can be eliminated. The shear and compression wave velocities and the unit weight for the material underlying the mesh can be entered, and the response of the mesh on top of that half-space can be modeled with greater accuracy.

In order for a two-dimensional finite mesh to represent the response of an infinite field condition, the artificial reflection of seismic waves from side boundaries, as well as from the underlying half-space, should be minimized. Lysmer and Kuhlemeyer (1969) introduced a simple procedure to accomplish this. They suggested the use of dampers as illustrated in Figure 3.11 for the case of a vibrating footing. In the case of a soil mass subjected to earthquake

vibrations, the implementation of a compliant base in QUAD4M is the same as the Lysmer and Kuhlemer scheme.

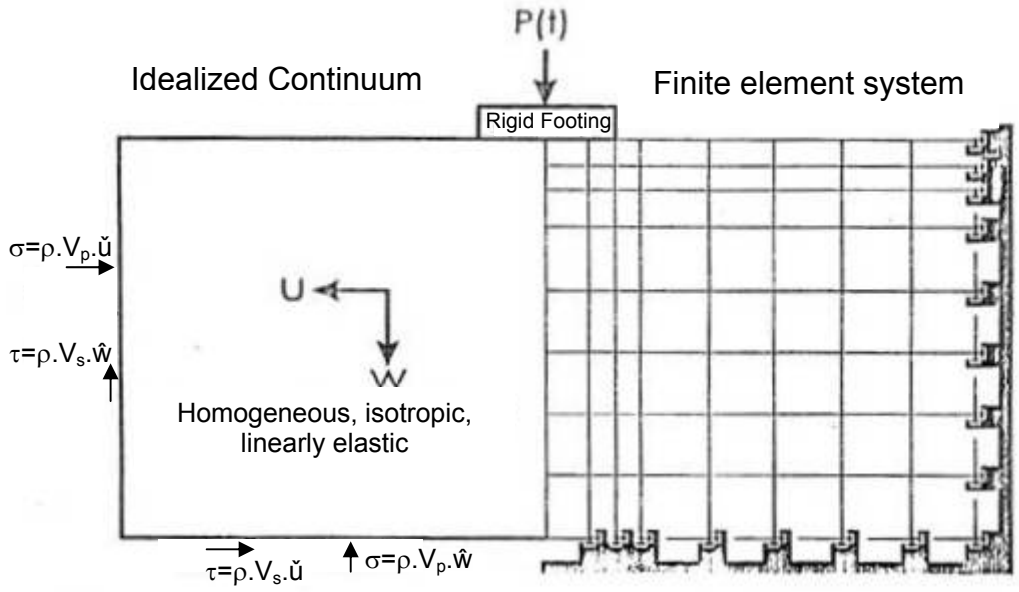

Figure 3.11: Finite models for dooting on half space; Lysmer and Kuhlemeyer (1969)

The implementation of these dampers involves adding damping at each of the nodes that make up the base and sides of the finite model.

For the formulation of the damping matrices, Rayleigh damping formulation is used. As is the case with all procedures that utilize a Rayleigh Damping formulation, the higher frequencies are over damped. Specifying the predominant period of the input motion obtained from the response spectrum controls the damping scheme.

In addition, seismic coefficients have been added in this version of the program. This feature is particularly useful in deformation analyses. A seismic coefficient is the ratio of the force induced by an earthquake in a block of the mesh, over the weight of that block.

The forces acting on the block are computed by multiplying the shear and normal stresses acting on an element by the width of that element.

An equivalent linear procedure (Seed and Idriss, 1970) is used in the program to account the nonlinearity of the soil using the iterative procedure.

The finite element procedure uses a system of equations represented in matrix form as:

$$[M]\,\underline{\ddot{u}} + [C]\,\underline{\dot{u}} + [K]\,\underline{u} = \underline{R} \qquad (3.15)$$

where;

[*M*] = Mass matrix (assumption of lumped mass formulation)

[*C*] = Damping matrix

[*K*] = Stiffness matrix,

$\underline{R}$ = Load vector which is given by:

$$\underline{R} = [M]\,\underline{\ddot{u}}_g \qquad (3.16)$$

$\underline{\ddot{u}}$ is the relative displacement vector and $\underline{\ddot{u}}_g$ is the outcrop acceleration.

The Newmark family of methods as Hughes (1987) and the Trapezoidal rule are used to solve the equation.

CHAPTER 4

A STUDY ON THE EFFECT OF THE RESPONSE OF SOIL DEPOSITS

4.1. INTRODUCTION

Effects of basin edge slope on the dynamic response of horizontal soil deposits are investigated by using one-dimensional and two-dimensional numerical analyses which incorporate the non-linear stress strain behavior of soils by equivalent linear method. SHAKE91 software is used to analyze one-dimensional response and a finite-element computer code QUAD4M is employed for two-dimensional response evaluation. For the analyses, 24 basin models having trapezoidal cross section are conceived to represent different geometries (i.e. depth of basin, slope of basin edge). A relatively "soft" and a "stiff" soil profile are used to identify the effect of the soil type on the response. Harmonic base excitations with different periods are used in the analyses, with a maximum acceleration of 0.15g. Recorded acceleration time histories for 1 October, 1995 Dinar EQ and 2 May, 1983 Coalinga EQ are used as well. The detailed information and the obtained results are given in the following sections.

4.2. OVERVIEW OF BASIN EDGE MODELS

The subject model is a valley of trapezoidal cross-section with different dimensions, from wide and shallow to narrow and deep, along with different slopes of rock boundary. In order to assess the effects of basin edge slope

on dynamic soil response, 24 different models are considered. In these models, the soil continuum is assumed to consist of horizontal layers, each of which is homogeneous and isotropic. Relatively soft and stiff soil profiles are considered in the models in order to identify the effect of soil type on the response. Both recorded strong motions and harmonic base motions are used. The utilized harmonic base motions are synthetic with sinusoidal shape and have periods ranging from 0.12sec to 1.00sec with a maximum acceleration of 0.15g.

4.2.1 GEOMETRY OF THE MODEL

The trapezoidal geometry of the general model is presented in Figure 4.1 and related dimensions of each model are given in Table 4.1. Mainly there are three groups with basin depths (H) of 40m, 80m and 120m respectively. For each group the basin edge slope is varying between 9 and 76 degrees.

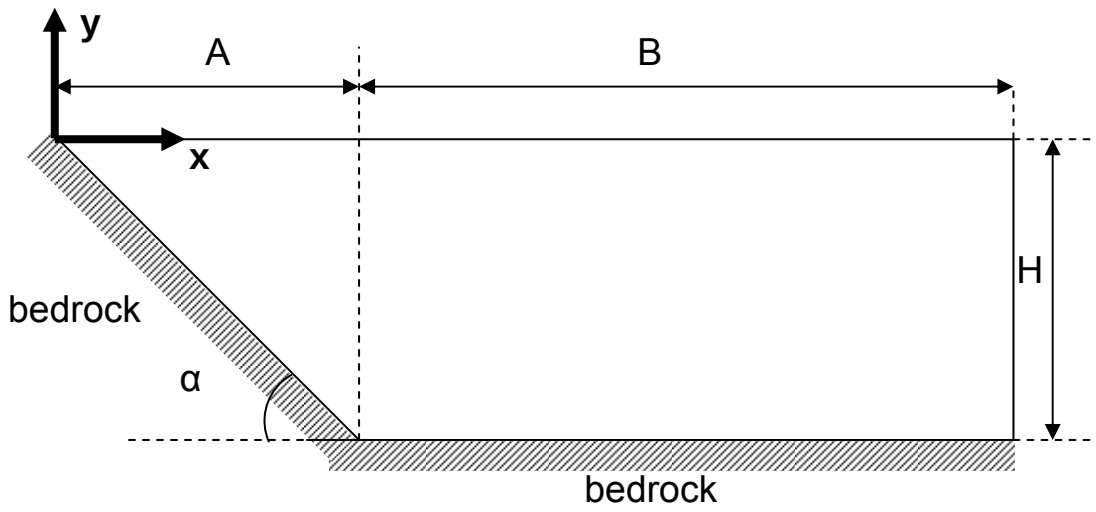

Figure 4.1: Geometric parameters of the trapezoidal models

Table 4.1: Geometric dimensions of models.

MODEL NO	α (degree)	A (m)	B (m)	H (m)
1	76	30	500	120
2	63	60	500	
3	53	90	500	
4	45	120	500	
5	34	180	500	
6	27	240	500	
7	14	480	500	
8	9	720	500	
9	76	20	500	80
10	63	40	500	
11	53	60	500	
12	45	80	500	
13	34	120	500	
14	27	160	500	
15	14	320	500	
16	9	480	500	
17	76	10	500	40
18	63	20	500	
19	53	30	500	
20	45	40	500	
21	34	60	500	
22	27	80	500	
23	14	160	500	
24	9	240	500	

4.2.2 INPUT SOIL PROPERTIES

Soil type for the basin is selected as clay. A relatively “soft” and a “stiff” clay profile were considered in the models to represent the effect of soil stiffness on the dynamic response. Figure 4.2 depicts the shear modulus at low strains (γ < 10-4 %) assumed for relatively soft and stiff clay profiles.

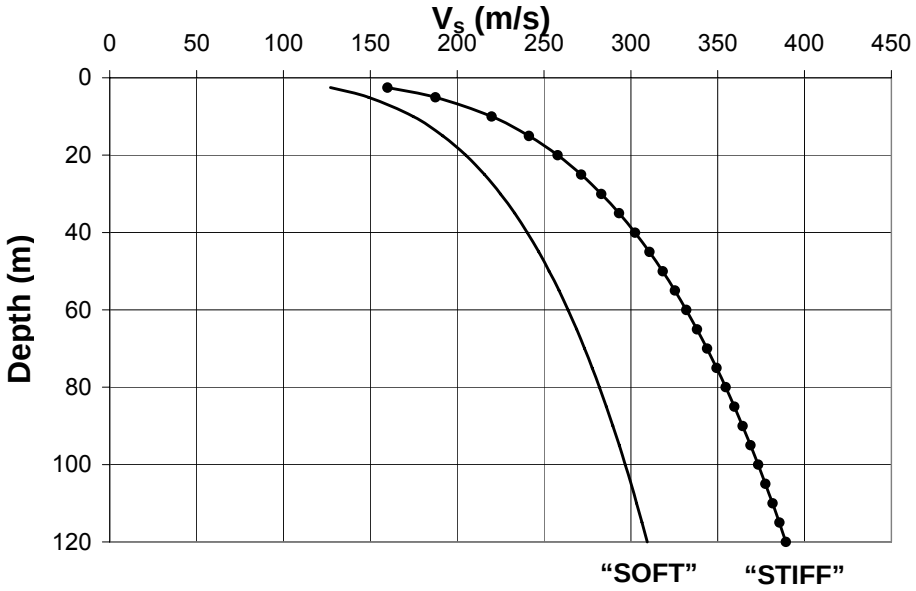

Figure 4.2: Shear wave velocity versus depth for relatively soft and stiff soil profile

The small strain dynamic shear modulus, G_{max}, can be expressed as a function of shear wave velocity, V_s, total unit weight of soil, γ, and gravitational acceleration, g, by manipulating Equation 4.1, as

$$G_{max} = V_s^2 . \gamma/g \qquad (4.1)$$

For the basin the total unit weight is taken as 20kN/m^3. Figure 4.3 shows the variation of maximum shear modulus with depth.

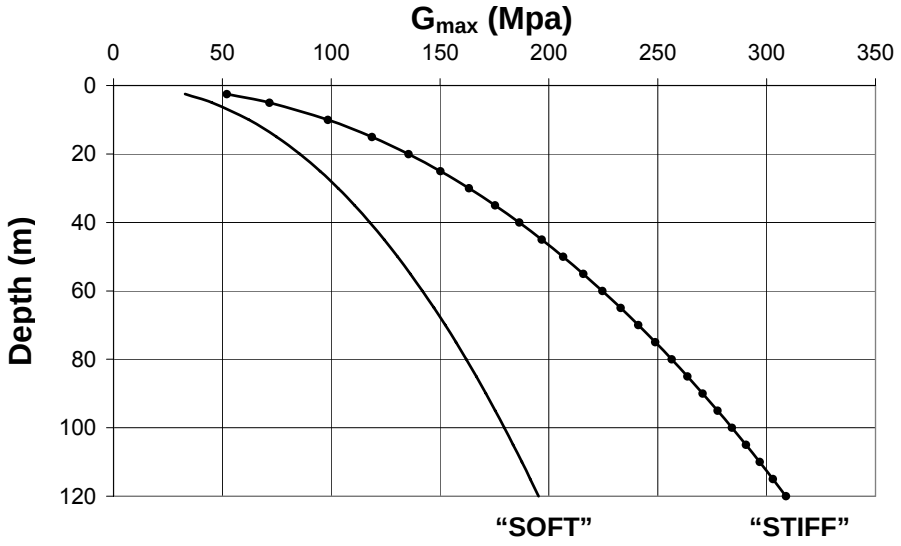

Figure 4.3: G_{max} versus depth for relatively soft and stiff soil profile

For clay type of soil, the modulus degradation curve by Idriss (1990) and Seed and Sun (1989) together with the damping curve proposed by Idriss (1990) is used as shown in Figure 4.4.

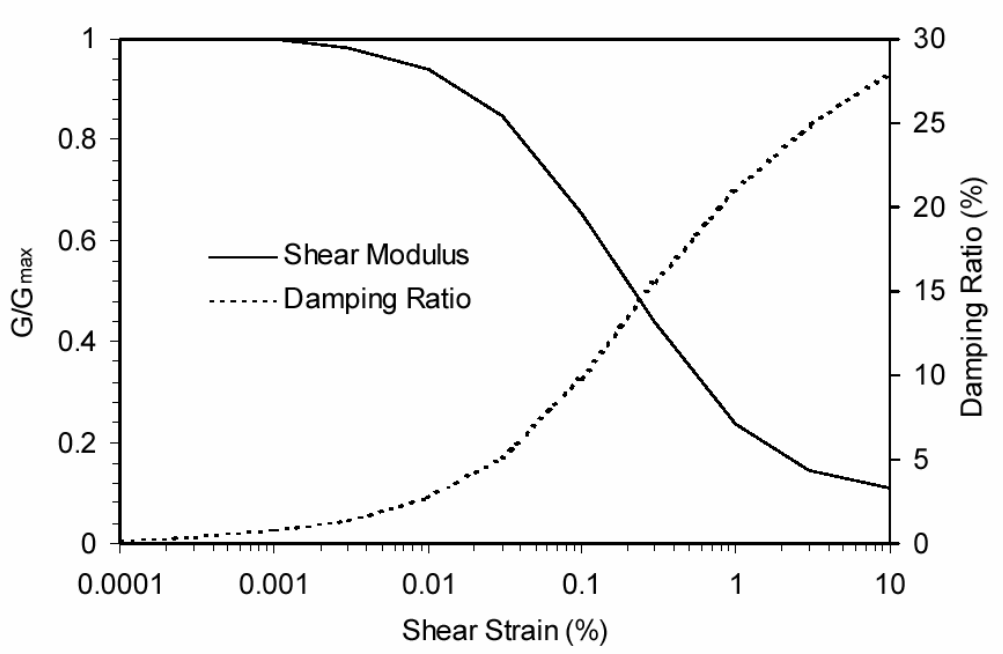

Figure 4.4: Modulus reduction and damping ratio curves

The unit weight, Poisson's ratio, small strain values of shear modulus and damping ratio are the required material property data to be specified for each element in QUAD4M. Their values are presented in Appendix A.

4.2.3 SELECTED INPUT MOTIONS

Two types of base motions are used in the analyses. The first type consists of sinusoidal base motions with predominant periods varying between 0.12sec and 1.00sec with a maximum acceleration of 0.15g. The second type consists of recorded strong motions of 1 October, 1995 Dinar and 2 May, 1983 Coalinga Earthquakes. The characteristic information for recorded and generated harmonic base motions is given in Table 4.2.

Table 4.2: Characteristic information for base motions.

BASE MOTION	PGA (g)	Predominant Period T_p (s)	Mean Period Tm (s)	Duration t (s)	Δt (s)	# data points
DINAR	0.1435	0.25	0.34	28	0.01	2800
COALINGA	0.3300	0.14	0.21	16	0.005	3200
S_012	0.1500	0.12	0.12	20	0.01	2000
S_032	0.1500	0.32	0.32	20	0.01	2000
S_052	0.1500	0.52	0.52	20	0.01	2000
S_072	0.1500	0.72	0.72	20	0.01	2000
S_100	0.1500	1.00	1.00	20	0.01	2000

4.2.3.1 HARMONIC BASE MOTION

Simple harmonic motion can be characterized by sinusoidal motion at constant frequency. The most important features can be defined by three components: amplitude, frequency and phase shown in Figure 4.5.

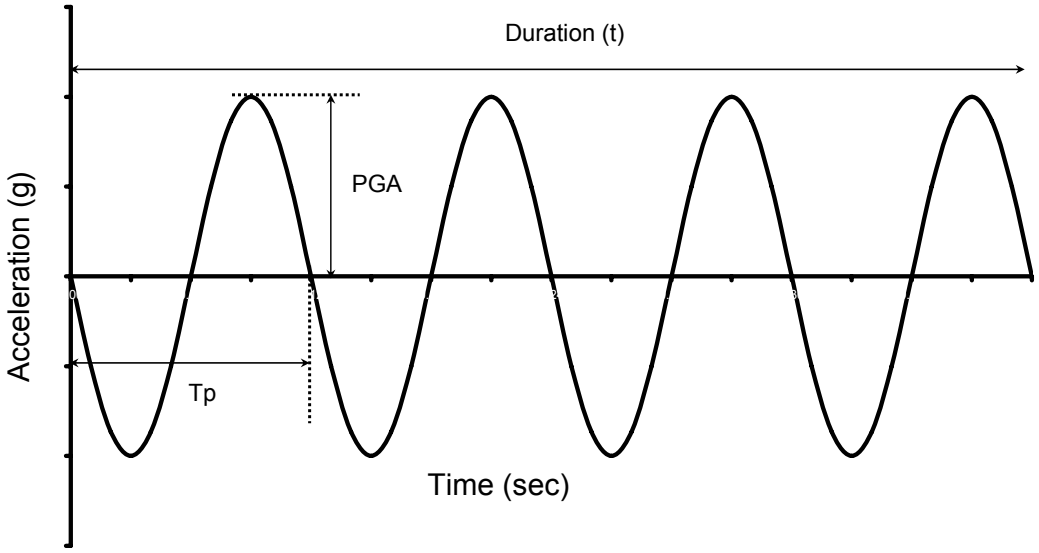

Figure 4.5: Harmonic base motion characteristics

4.2.3.2 RECORDED STRONG MOTION

On October 1, 1995 the main shock record obtained at Dinar Meteorology Station indicated a horizontal peak ground acceleration (PGA) of 0.275 g in the north-south direction, 0.294 g in the east-west direction and 0.111 g in the vertical direction. The duration of strong shaking was around 25sec. The acceleration time history and acceleration response spectra for the horizontal components calculated for 5% damping of Dinar Earthquake (Mw=6.0, USGS) are given in the Figure 4.6 (a) and (b) respectively.

Reference base motion used in the analyses was obtained by deconvolution of the recorded horizontal accelerograms to the assumed bedrock depth of 100m. The obtained acceleration time history and acceleration response spectrum after deconvolution are given in the Figure 4.6 (c) and (d) respectively.

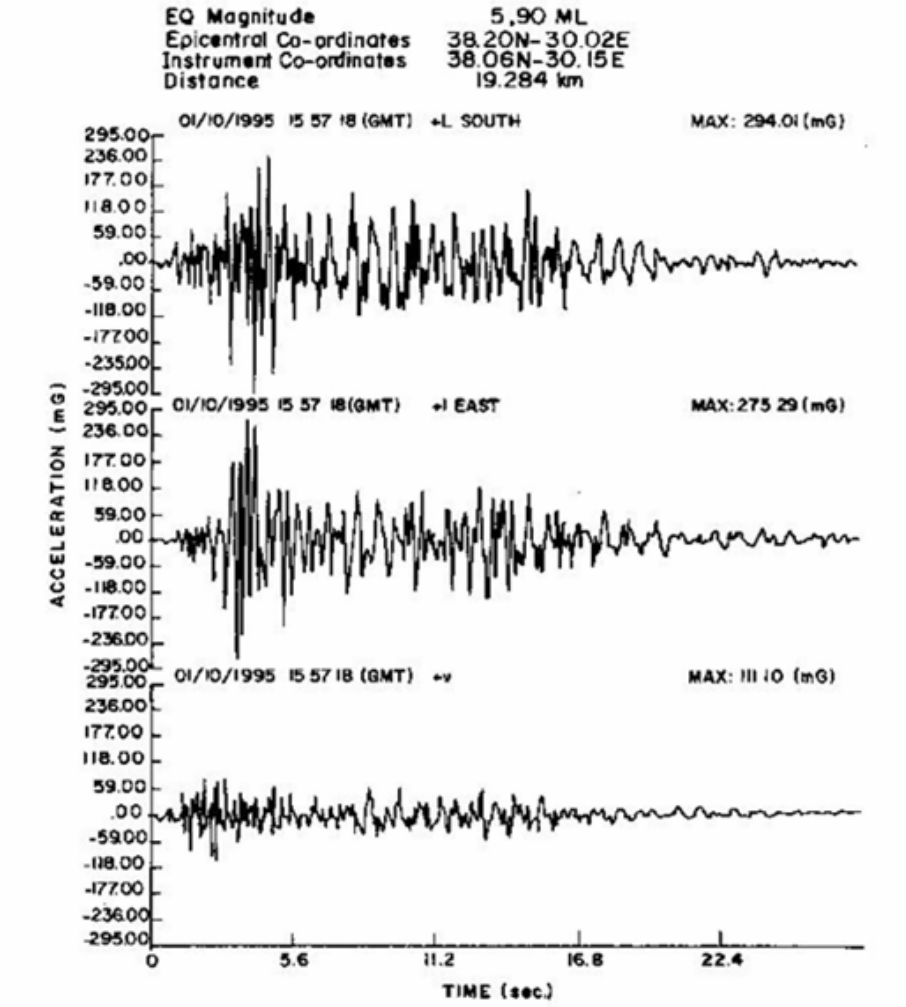

(a)

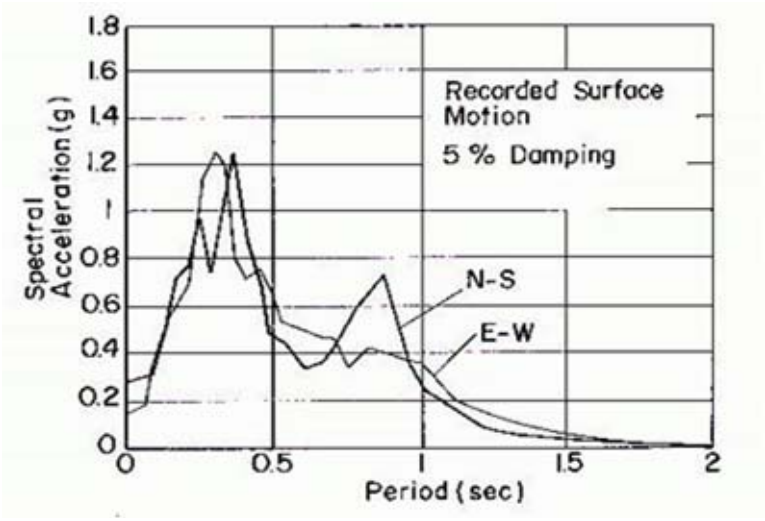

(b)

Figure 4.6: Characteristics of Dinar Earthquake

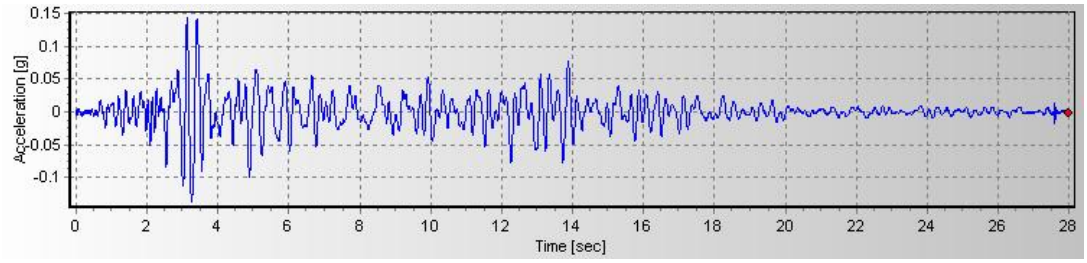

(c)

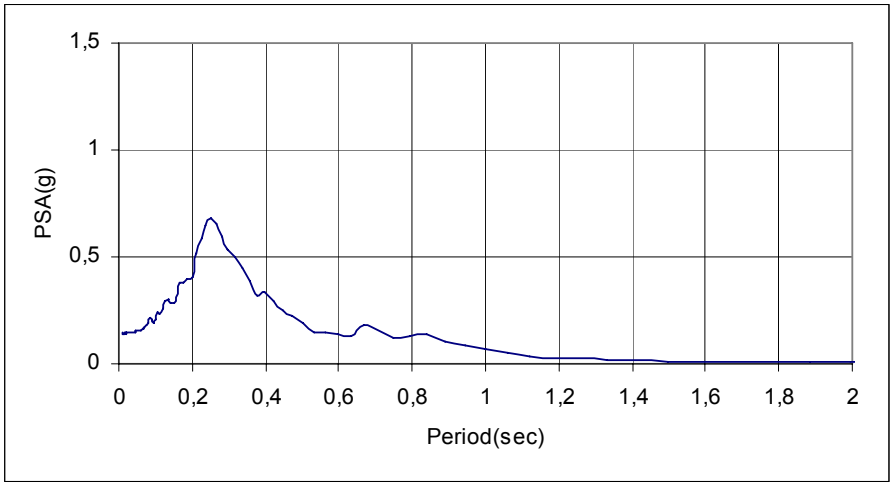

(d)

Figure 4.6: (continued)

On Monday, May 2, 1983, at 4:42 p.m., an earthquake of moderate magnitude struck the rural oil and farming community of Coalinga in the San Joaquin Valley, California. The magnitude of the earthquake was measured as 6.5 on the Richter scale and the epicenter was approximately nine miles north-northeast of Coalinga. The causative fault type is near-surface strike-slip along the San Andreas Fault. This earthquake destroyed over 800 homes and other buildings, and was felt as far away as Los Angeles and western Nevada. The acceleration time history and acceleration response spectrum are given in the Figure 4.7 (a) and (b) respectively.

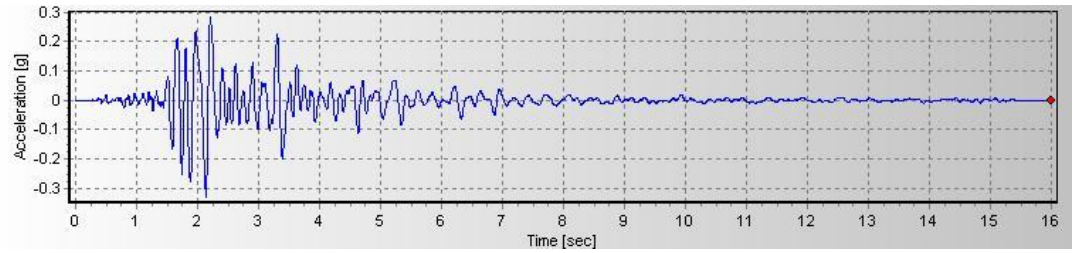

(a)

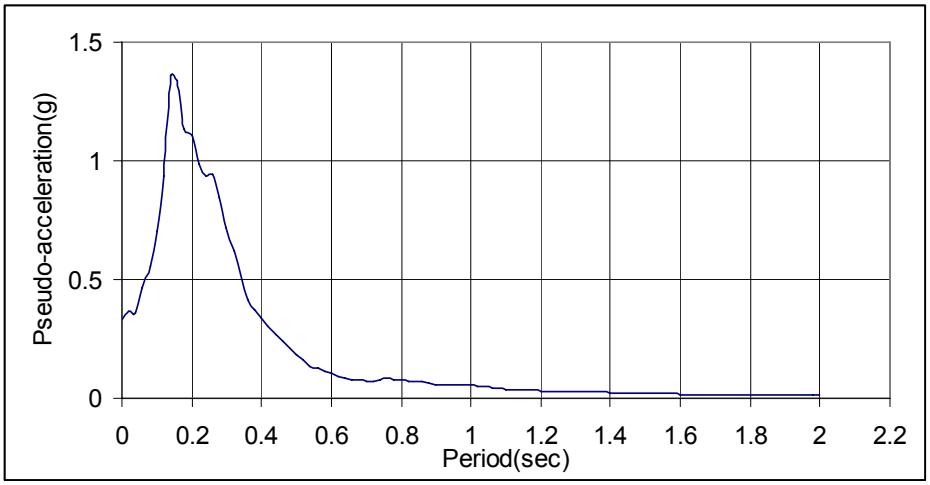

(b)

Figure 4.7: Characteristics of Coalinga Earthquake

4.3. SEISMIC RESPONSE ANALYSES OF SELECTED SOIL PROFILES

Dynamic response of soil deposits are obtained by one-dimensional and two-dimensional numerical analyses which incorporate the non-linear stress strain behavior of soils by equivalent linear method. SHAKE91 software is used to evaluate one-dimensional response and a finite-element computer code QUAD4M is employed for two-dimensional response evaluation. Equivalent Linear Method accounts for the nonlinearity of the soil using an iterative procedure to obtain values for modulus and damping that are compatible with the equivalent uniform strain induced in each sub layer. The input parameters of Finite Element Models, methods of analyses and obtained results are discussed in the following sections.

4.4. FINITE ELEMENT MODEL

Soil is modeled as solid elements that are isoparametric four-node quadrilateral and three-node triangular constant strain elements as shown in Figure 4.8. The lateral boundary of the models beyond the slope of bedrock is established so as to detect the extent and variation of the effect of buried topography on the base motion. The bedrock is assumed to be infinitely rigid and the input motion is uniform and in phase on the whole sediment/bedrock interface. For the vertical boundary on the alluvial plain, nodal points are constrained in such a way that they can move in the horizontal direction only.

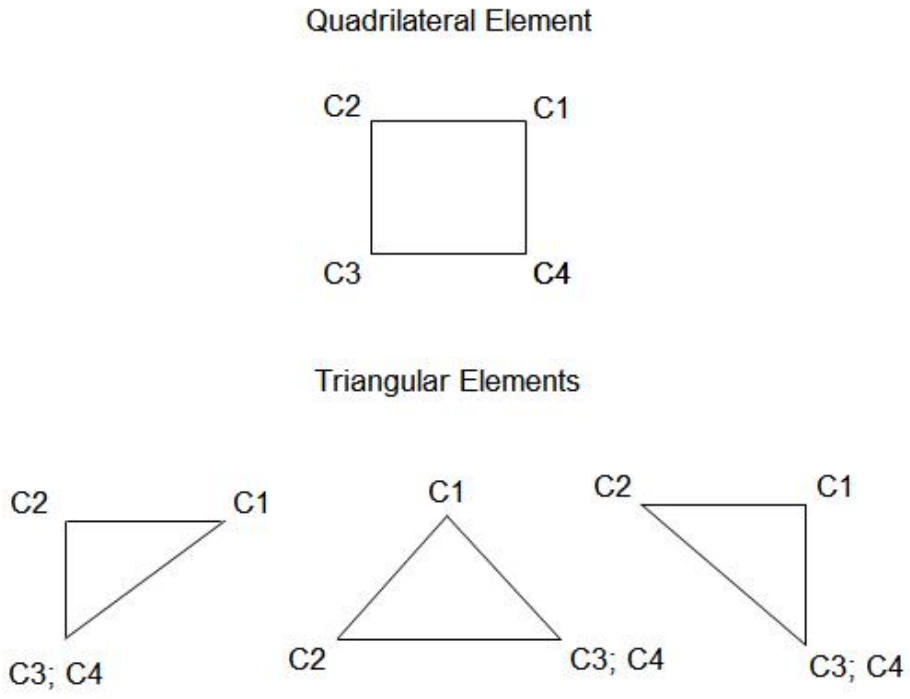

Figure 4.8: Strain Elements

To assess convenient dimensions of the strain elements, series of runs are performed on the representative trapezoidal geometry using QUAD4M with harmonic base motions having predominant periods of Tp = 1sec, 0.73sec, 0.5sec, 0.3sec, 0.2sec and 0.1sec. Model 24 with a basin

edge slope of 9^o and a basin depth of 40m is used as shown in Figure 4.9. The aspect ratio defined as the ratio of vertical dimension of the strain element (D_v) to horizontal dimension (D_h) is kept lower than 1.5. Three different mesh sizes are evaluated to understand the effect of mesh size on the response as;

(1) "coarse mesh" with dimensions of D_h=7.5m and D_v=5m

(2) "2X fine mesh", a medium size mesh with dimensions of D_h=3.75m and D_v=2.5m

(3) "4X fine mesh", a finer mesh with dimensions of D_h=1.875m and D_v=1.25m

The peak ground acceleration, PGA, versus horizontal distance values are plotted as shown in Figure 4.10 (a), (b), (c), (d), (e), and (f). It is seen that "2X fine mesh" and "4X fine mesh" yield very close results, whereas "coarse mesh" give relatively lower PGA values. Thus, it is concluded that 2X fine mesh (D_h=3.75m and D_v=2.5m with an aspect ratio < 1.5) is fine enough and can be used throughout the study.

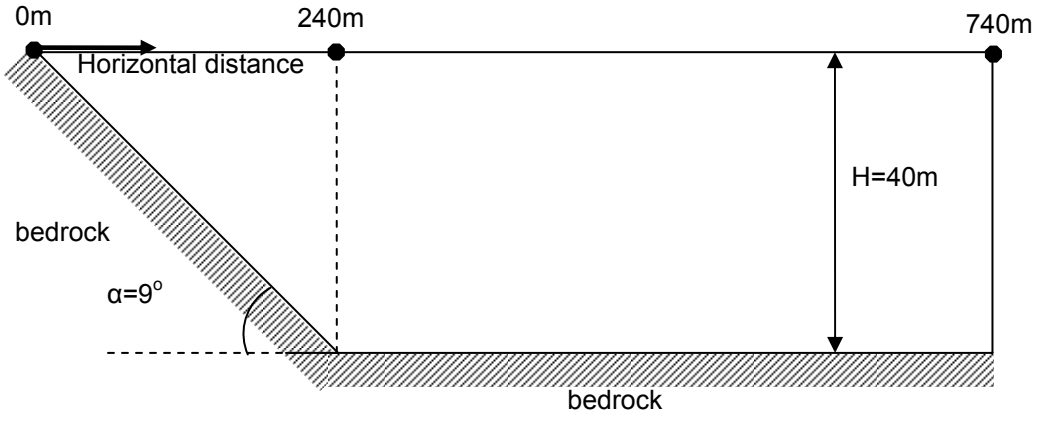

Figure 4.9: Model 24 geometry

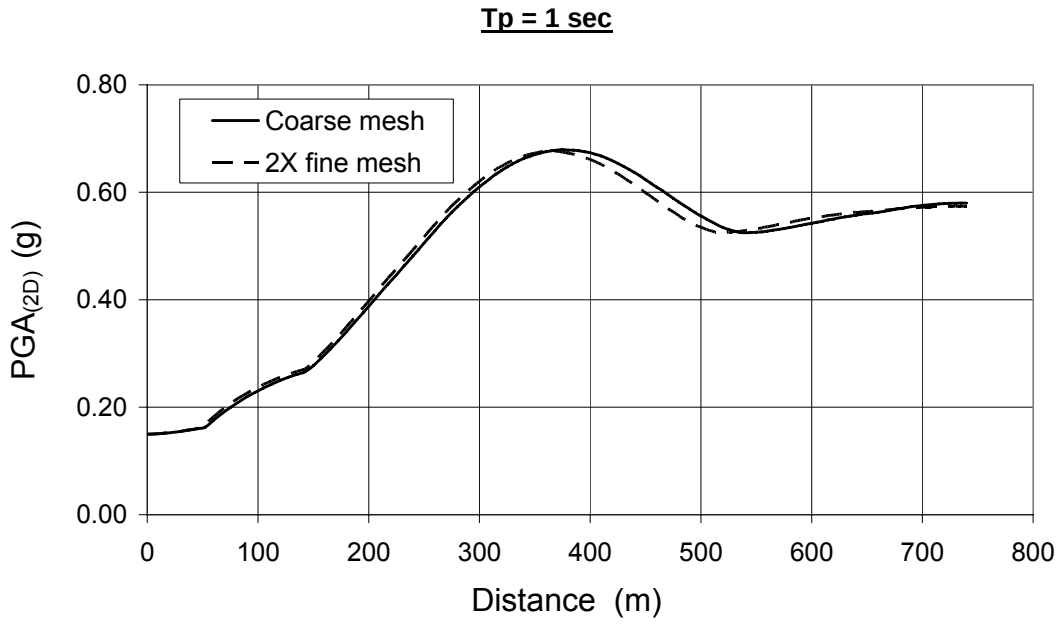

(a)

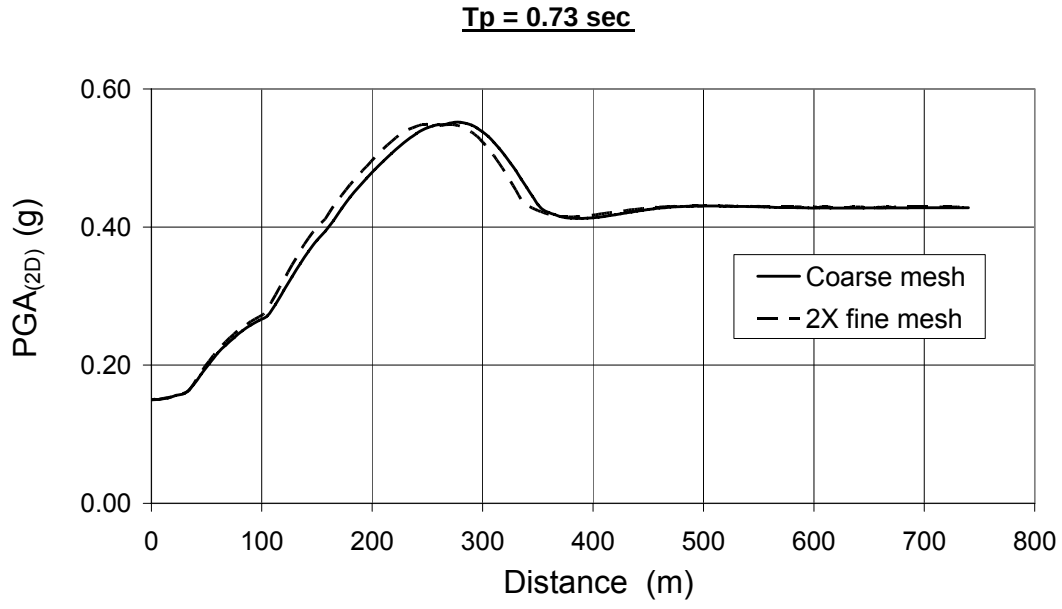

(b)

Figure 4.10: Effect of mesh size on the results

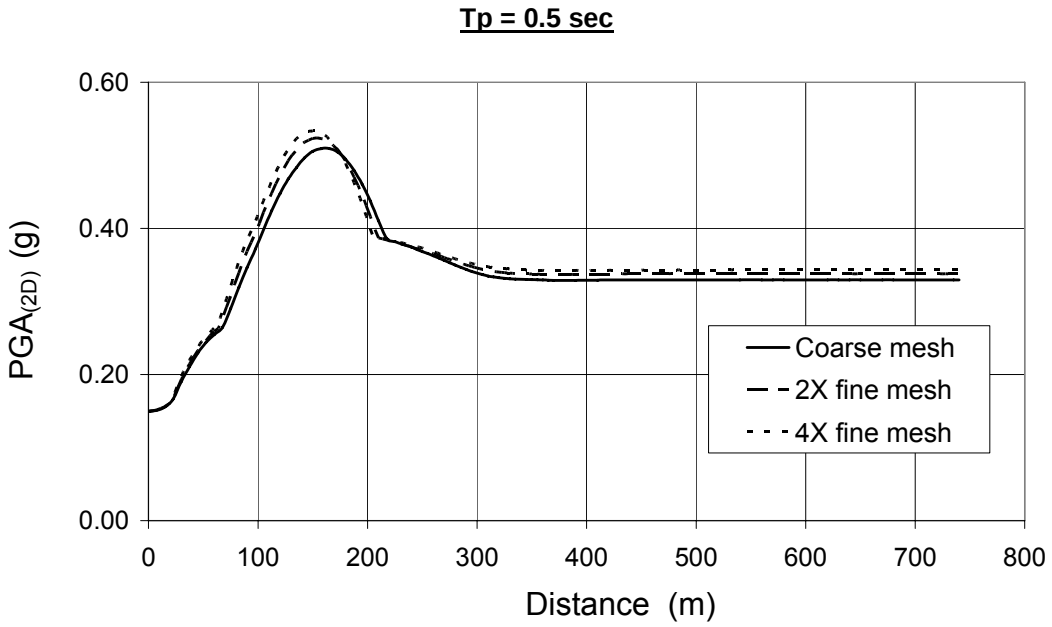

(c)

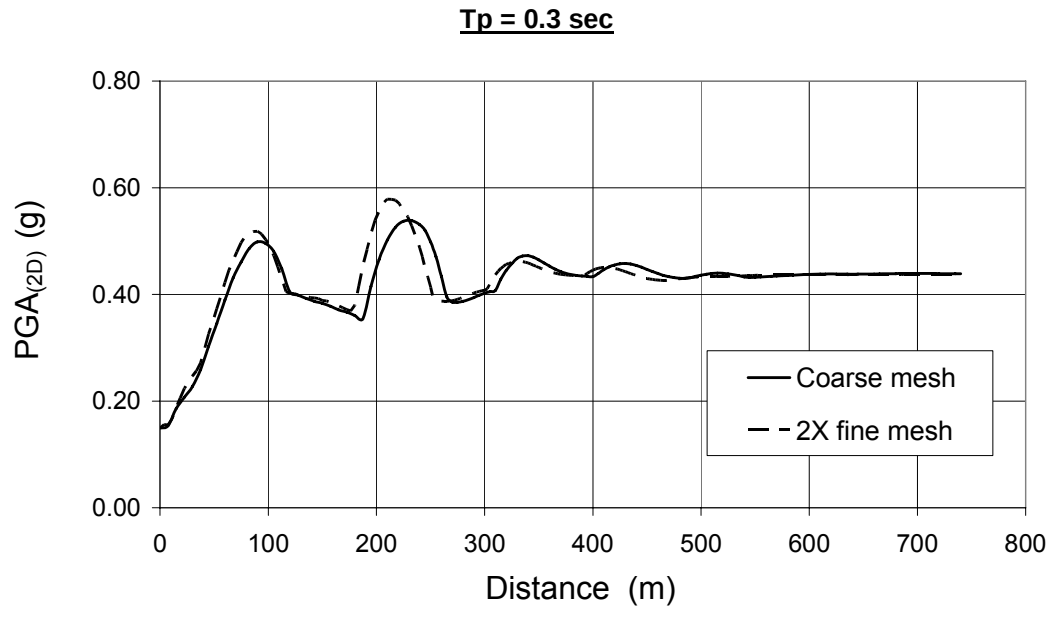

(d)

Figure 4.10: (Continued)

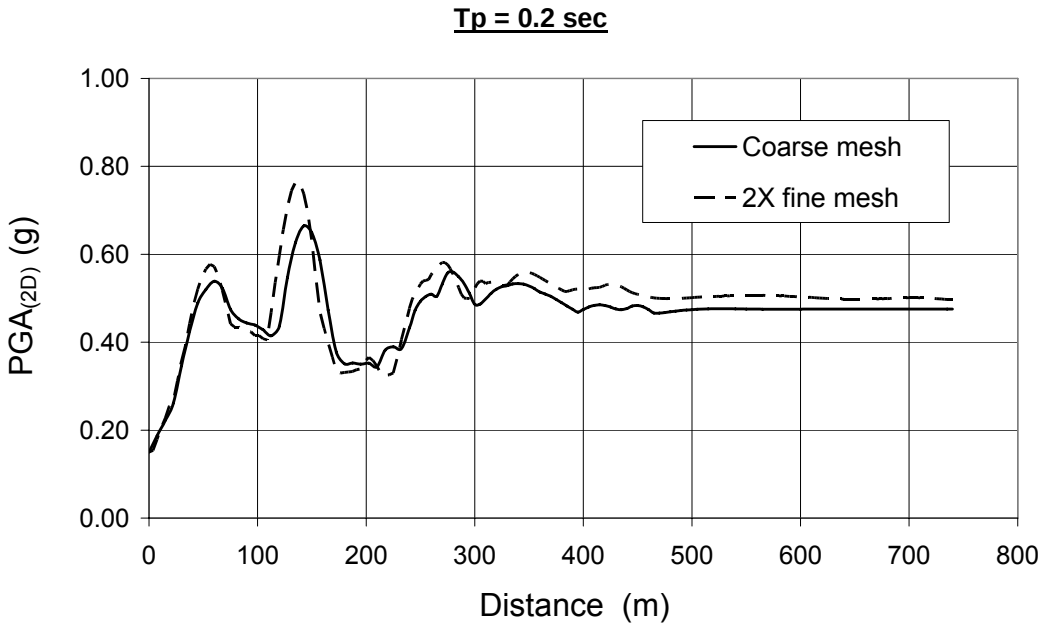

(e)

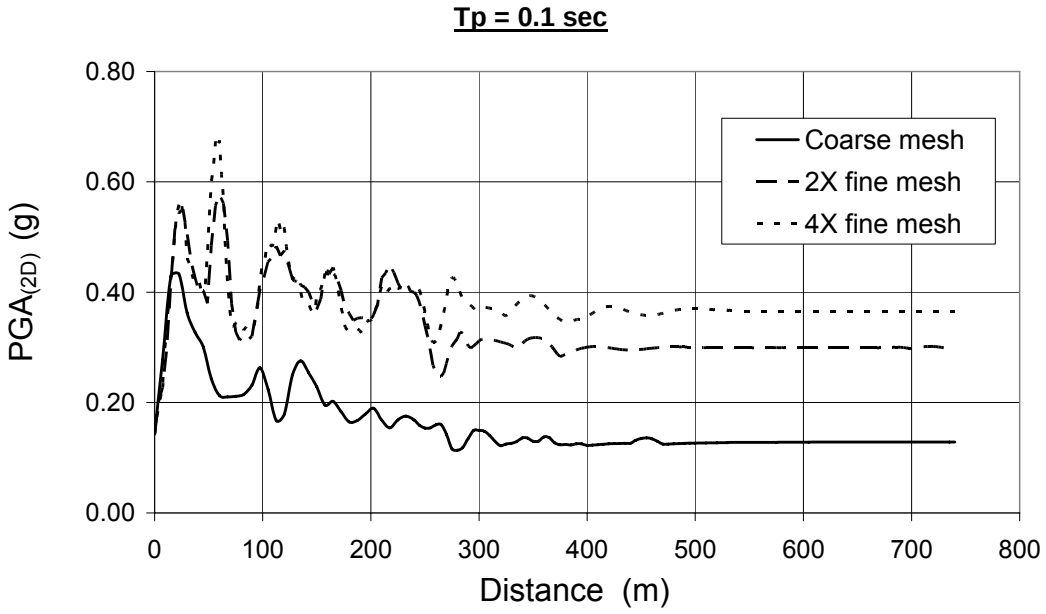

(f)

Figure 4.10: (Continued)

To verify the mesh size of “2X fine mesh”, a series of amplification studies on soil columns of the representative profiles are performed using program QUAD4M and SHAKE91. In these studies, a single column of rectangular elements is used to represent the soil layers in the free field. All nodal points are constrained such that they can move only in the horizontal direction. The vertical dimension of the “2X fine mesh” is tested with SHAKE91 program and it is found that the results obtained from QUAD4M analyses were reasonably close to those obtained from SHAKE91 analyses. The computed response is less sensitive to the choice of the horizontal mesh size. So, in some of the models, horizontal mesh dimensions are taken larger than the vertical mesh dimensions. Finite element mesh for each model is given in Figure 4.11.

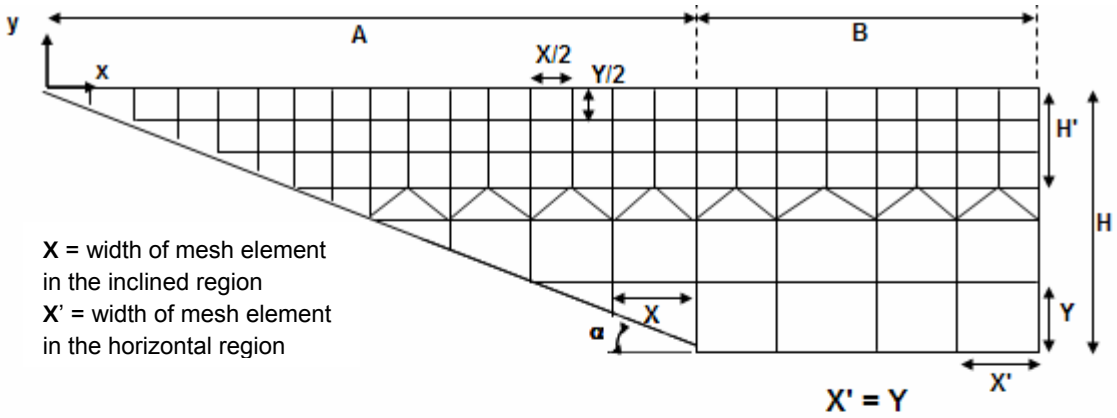

MODEL NO	α (degree)	A (m)	B (m)	H (m)	H' (m)	X/2 (m)	Y/2 (m)	# nodes	# elements	Output interval in A	Output interval in B
1	76	30	500	120	37.5	2.500	2.500	5141	5112	2.500	2.500
2	63	60	500	120	37.5	2.500	2.500	5333	5308	2.500	2.500
3	53	90	500	120	37.5	1.875	2.500	5717	5700	1.875	2.500
4	45	120	500	120	37.5	2.500	2.500	5717	5700	2.500	2.500
5	34	180	500	120	37.5	3.750	2.500	5717	5700	3.750	2.500
6	27	240	500	120	37.5	2.500	2.500	6533	6500	2.500	2.500
7	14	480	500	120	37.5	2.500	2.500	8165	8100	2.500	2.500
8	9	720	500	120	37.5	3.750	2.500	8165	8100	3.750	2.500
9	76	20	500	80	37.5	2.500	2.500	4241	4218	2.500	2.500
10	63	40	500	80	37.5	2.500	2.500	4345	4324	2.500	2.500
11	53	60	500	80	37.5	1.875	2.500	4553	4536	1.875	2.500
12	45	80	500	80	37.5	2.500	2.500	4553	4536	2.500	2.500
13	34	120	500	80	37.5	3.750	2.500	4553	4536	3.750	2.500
14	27	160	500	80	37.5	2.500	2.500	5005	4972	2.500	2.500
15	14	320	500	80	37.5	2.500	2.500	5909	5844	2.500	2.500
16	9	480	500	80	37.5	3.750	2.500	5909	5844	3.750	2.500
17	76	10	500	40	37.5	2.500	2.500	3357	3340	2.500	2.500
18	63	20	500	40	37.5	2.500	2.500	3389	3372	2.500	2.500
19	53	30	500	40	37.5	1.875	2.500	3453	3436	1.875	2.500
20	45	40	500	40	37.5	2.500	2.500	3453	3436	2.500	2.500
21	34	60	500	40	37.5	3.750	2.500	3453	3436	3.750	2.500
22	27	80	500	40	37.5	2.500	2.500	3605	3572	2.500	2.500
23	14	160	500	40	37.5	2.500	2.500	3909	3844	2.500	2.500
24	9	240	500	40	37.5	3.750	2.500	3909	3844	3.750	2.500

Figure 4.11: The details of the mesh for each model

4.5. DISCUSSION OF RESULTS

4.5.1 EFFECT OF SOIL NONLINEARITY ON THE BEHAVIOUR OF ONE-DIMENSIONAL SOIL MODEL

To assess the soil/rock amplification ratio for one-dimensional soil model, site response analyses are carried out using various harmonic base motions. SHAKE91 program is used for the analysis under the following assumptions:

- The soil system extends infinitely in the horizontal direction.
- Each layer in the system is completely defined by its value of shear modulus, critical damping ratio, density, and thickness. These values are independent of frequency.
- The responses in the system are caused by the upward propagation of shear waves from the underlying rock formation.
- The shear waves are given as acceleration values of equally spaced time intervals. Cyclic repetition of the acceleration time history is implied in the solution.
- The strain dependence of modulus and damping is accounted for by an equivalent linear procedure based on an average effective strain level computed for each layer.

The input soil data and one-dimensional model geometry is shown in Figure 4.12 and Figure 4.13 respectively.

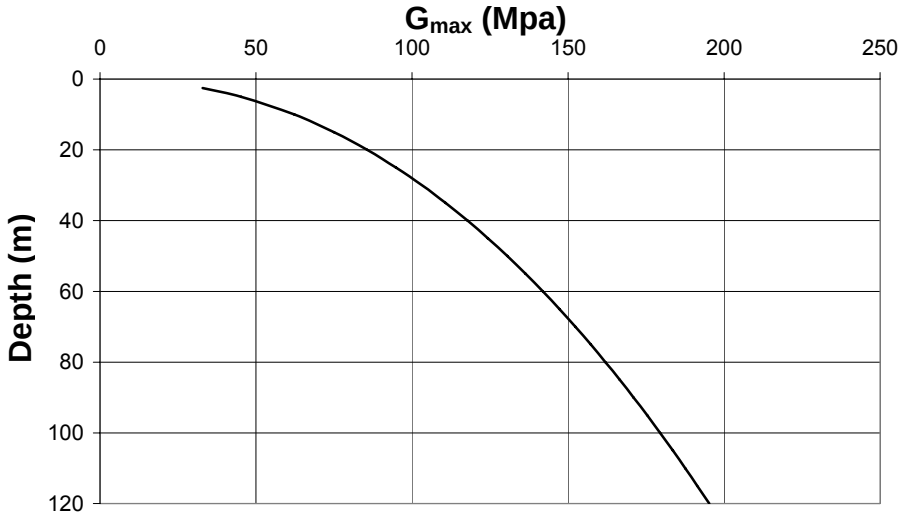

Figure 4.12: Input soil parameter for one-dimensional analyses

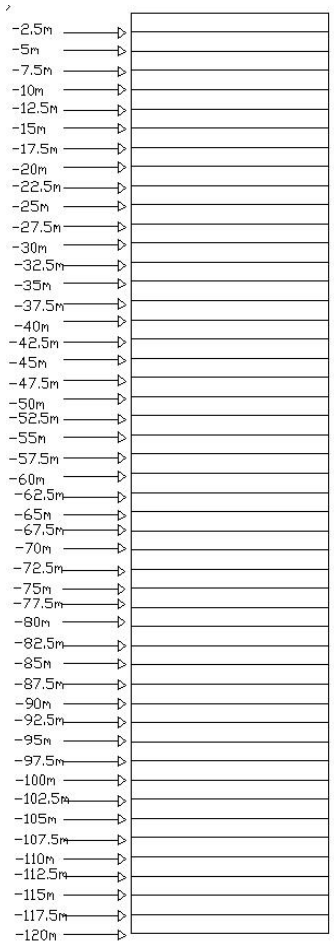

Figure 4.13: Common soil column used in one-dimensional model

PGA_{1D}/PGA_{rock} ratios, where PGA_{1D} is the acceleration on top of the soil and PGA_{rock} is the acceleration on rock outcrop, are calculated for soil columns having thicknesses varying from 2.5m to 120m with 2.5m sublayer thickness. The fundamental period of the site, T_{before}, increases due to softening of the soil layers and becomes equal to T_{after} which is the fundamental period obtained at the end of the analysis. The variation of PGA_{1D}/PGA_{rock} with T_{after} and T_{before} are shown in Figure 4.14 and Figure 4.15 respectively and a comparison between T_{after} and T_{before} is given in Figure 4.16.

The results of the analysis shows that, the maximum amplification is obtained for soil columns having a fundamental period T_{after} equal to the predominant period of the base motion. It is also found that PGA_{1D}/PGA_{rock} exhibits a decreasing trend with increasing values of T_{after} and predominant period of the base motion as well. It is noted that, analyses performed by Roesset (1977), the details of which are mentioned in chapter 2, yields the similar conclusions obtained here.

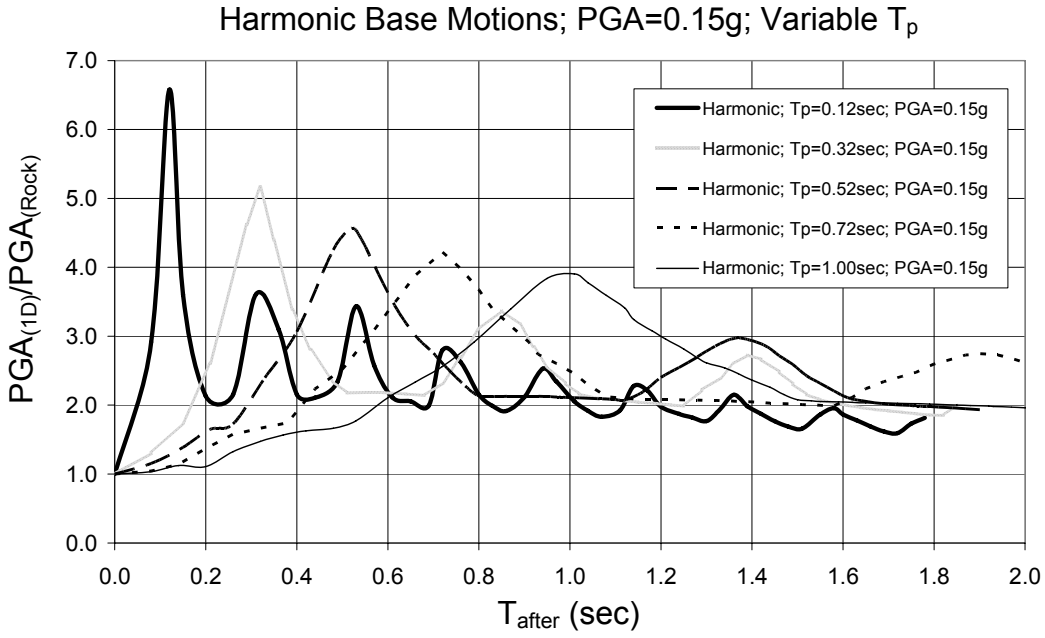

Figure 4.14: Variation of PGA_{1D}/PGA_{rock} with T_{after}

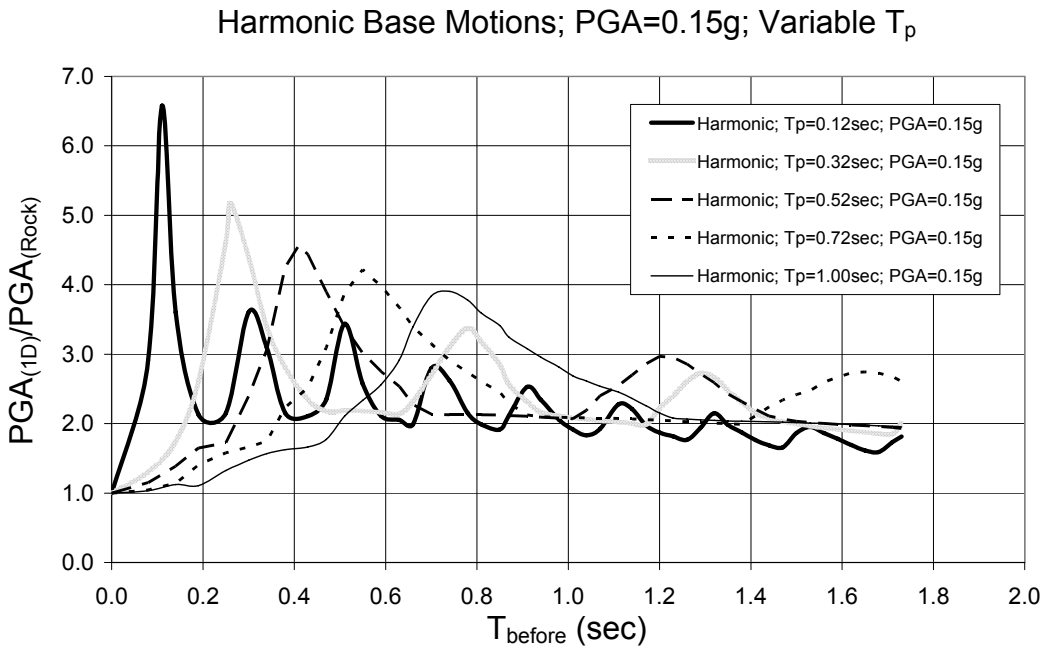

Figure 4.15: Variation of PGA_{1D}/PGA_{rock} with T_{before}

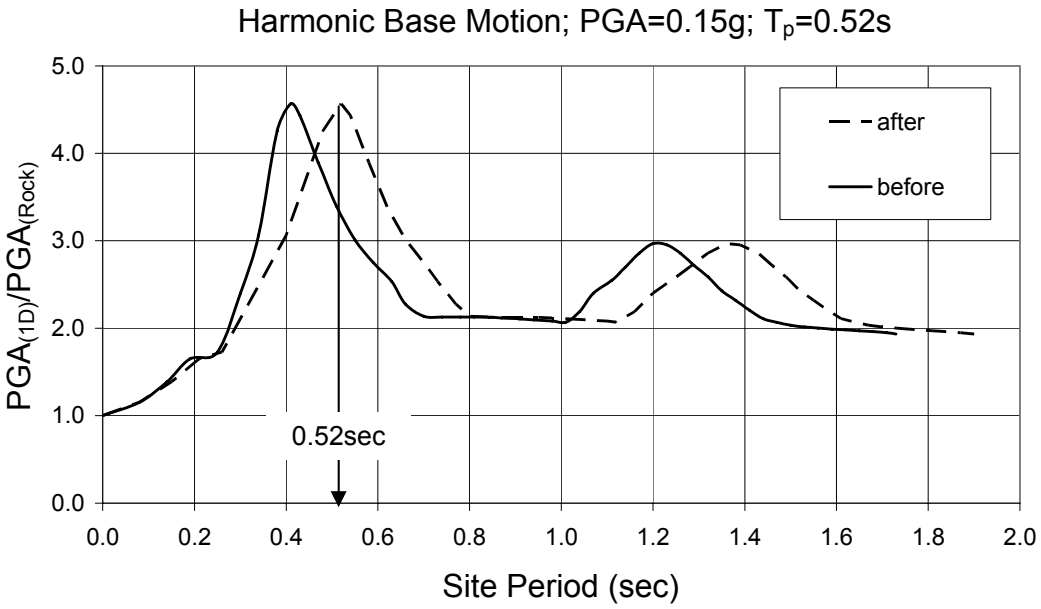

Figure 4.16: The comparison between T_{after} and T_{before}

In the second set of runs, site response is investigated under harmonic base motions having acceleration amplitudes of 0.15g, 0.30g and 0.60g. It is found that the ratio PGA_{1D}/PGA_{rock} decreases with increasing acceleration amplitude of the base motion as indicated in Figure 4.17.

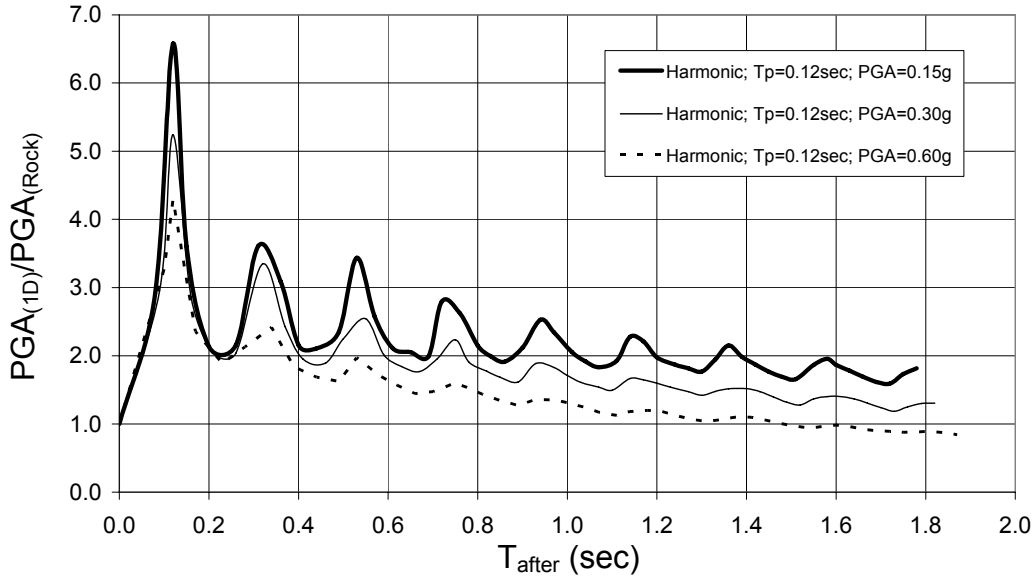

Figure 4.17: Effect of PGA of motion on amplification

4.5.2 RESPONSE OF SELECTED SOIL PROFILES UNDER HARMONIC AND RECORDED MOTIONS

The effects of frequency content and the acceleration amplitude of base motions on the site response are assessed using Dinar Earthquake and harmonic base motions. Harmonic base motions are generated by changing two parameters; (1) the period of the motion as 0.25sec, 0.34sec and 0.29sec which are predominant period, mean period and average of predominant and mean period of Dinar EQ respectively and (2) the amplitude of the motion as 0.50, 0.65 and 0.75 times the PGA of the Dinar Earthquake. Table 4.3 indicates the parameters of the base motions.

Table 4.3: Basic parameters of the base motions

Base Motion	PGA (g)	Predominant Period Tp (sec)	Mean Period Tm (sec)	Duration T (sec)
Dinar	0.1435	0.25	0.34	28
Sin 0.25_0.5	0.5 x 0.1435	0.25	0.25	28
Sin 0.25_0.65	0.65 x 0.1435	0.25	0.25	28
Sin 0.25_0.75	0.75 x 0.1435	0.25	0.25	28
Sin 0.34_0.65	0.65 x 0.1435	0.34	0.34	28
Sin 0.29_0.65	0.65 x 0.1435	(0.24+0.34)/2	(0.24+0.34)/2	28

The variation of $PGA_{(2D)}/PGA_{(Rock)}$ with normalized distance is shown in Figure 4.18 for harmonic base motions having constant amplitude but variable periods, while in Figure 4.19 it is denoted for harmonic base motions having constant period but variable amplitudes.

Normalized distance, ND, is defined as (refer to Figure 4.11);

For $x < A$; $ND=x/A$

For $x > A$; $ND=1+(x-A)/B$

where, x is the distance measured from the rock soil contact point on the ground surface

It is found that the location of the peak amplification for a selected soil profile is very sensitive to the period of the harmonic base motion rather than its amplitude. An increase in the period of harmonic base motion shifts the peak amplification away from the slope towards the horizontal region where the basin is deep, which is expected, since the natural period of the site increases with depth. It is also seen that harmonic base motion having a period equal to the predominant period of the recorded base motion predicts the response of the soil profile under recorded base motion reasonably good at the locations away from the slope (ND >1).

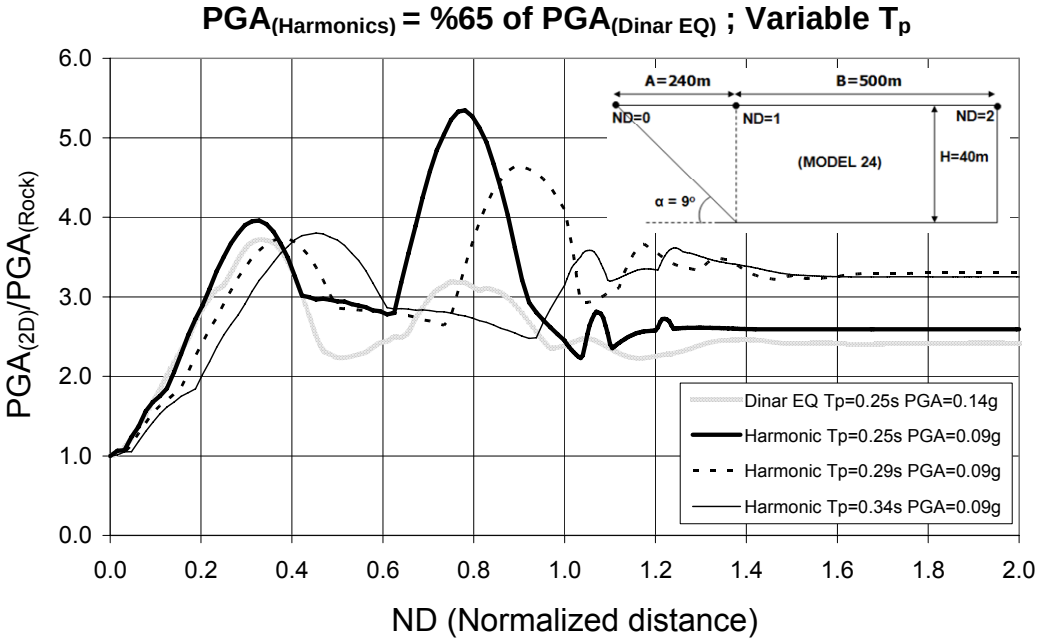

Figure 4.18: Variation of $PGA_{(2D)}/PGA_{(Rock)}$ with normalized distance for constant amplitude, variable periods

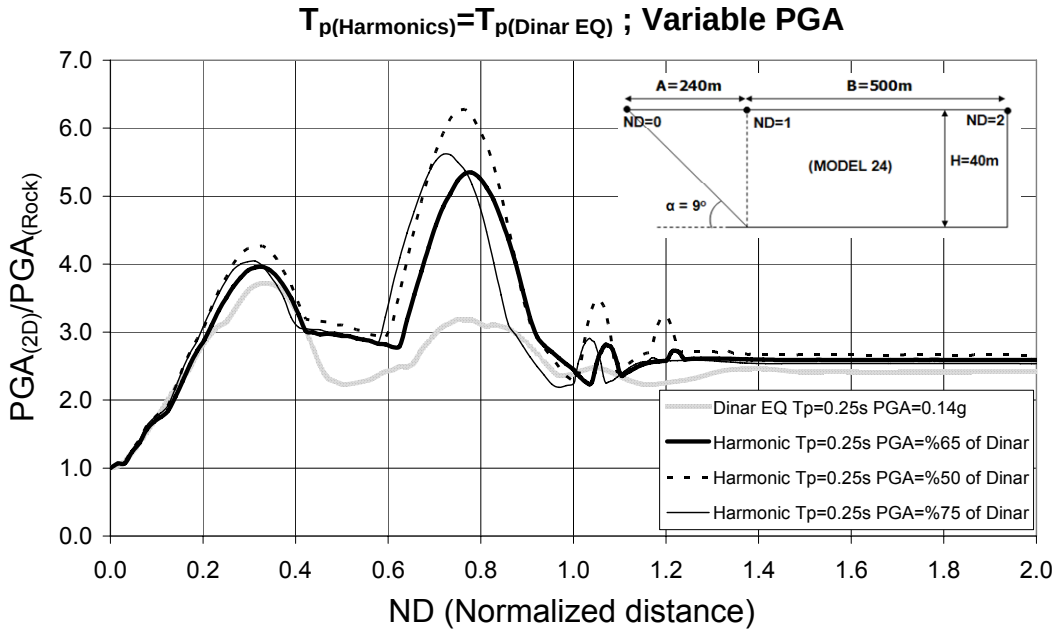

Figure 4.19: Variation of $PGA_{(2D)}/PGA_{(Rock)}$ with normalized distance for constant period, variable amplitudes

4.5.3 EFFECT OF EQ DURATION ON SOIL RESPONSE

The effect of the duration of base motion on the soil response is investigated through Model 8 and Model 19. Model 8 has 9^o basin edge slope and 120m basin depth while Model 19 has 53^o basin edge slope and 40m basin depth. Harmonic base motions having an acceleration amplitude of 0.15g and a period of 0.12 sec are used with durations varying from 1.2sec to 40sec, as shown in Figure 4.20.

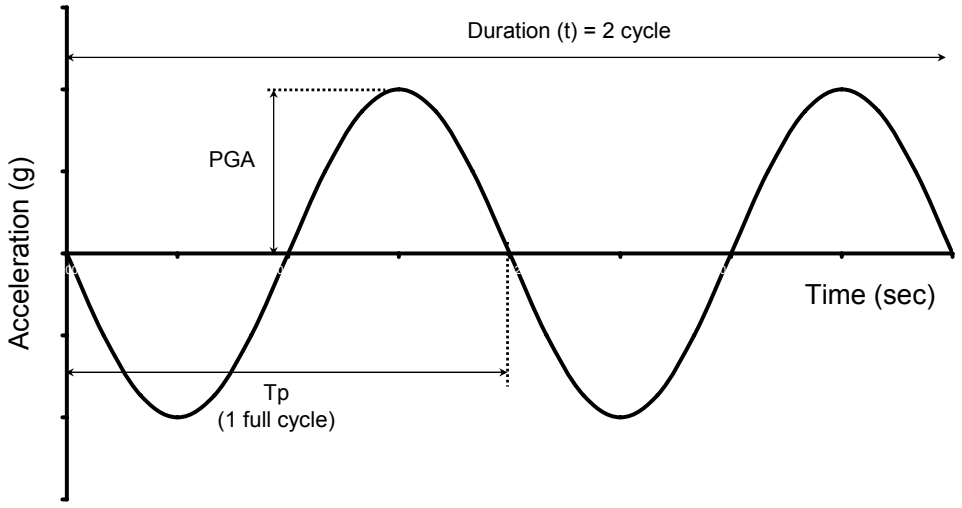

Number of cycle of harmonic base motion	Predominant Period Tp (sec)	Amplitude of base motion PGA (g)	Corresponding Duration T (sec)
10 cycle	0.12	0.15	1.2
20 cycle	0.12	0.15	2.4
40 cycle	0.12	0.15	4.8
83 cycle	0.12	0.15	10
167 cycle	0.12	0.15	20
333 cycle	0.12	0.15	40

Figure 4.20: Cycle definition and characteristics of harmonic base motions

The variation of PGA_{2D}/PGA_{rock} with normalized distance under harmonic base motions with different durations but with the same peak acceleration are obtained and depicted in Figure 4.21 and Figure 4.22 for Model 8 and Model 19 respectively.

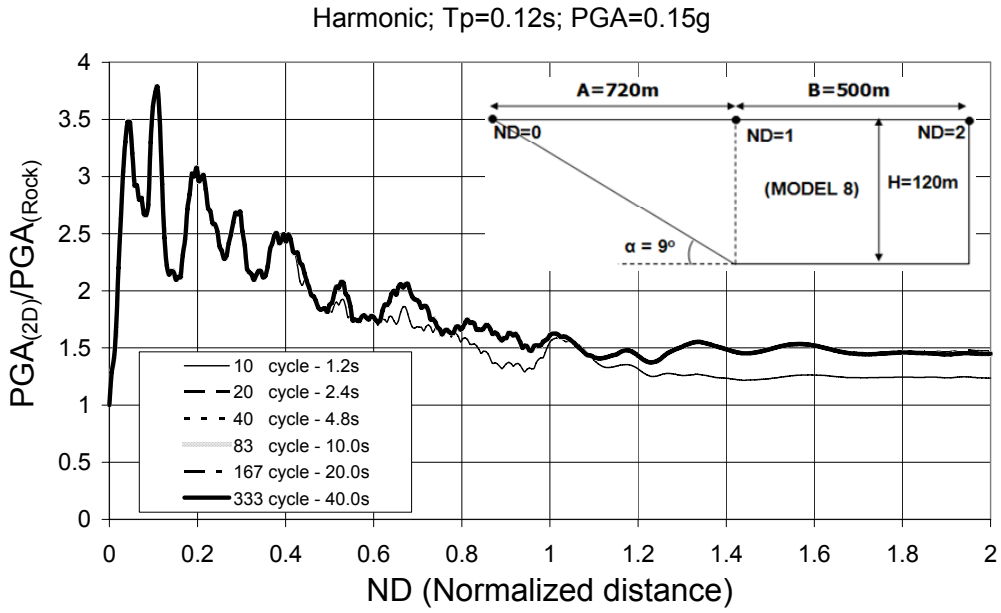

Figure 4.21.a: Effect of duration on amplification for Model 8

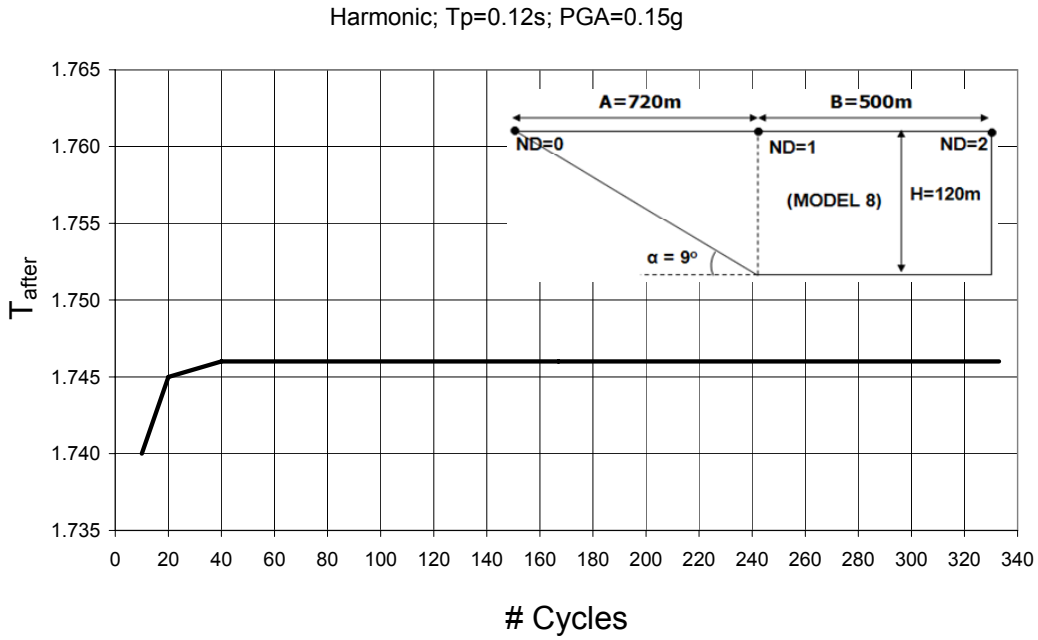

Figure 4.21.b: Effect of duration on T_{after} for Model 8

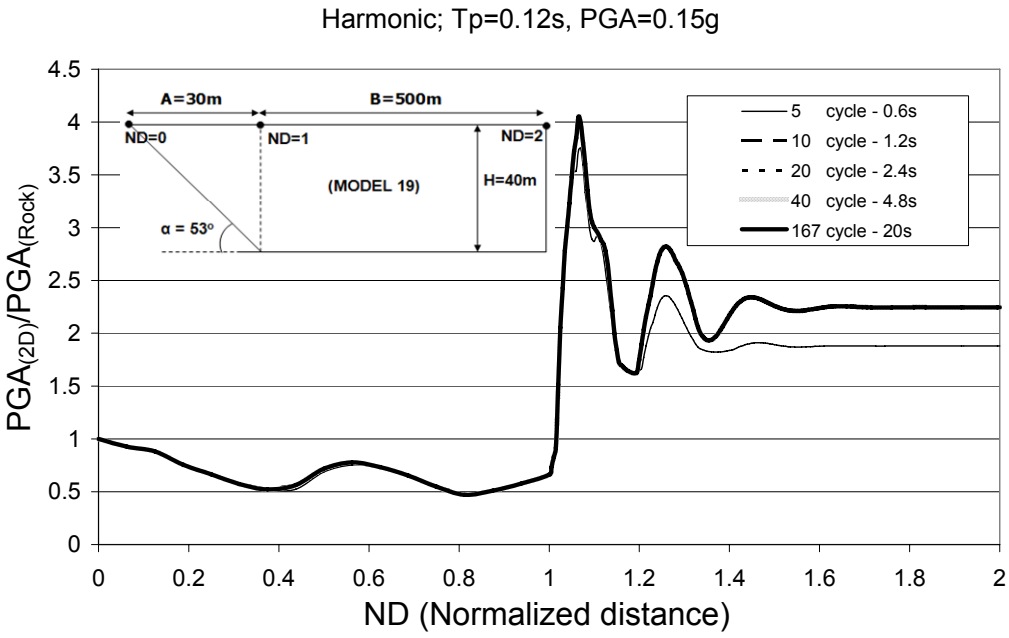

Figure 4.22.a: Effect of duration on amplification for Model 19

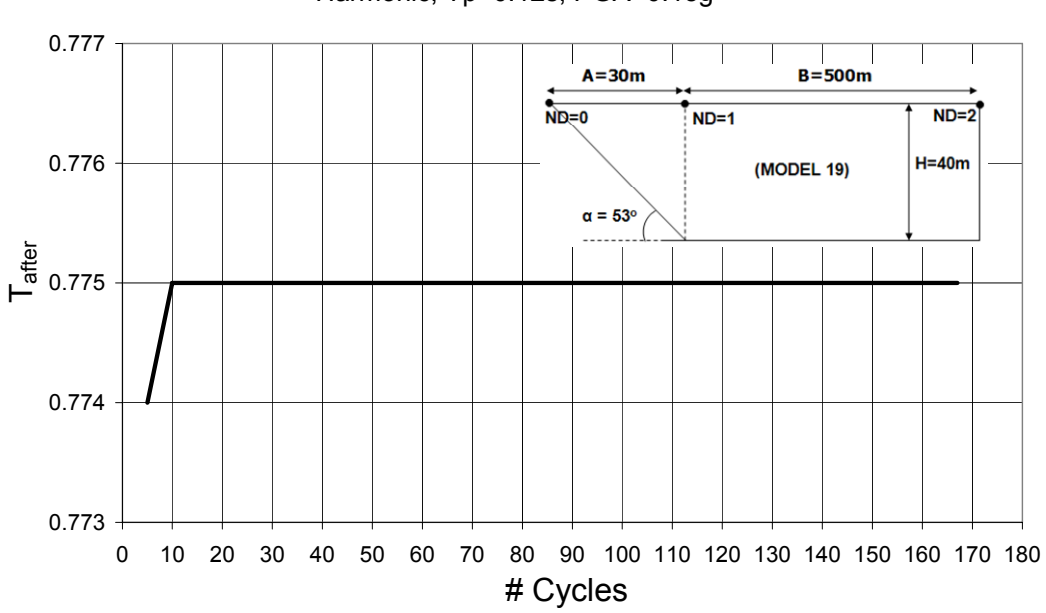

Figure 4.22.b: Effect of duration on T_{after} for Model 19

It can be observed that for neither deep and slightly inclined basin (Model 8; 120m, 9^o) nor relatively shallow and steep-sloped basin (Model 19; 40m, 53^o), the amplification does not significantly change with the increase of the duration of harmonic base motion except the ones with a very short duration of 2.4sec and 1.2sec for deep and shallow profiles respectively. [For deep and slightly inclined basins, the minimum duration of the harmonic base motion which maximizes the amplification is around 2.4sec, which corresponds to 20 cycles (20 times Tp) and for shallow and steep-sloped basins it is around 1.2sec, which corresponds to 10 cycles (10 times Tp) as shown in Figure 4.21 (a) and Figure 4.22 (a)]. Nevertheless, the minimum duration of the harmonic base motion which maximizes the amplification can be taken as 20 times the predominant period of the motion, Tp. The minimum number of cycles which will maximize the amplification can also be predicted from Figure 4.21 (b) and Figure 4.22 (b), which shows the variation of the fundamental period of the site after the analysis (T_{after}) with number of cycles. It is seen that T_{after} increases slightly up to certain level and then does not change with increasing duration.

4.5.4 EFFECTS OF BASIN EDGE SLOPE ON SOIL RESPONSE

To assess the effects of the basin edge slope on the dynamic response of soil deposits, one-dimensional and two-dimensional numerical analyses which incorporate the non-linear stress strain behavior of soils by equivalent linear method are used. One-dimensional approach is based on the assumption that the main response in soil is due to upward propagation of shear waves from the underlying bedrock. SHAKE91 software is used to analyze one-dimensional response. A finite-element computer code QUAD4M is employed for two-dimensional response evaluation.

For the analyses, 24 basin models are developed. The basin models consist of a valley of trapezoidal cross-section having different dimensions varying from wide and shallow to narrow and deep, along with different

slopes of rock boundary. In these models, the soil continuum is assumed to consist of horizontal layers, each of which is homogeneous and isotropic. A relatively “soft” and a “stiff” soil profile are incorporated in the models in order to identify the effect of soil type on the response.

Harmonic base motions are used in the analyses with a maximum acceleration of 0.15g. Harmonic base motions are sinusoidal functions with periods ranging from 0.12sec to 1.00sec.

Effect of basin topography is investigated by the amplification ratio, $PGA_{(2D)}/PGA_{(Rock)}$, defined as the ratio of PGA_{soil} estimated by two-dimensional analysis to PGA_{rock}. In order to make a comparison between the results of one-dimensional and two-dimensional analyses, $PGA_{(2D)}/PGA_{(1D)}$ is defined as a dimensionless ratio. If this ratio is closer to 1, it implies that, both two-dimensional and one-dimensional analyses yield the same amplification for the site.

The main parameters governing the variations of seismic response of alluvial valley are analyzed and following results are arrived at from those analyses:

1) For a constant value of basin edge slope and a constant ratio of fundamental period of site to the predominant period of base motion, (T_n/T_p), the variations of $PGA_{(2D)}/PGA_{(1D)}$ with normalized distance exhibit almost the same behavior for different soil types, basin depths and predominant period of base motions as can be seen in Figure 4.23. Same trend is obtained for the variations of $PGA_{(2D)}/PGA_{(Rock)}$ as shown in Figure 4.24.

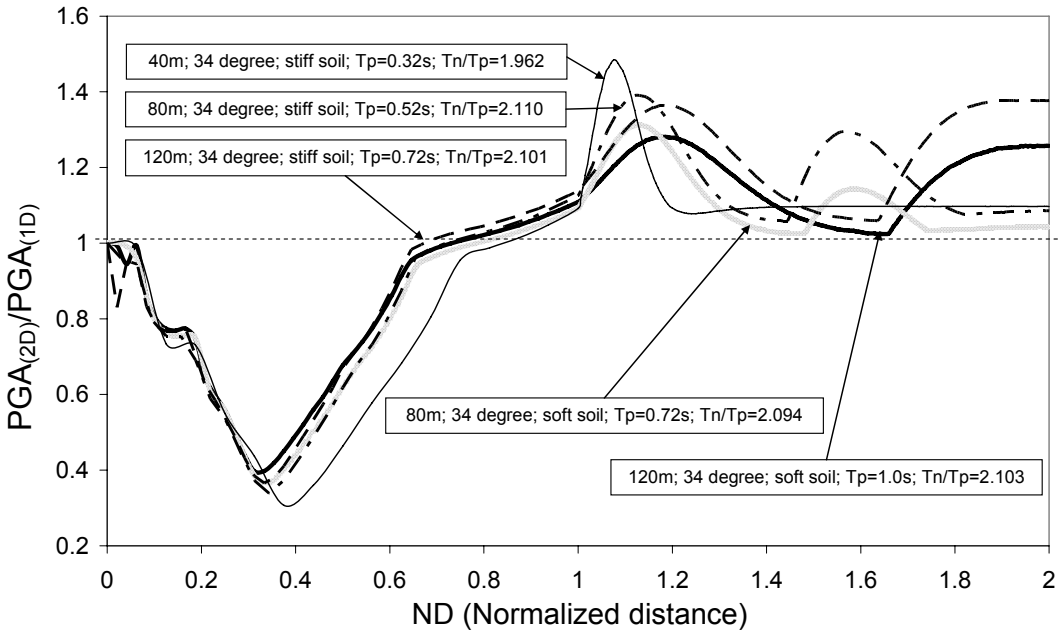

Figure 4.23: Variation of $PGA_{(2D)}/PGA_{(1D)}$ with normalized distance

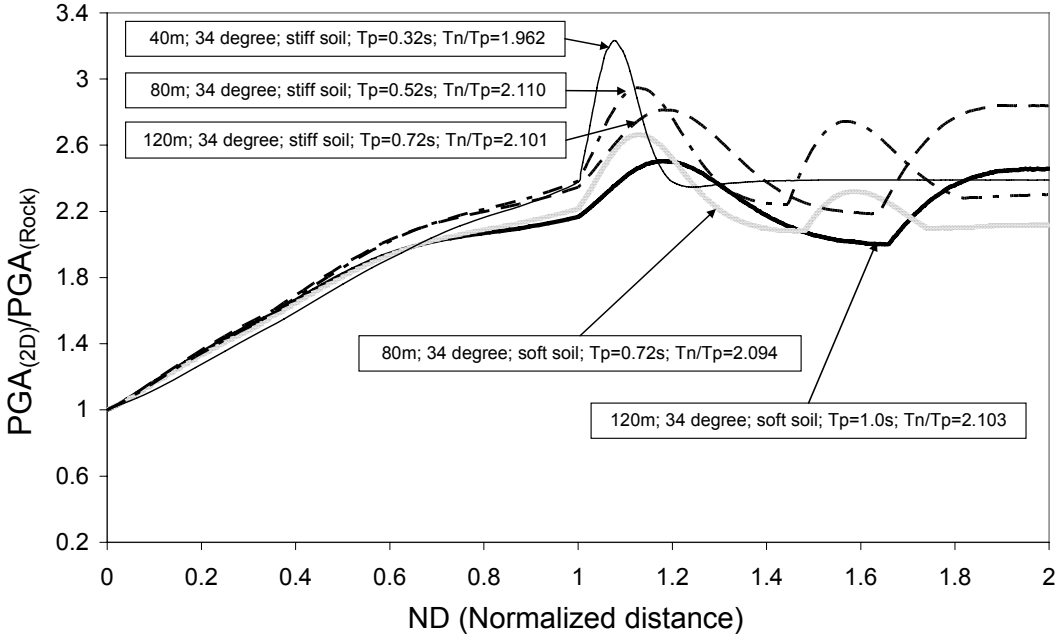

Figure 4.24: Variation of $PGA_{(2D)}/PGA_{(Rock)}$ with normalized distance

2) As shown in Figure 4.25, It is observed that one-dimensional analysis may not accurately predict the effect of the basin edge and that it may overestimate the amplification for ND<1 and underestimate when ND~1. It can be concluded that, one-dimensional seismic response analysis predictions are conservative by a factor of as low as 0.30 in the sloping edge region. However, beyond this region, one-dimensional analysis results are unconservatively biased by a factor as high as 1.2. The critical region where one-dimensional results are found to be unconservative falls in the normalized distance range of 0.8 to 1.5.

3) Keeping Tn/Tp constant, the ratio $PGA_{(2D)}/PGA_{(1D)}$ increases and approaches to 1 within the inclined region of the basin (ND<1) with decreasing slope as shown in Figure 4.25. It is also seen that $PGA_{(2D)}/PGA_{(1D)}$ is about 0.97, which is very close to 1 for ND>>1, expected for horizontal layer, where the small discrepancy can be attributed to basin edge effect and the finite element modelling.

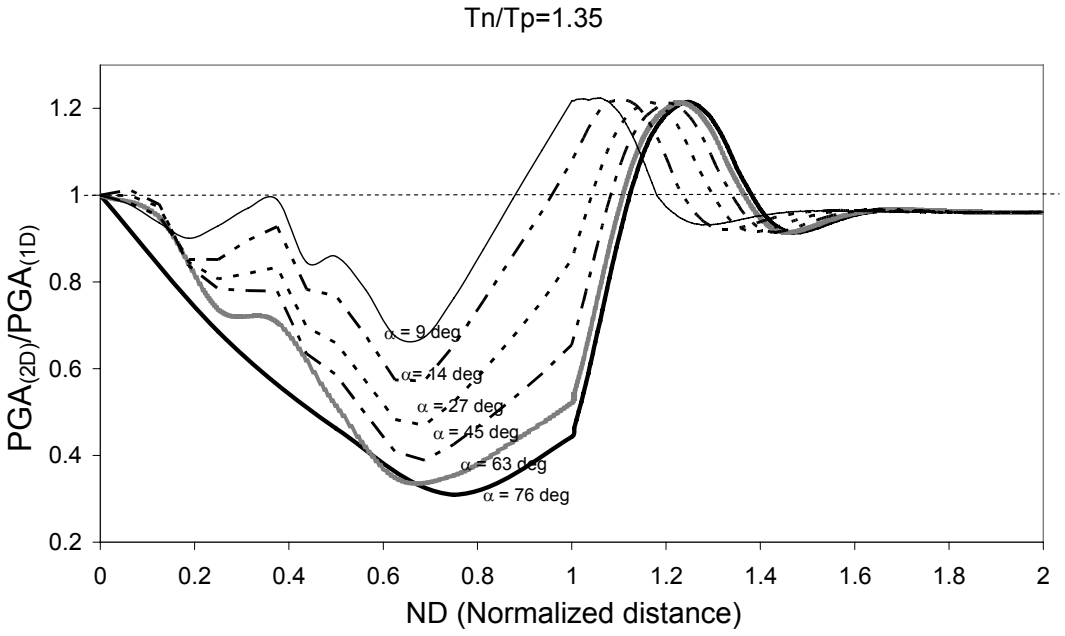

Figure 4.25: Variation of $PGA_{(2D)}/PGA_{(1D)}$ with normalized distance for constant Tn/Tp=1.35

4) Keeping Tn/Tp constant, the ratio $PGA_{(2D)}/PGA_{(rock)}$ increases within the inclined basin (ND<1) with decreasing slope as shown in Figure 4.26. The increase in the "amplification" is smooth in basins with gentle slopes as compared to the basins with steep slopes. For steep slope basins, the amplification sharply increases at ND = 1. Usually, the critical region where maximum amplification is observed falls in the normalized distance range of 0.6 to 1.5 and the critical region shifts towards ND=1.5 with increasing slope.

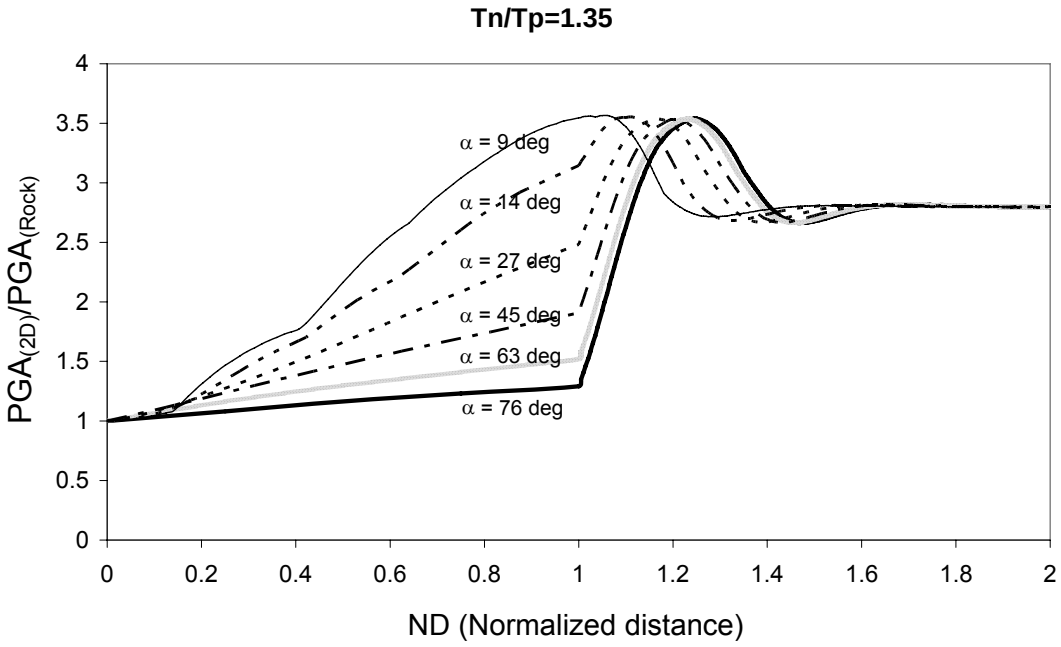

Figure 4.26: Variation of $PGA_{(2D)}/PGA_{(rock)}$ with normalized distance for constant Tn/Tp=1.35

5) Figure 4.27 and Figure 4.28 presents variation of boundaries of critical region with changing basin edge slope, where maximum amplifications ($PGA_{(2D)}/PGA_{(rock)}$) are observed, for values of T_n/T_p=1.35 and T_n/T_p=1.70, respectively. It is seen that, generally the critical region where maximum amplifications are observed falls in a range where normalized distance varies from 1.0 to 1.4 for basins having slopes greater than 30^o. The lower boundary of critical region approaches

towards ND = 0.7 and ND = 0.4 for basins with slopes less than 30^{o}, for values of T_n/T_p=1.35 and T_n/T_p=1.70 respectively.

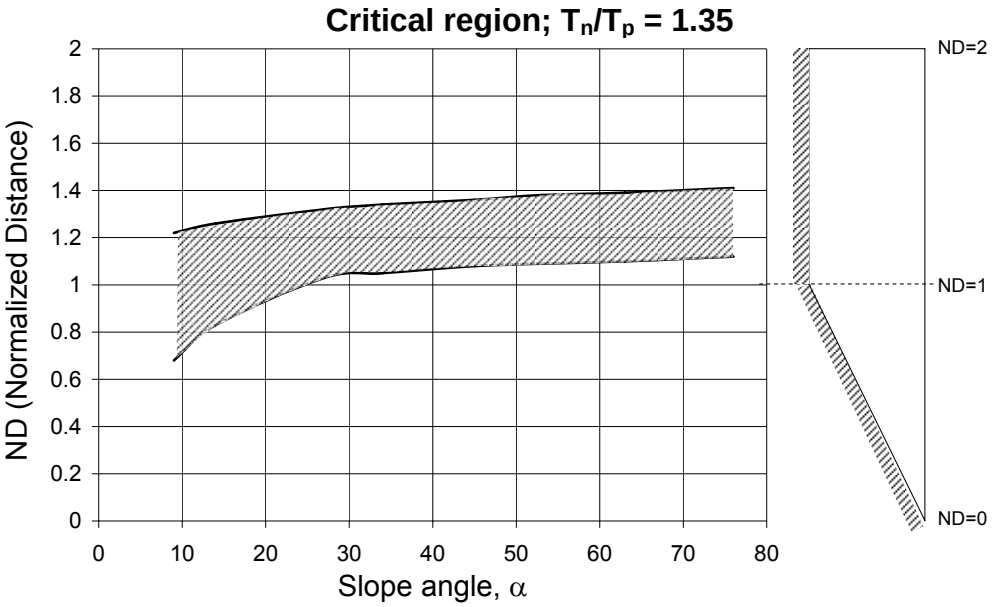

Figure 4.27: Critical region where max amplification due to basin edge effect is observed for T_n/T_p =1.35

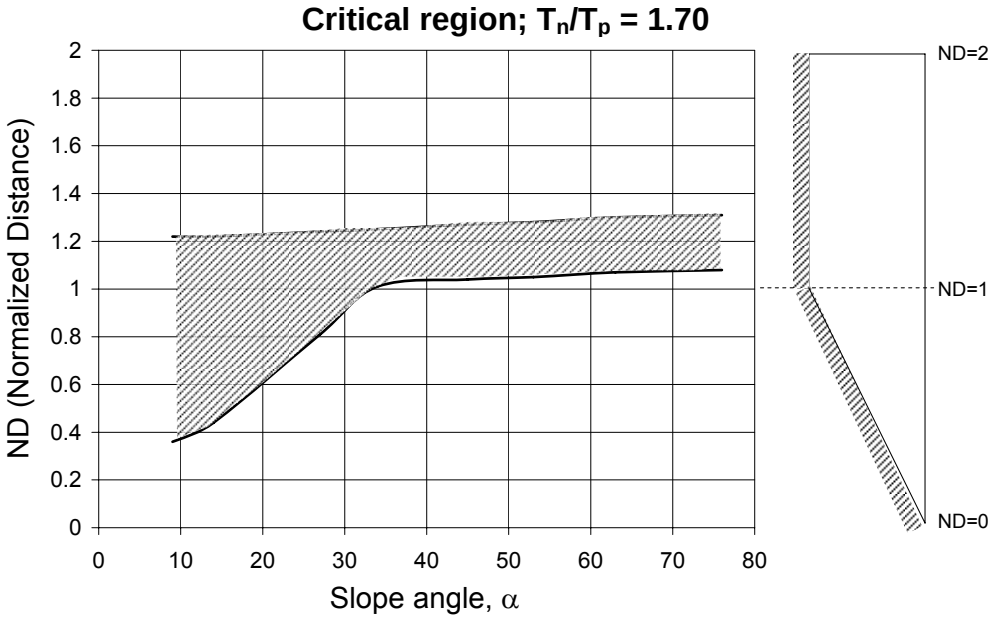

Figure 4.28: Critical region where max amplification due to basin edge effect is observed for T_n/T_p =1.70

6) As shown in Figure 4.29, keeping basin edge slope constant, a decrease of (T_n/T_p), where T_n/T_p >1, results in a shift of points of minima of $PGA_{(2D)}/PGA_{(1D)}$ towards the region where the basin is horizontal (ND>1). The PGA predictions by two-dimensional analyses are found to be as high as 50% of those found by one-dimensional analyses in the critical region which falls in a range where normalized distance varies from 0.8 to 1.5.

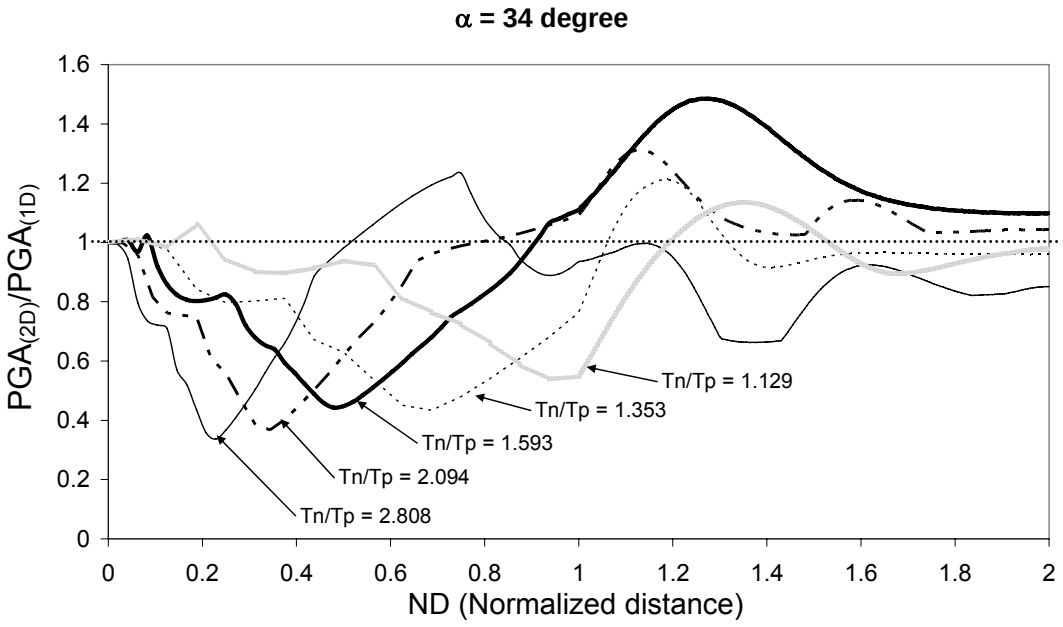

Figure 4.29: Variation of $PGA_{(2D)}/PGA_{(1D)}$ with normalized distance for constant $\alpha=34^0$

7) Figure 4.30 illustrates that, for a basin and earthquake couple approaching to resonance state (T_n/T_p=1), the amplification ($PGA_{(2D)}/PGA_{(Rock)}$) due to the basin edge effect for the region where ND is slightly greater than 1 is found to be as high as 100% of that is found for the region where ND~1. As T_n/T_p increases, $PGA_{(2D)}/PGA_{(Rock)}$ decreases exponentially as shown in Figure 4.31.

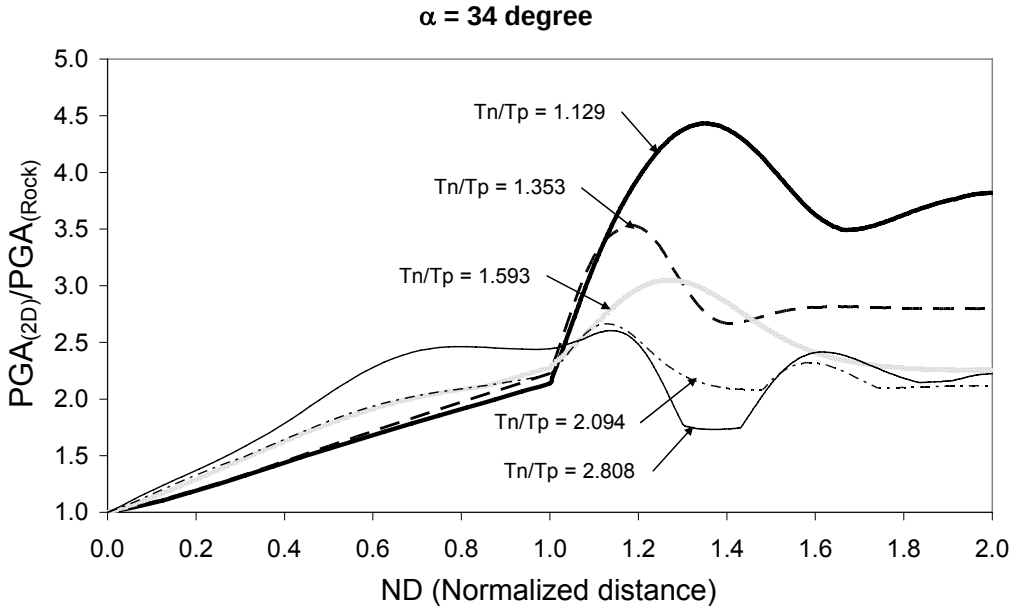

Figure 4.30: Variation of $PGA_{(2D)}/PGA_{(Rock)}$ with normalized distance for constant $\alpha=34^0$

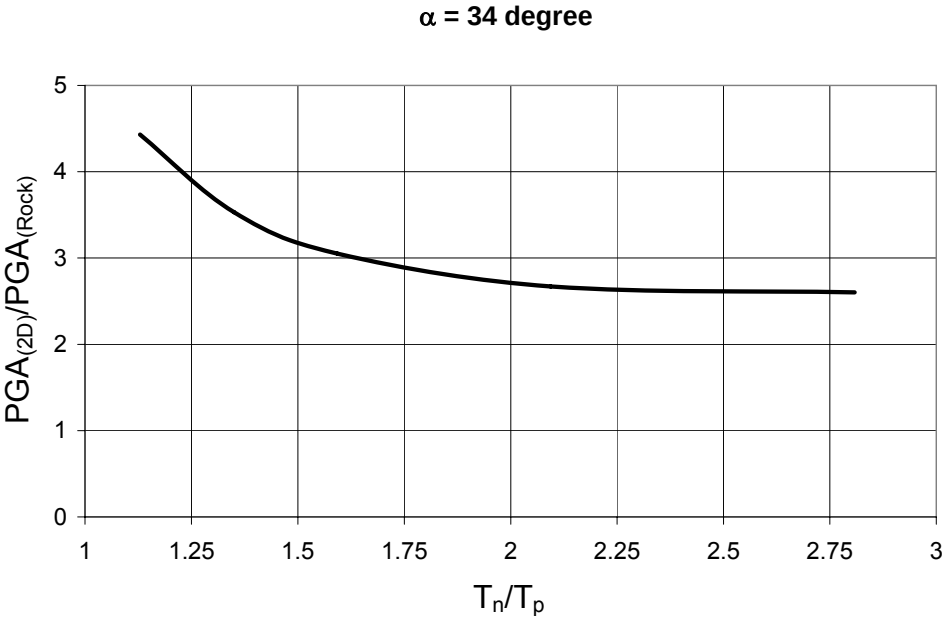

Figure 4.31: Variation of $PGA_{(2D)}/PGA_{(Rock)}$ with T_n/T_p for constant $\alpha=34^0$

CHAPTER 5

CONCLUSIONS

Effect of basin geometry on the dynamic response of horizontal soil deposits is investigated by using one-dimensional and two-dimensional computer programs which incorporate the non-linear stress strain behavior of soils by equivalent linear method. Basin geometry consists of trapezoidal sections with different slope angles and depths. A total number of 24 models are used together with different soil types. Harmonic base motions with different predominant periods (T_p) with a maximum acceleration of 0.15g and Dinar Earthquake motion are used in the analyses in order to assess the effects of base motion parameters on the response of soil deposits.

Following dimensionless soil amplification ratios are defined in order to represent the results, as:

(1) $PGA_{(2D)}/PGA_{(Rock)}$

(2) $PGA_{(1D)}/PGA_{(Rock)}$

(3) $PGA_{(2D)}/PGA_{(1D)}$

where,

$PGA_{(2D)}$: the peak ground acceleration at top of the soil deposit for two-dimensional analysis.

$PGA_{(1D)}$: the peak ground acceleration at top of the soil deposit for one-dimensional analysis.

$PGA_{(Rock)}$: the peak ground acceleration on rock outcrop.

Results are represented in terms of normalized distance (ND) which is again a dimensionless ratio defined as;

For $x < A$; x/A

For $x \geq A$; $1+(x-A)/B$

where, x is the distance measured from the rock soil contact point on the ground surface

The following conclusions can be drawn from the results of the analyses.

1. Results of one-dimensional analyses indicate that
   a. For a given base motion, the maximum amplification PGA_{1D}/PGA_{rock} is obtained for the soil profile having a fundamental period T_{after} equal to the predominant period of the base motion T_p, where T_{after} is the fundamental period of the site obtained at the end of the analysis.
   b. The soil/rock amplification ratio PGA_{1D}/PGA_{rock} exhibits a decreasing trend with increasing values of fundamental period of the soil profile T_{after} and predominant period of the base motion T_p as well.
   c. The soil/rock amplification ratio PGA_{1D}/PGA_{rock} decreases with increasing amplitude of the harmonic base motion.
2. Results of two-dimensional analyses indicate that
   a. The ratio of fundamental period of site to the predominant period of base motion, T_n/T_p, significantly affects the location and the magnitude of the peak amplification for a selected soil profile.
   b. For a constant value of basin edge slope and a constant ratio of fundamental period of site to the predominant period of base motion, (T_n/T_p), the variations of $PGA_{(2D)}/PGA_{(1D)}$ with

normalized distance exhibit almost the same behavior for different soil types, basin depths and predominant periods of base motion. Same trend is also obtained for the variations of $PGA_{(2D)}/PGA_{(Rock)}$ with normalized distance.

c. One-dimensional analysis may not accurately predict the effect of the basin edge and it may overestimate the amplification for ND<1 and underestimate for ND~1. However, $PGA_{(2D)}/PGA_{(1D)}$ ratio approaches to 1, expected for a horizontal layer, at a certain distance away from the inclined basin (ND >> 1).

d. In the sloping edge region, one-dimensional seismic response analysis predictions of peak ground accelerations are conservative by a factor of as high as 5, where it decreases with decreasing basin edge slope angle and T_n/T_p value as well. However, beyond this region, one-dimensional analysis results are unconservatively predisposed by a factor as high as 1.5. The critical region where one-dimensional results are found to be unconservative falls in the normalized distance range of 0.8 to 1.5 as basin edge slope increases. Therefore it is recommended to multiply the amplification obtained from one-dimensional analysis by a factor of 1.5 in order to take into consideration the effect of the basin edge slope for the critical region mentioned above.

e. Keeping Tn/Tp constant, the ratio $PGA_{(2D)}/PGA_{(rock)}$ increases within the sloping edge region (ND<1) with decreasing slope. The increase in the “amplification” is smooth in basins with gentle slopes as compared to the basins with steep slopes. For steep slope basins, the amplification sharply increases at ND=1.

f. For basins having slopes greater than 30 degrees, the critical region where maximum amplification due to the basin edge

slope is observed falls in the normalized distance range of 1.0 to 1.5 and the variation of T_n/T_p have slight influence on this range. The bandwidth of the critical region does not change with changing slope angle but the critical region shifts gradually towards ND=1.5 as the basin edge slope increases.

For basins having slopes less than 30 degrees, the critical region where maximum amplification due to the basin edge slope is observed falls in the normalized distance range of as low as 0.2 to as high as 1.4. As slope decreases, the bandwidth of the critical region increases. For a constant slope, as T_n/T_p increases, the bandwidth of the critical region also increases.

g. For a basin and earthquake couple approaching to resonance state (T_n/T_p=1), the amplification due to the basin edge slope, for the region where ND is slightly greater than 1 is found to be as high as 100% of that is found for the region where ND~1. As T_n/T_p increases, amplification decreases exponentially.

REFERENCES

1. Aki K and Larner KL. "Surface motion of a layered medium having an irregular interface due to incident plane SH-waves," Journal of Geophysical Research, vol. 75, 1970, pg. 1921–1941.

2. Aki K. “Local site effects on strong ground motion. In: Van Thun JL, editors. Earthquake engineering and soil dynamics — recent advances in ground-motion evaluation, “ASCE Geotechnical Special Publication, no. 20, 1988, pg. 103–55.

3. Ashford, S.A., Sitar, N., Lysmer, J., and Deng, N. (1997). “Topographic effects on the seismic response of steep slopes,” Bull. Seism. Soc. Am., 87, 701-709.

4. Assimakia D.,Kausel E.,Gazetas G., "Wave propagation and soil–structure interaction on a cliff crest during the 1999 Athens Earthquake, " Soil Dynamics and Earthquake Engineering, vol.25 ,2005, pg.513–527.

5. Athanasopoulos GA, Pelekis PC, Leonidou EA. "Effects of surface topography on seismic ground response in the Egion (Greece) 15 June 1995 earthquake,"Soil Dynamics and Earthquake Engineering, vol. 18, 1999, pg. 135-149.

6. Athanasopoulos GA, Zervas S. "Effects of ridge-like surface topography on seismic site response, " Bath, UK. In: Carmak AS, Brebbia CA, editors. Proceedings of 6th international conference on soil dynamics and earthquake engineering, Computational Mechanics Publications, Southampton, 1993.

7. Bakir S., Ozkan M.Y., Ciliz S. "Effect of basin edge on the distribution of damage in 1995 Dinar Turkiye Earthquake" Soil Dynamics and Earthquake Engineering , vol. 22, page 335-345, 2002.

8. Brambati A., Faccioli E., Carulli G.B., Cucchi F., Onofri R., Stefanini S. & Ulcigrai F. (1980) - Studio di microzonazione sismica dell'area di Tarcento (Friuli). Regione Autonomia Friuli-Venezia Giulia & Università degli Studi di Trieste con la collaborazione del Politecnico di Milano. Trieste.

9. Bard P-Y. "Diffracted waves and displacement field over two-dimensional elevated topographies," Journal of Royal Astronomy Society, 1982, pg. 731-760.

10. Bard, PY and Gariel JC. "The seismic response of two-dimensional sedimentary deposits with large vertical velocity gradients," Bulletin of the Seismological Society of America, 1986, vol. 76, pp. 343-366.

11. Bard, P-Y. (1995). "Effects of surface geology on ground motion: recent results and remaining issues," Proc. 10th European Conference on Earthquake Engineering, Duma (ed.), Rotterdam, 305-323.

12. Bielak J, Xu J and Ghattas O. "Earthquake ground motion and structural response in alluvial valleys," Journal of Geotechnial and Geoenvironmental Engineering, May 1999, pp. 413-423.

13. Boore, D. M., 1972: A note on the effect of simple topography on sesimic SH waves. Bulletin of the Seismological Society of America,Vol.62,No.1,pp. 275-284.

14. Bouchon M. "Effect of topography on surface motions," Bulletin of the Seismological Society of America, vol. 63 (3), 1973, pp. 615–632.

15. Bouckovalas GD, Kouretzis G. "Review of soil and topography effects in the September 7, 1999 Athens (Greece) earthquake, " Proceedings: Fourth International Conference on Recent Advances in Geotechnical Earthquake Engineering, San Diago, California, March 26-31, 2001.

16. Bouckovalas G., Papadimitriou Ach. (2004), "Numerical evaluation of slope topography effects on seismic ground motions", 11th ICSDEE and 3rd ICEGE, January 7-9, Berkeley, U.S.A.

17. Brune JN. "Preliminary results on topographic seismic amplification effect on a foam rubber model of the topography near Pacoima Dam, " In: proceedings of the eighth world conference on earthquake engineering, San Francisco, vol. II, 1984, pg. 663–9.

18. Cao, H. and Lee, V.W. (1990). “Scattering and Diffraction of Plane P Waves by Circular Cylindrical Rigid Foundations with Variable Depth-to-Width Ratios”, Soil Dynamics and Earthquake Engineering, Vol. 9, No. 3, pp. 141-150.

19. Castellani A., Chesi C., Peano A., Sardella L. "Seismic response of topographic irregularities, " In: Cakmak AS, Abdel-Ghaffar AM, Brebbia CA. Balkema/Rotterdam, editors. Proceedings of soil dynamics and earthquake engineering conference, Southampton, July, 1982, vol. 1, 1982, pg. 251–268.

20. Castellani A, Peano A, Sardella L. "Seismic response of topographic irregularities," In: Proceedings of the third international earthquake microzonation conference, Seattle, vol. II, 1982, pg. 533–40.

21. Chang, S.W., Bray, J.D., and Seed, R.B. (1996). “Engineering implications of ground motions from the Northridge earthquake,” Bull. Seism. Soc. Am., 86, S270-S288.

22. Cha´vez-Garcia F.J., Faccioli E. “Complex site effects and building codes: making the leap. J Seismol 2000;4:23–40.

23. Celebi M. "Topographical and geological amplifications determined from strong motion and aftershock records of the 3 March 1985 Chile earthquake," Bulletin of the Seismological Society of America 88 (4), 1987, pg. 1147–1167.

24. Davis, L.L., and West, L.R. (1973). “Observed effects of topography on ground motion,” Bull. Seism. Soc. Am., 63, 283-298.

25. Davis, P.M., Rubenstein, J.L., Liu, K.H., Gao, S.S. and Knopoff, L. (2000). “Northridge earthquake damage caused by geologic focusing of seismic waves,” Science, 289, 1746-1750.

26. Dobry R.,Vucetic M., Dynamic properties and seismic response of soft clay deposits, Proc. Int. Symp. on Geotechnical Engineering of Soft Soils,2,MexicoCity,1987,51–87.

27. Eurocode 8: Design of structures for earthquake resistance. Part 5: Foundations, retaining structures and geotechnical aspects, November 2001.

28. Faccioli E. "Seismic amplification in the presence of geological and topographic irregularities," In: Proceedings of the second international conference on recent advances in geotechnical earthquake engineering and soil dynamics. St Louis, Missouri, vol. II, 1991, pg. 1779–97.

29. Field, E.H. et al. (2000). “Accounting for site effects in probabilistic seismic hazard analyses of southern California: Overview of the SCEC Phase III report,” Bull. Seism. Soc. Am., 90, S1-S31.

30. Figueroa, A. 1960. Some Consideration about the Effect of Mexican Earthquakes, Volume III, Proceedings: Second World Conference on Earthquake Engineering. 1553-1561.

31. Finn WD Liam, Lai S., Matsunaga Y. "The effects of site conditions on ground motions, " 10 th European Conference on Earthquake Engineering, 1995, pp. 2607-2612.

32. Finn LWD. "Site conditions and seismic response. In: Proceedings of the international symposium, on the effects of surface geology on seismic motion (ESG 1992) ". Odawara, Japan, vol. I, 1984, pg. 3–31.

33. Finn, W.D.L., M. Yogendrakumar, N., Yoshida, and H.Yoshida. 1986. TARA-3: A program for non-linear static and dynamic effective stress analysis. Soil Dynamics Group, Univ. of British Columbia, Vancouver, BC

34. Frankel A, Meremonte M, Cranswick E, Carver, Worley D, Odum J, Williams R. "Observations from Northridge aftershocks recorded by seismometers deployed in the San Fernando valley and at the interstate-10 collapse, "Seismological Society of America, Annual Meeting, April 5-7 1994, Pasedana, California.

35. Graves, R. W., Pitarka A., and Somerville G., ‘’Ground motion amplification in the Santa Moniuca Area: Effect of shallow basin edge structure,’’ Bulletin of Seim. Soc. Am., 88, 1224-1242, 1998.

36. Graves, R.W. (1993). “Modeling three-dimensional site response effects in the Marina District, San Francisco, California,” Bull. Seism. Soc. Am., 83, 1042-1063.

37. Geli L, Bard PY, Jullien B. "The effect of topography on earthquake ground motion: a review and new results," Bulletin of the Seismological Society of America, vol. 78: (1), 1988, pg.42–63.

38. GovindaRaju L., Ramana G. V., HanumanthaRao C. , Sitharam T. G. "Site-specific ground response analysis" Special Section: Geotechnics and Earthquake Hazards. Current Science, vol. 87, no. 10, 25 November 2004.

39. Green R.A., Cameron W.I. "The influence of ground motion characteristics on site response coefficients " 2003 Pacific Conference on Earthquake Engineering

40. Gutenberg, B. and C.F. Richter. 1956. Earthquake Magnitude, Intensity, Energy, and Acceleration (Second Paper), Bulletin of the Seismological Society of America. 46(2). 105-145.

41. Hanks, TC. "Strong ground motion of the San Fernando California earthquake, ground displacement," Bulletin of the Seismological Society of America, 1975, vol. 65, pp.193-225.

42. Hardin, O.B., Drnevich V.P., " Shear modulus and damping in soils: Measurement and parameters effects, " Journal of the Soil Mechanics and Foundations Division, ASCE, Vol.98, No. SM6, pp. 603-624, June, 1972a.

43. Hardin, O.B., Drnevich V.P., " Shear modulus and damping in soils :Design equations and curves, " Journal of the Soil Mechanics and Foundations Division, ASCE, Vol.98, No. SM7, pp. 667-692, July, 1972b.

44. Hardin, B.O., Black, W.L., 1969. Closure to vibration modulus of normally consolidated clay: design equations and curves. Journal of the Soil mechanics and Foundation Engineering Division, ASCE, 95(6):1531-1537.

45. Hartzell, S.A., Carver, D., Cranswick, E., and Frankel, A. (2000). “Variability of site response in Seattle, Washington,” Bull. Seism. Soc. Am., 90, 1237-1250.

46. Heymsfield E.,”2D scattering of SH waves in a soil layer underlain with a sloping bedrock,” Soil Dynamics and Earthquake Engineering, vol. 19, page 489-500, 2000.

47. Hudson, M., Idriss, I. M., Beikae M. "QUAD4M: A Computer Program to evaluate the seismic response of soil structures using finite element procedures and incorporating a compliant base manual" Center for Geotechnical Modeling. Department of Civil and Environmental Engineering, University of California, Davis, California, May 1994.

48. Hughes T. J.R. (1987) "The Finite Element Method.London."Prentice Hall.

49. Jibson R. "Summary of research on the effects of topographic amplification of earthquake shaking on slope stability," US Geological Survey, Open-file Report 87-268, Menlo Park, California, 1987.

50. Idriss, I.M. and Seed, H. Bolton (1968) "Seismic Response of Horizontal Soil Layers,” Journal of the Soil Mechanics and Foundations Division, ASCE, Vol. 94, No.SM4, July.

51. Idriss I.M., Lysmer J., Hwang R. and Bolton Seed H. (1973) " Quad4: A computer program for evaluating the seismic response of soil structures by variable damping finite element procedures, EERC Report 73-16, University of California, Berkeley.

52. Idriss, I.M., and Sun, J.I. (1992). “SHAKE91: A computer program for conducting equivalent linear seismic response analyses of horizontally layered soil deposits,” Center for Geotech. Modeling, Univ. of California, Davis.

53. Ishibashi, I. and Zhang, X.,"Unified Dynamic Shear Moduli and Damping Ratios of Sand and Clay," Soils and Foundations, Japanese Society of Soil Mechanics and Foundation Engineering, Vol. 33 ,No. 1 , March 1993, pp.182-191.

54. King JL and Tucker BE. "Observed variations of earthquake motion across sediment filled valley," Bulletin of the Seismological Society of America, 1984, vol. 74, pp.137-151.

55. Kawase, H. (1996). “The cause of the damage belt in Kobe:‘The basin edge effect,’ constructive interference of the direct S-wave with the basin induced diffracted/Rayleigh waves,” Seism. Res. Lett., 67(5), 25-34.

56. Kokushu T., Yoshida Y.,Esashi Y.,Dynamic properties of soft clay for wide strain range,Soils and Foundations,22(4), 1982,1–18.

57. Kramer S.L. Geotechnical Earthquake Engineering, Prentice Hall, 1996, pp. 309-345.

58. Lee, V.W., and Cao, H. (1989). “Diffraction of SV waves by circular canyons of various depths,” J. Engrg. Mech., ASCE, 115 (9), 2035-2056.

59. Lee, Y., and Anderson, J.G. (2000). “A custom southern California ground motion relationship based on analysis of residuals,” Bull. Seism. Soc. Am., 90, S170-S187.

60. Liu, H.L., and Heaton, T.H. (1984). “Array analysis of the ground velocities and accelerations from the 1971 San Fernando California earthquake,” Bull. Seism. Soc. Am., 74, 1951-1968.

61. Lysmer J., Kuhlemeyer R.L. (1969). “Finite Dynamic Model for Infinite Media“ Journal of the Engineering Mechanics Division, Proceedings of the American Society of Civil Engineers.EM4:859-877.

62. Makra K., Cha’vez-Garcia F.J., Raptakis D., Pitilakis K. ’’Parametric analysis of the seismic response of a 2D sedimentary valley: implications for code implementations of complex site effects,’’ Soil Dynamics and Earthquake Engineering 25 (2005) 303–315.

63. Narayan J.P. “2.5D Simulation of basin-edge effects on the ground motion characteristics,“ Proc.Indian Acad. Sci. (Earth Planet. Sci.),112, No.3, September 2003, pp.463-469.

64. Narayan J.P. “Effects of soil layering of soil layering on the characteristics of basin-edge induced surface waves and differential ground motion, “Journal of Geophy. and Engineering, 2006.

65. Ohtsuki A, Yamahara H. "Effect of topography and subsurface in homogeneity on seismic SV waves and Rayleigh waves," In: Proceedings of the eighth world conference on earthquake engineering. San Francisco, vol. II, 1984, pg. 655–62.

66. Ordonez G.A. “SHAKE2000: A Computer Program for the 1D Analysis of Geotechnical Earthquake Engineering Problems”, 2005.

67. Pedersen, H.A., Le Brun, B., Hatzfeld, D., Campillo, M., and Bard, P.-Y. (1994). “Ground motion amplification across ridges,” Bull. Seism. Soc. Am., 84, 1786-1800.

68. Pitarka, A., Irikura, K., T. Iwata and H. Sekiguchi (1998). Three-dimensional simulation of the near-fault ground motion for the 1995 Hyogo-ken Nanbu (Kobe), Japan, earthquake. Bull. Seism. Soc. Am. 88, 428-440.

69. Prévost, J.H., “DYNAFLOW: A Nonlinear Transient Finite Element Analysis Program”, Princeton University,Princeton, New Jersey, (1981), last revision (2004).

70. Rassem M., Ghobarah A. and Heidebrecht A. C., “Engineering Perspective for the Seismic Site Response of Alluvial Valleys ", Earthquake Engineering and Structural Dynamics, vol. 26, 477-493, 1997.

71. Rathje, E.M., Abrahamson, N.A., and Bray, J.D. (1998). “Simplified frequency content estimates of earthquake ground motions,” J. Geotech.& Geoenv. Engrg., ASCE, 124(2), 150-159.

72. Reinoso E, Wrobel LC and Power H. "Three-dimensional scattering of seismic waves from topographical structures," Soil Dynamics and Earthquake Engineering, 1998.

73. REGLES (1995). “Règles de Construction Parasismique, Règles PS Applicables Aux Bâtiments”, Dites Règles PS 92, Norme Française, AFNOR, France.

74. Roesset, J.M., " Fundamental of Soil Amplification, " Seismic Design for Nuclear Power Plants, Edited by R.J. Hansen, M.I.T. Press., pp. 183,1970.

75. Roesset, J.M., "Soil amplification of earthquake," In Numerical Methods in Geotechnical Engineering, edited by C.S. Desai and J.T. Christian, Chapter 19,pp. 639-682.New York: McGraw-Hill (1977).

76. Rollins M., Evans M.D., Diehl N.B., Daily W.D. “Shear modulus and damping relationships for gravel, “ Journal of Geotechnical and Geoenviromental Engineering, vol. 124,No.5,page 396-405,May 1998.

77. Sanchez-Sesma FJ, Chavez-Perez S, Aviles J. "Scattering of elastic waves by three-dimensional topographies," Proceedings of the 8th world conference on earthquake engineering, San Francisco, vol. II, 1994, pg. 639–46.

78. Sanchez-Sesma FJ, Bravo MA and Herrera J. "Surface motion of topographical irregularities for incident P, SV, Rayleigh waves," Bulletin of the Seismological Society of America, vol. 75, 1985, pg. 263–269.

79. Schnabel, P.B., Lysmer, J., and Seed, H.B. (1972). SHAKE: A computer program for earthquake response analysis of horizontally layered sites, Rpt. No. EERC 72/12, Earthquake Engineering Research Center, Univ. of California, Berkeley.

80. Schneider, J.F., Silva, W.J., and Stark, C.L. (1993). “Ground motion model for the 1989 m6.9 Loma Prieta earthquake including effects of source, path, and site,” Earthquake Spectra, 9(2), 251-287.

81. Seed, H.B., I.M. Idriss, and F.W. Kiefer. 1969. Characteristics of Rock Motions during Earthquakes, ASCE Journal of the Soil Mechanics and Foundation Division. 95(5). 1199-1218.

82. Seed H.B., Idriss I.M., “Soil moduli and damping factors for dynamic response analysis, "Report no. UCB/EERC-70/10, University of California, Berkeley, December, 1970.

83. Seed H.B., Wong R.T., Idriss I.M., Tokimatsu K., “ Moduli and damping factors for dynamic analyses of cohesionless soil, “ Journal of Geotechnical Engineering, ASCE, vol. 112,No. 11,page 1016-1032, 1986.

84. Semblat JF, Dangla P and Duval AM. "Numerical analysis of seismic wave amplification in Nice (France) and comparisons with experiments," Soil Dynamics and Earthquake Engineering, vol. 19, 2000, pg. 347-362.

85. Semblat JF, Dangla P, Kham M and Duval AM. "Seismic site effects for shallow and deep alluvial basins: in-depth motion and focusing effect," Soil Dynamics and Earthquake Engineering, vol. 22, 2002, pg. 849-854.

86. Semblat JF, Dangla P and Duval AM. "Seismic site effects in a deep alluvial basin: Numerical analysis by the boundary element method," Computer and Geotechnic, vol. 29, 2002, pg. 573.

87. Semblat JF, Kham M., Parara E., Bard P.Y., Pitilakis K., Makra K., Raptakis D. "Seismic wave ampli cation: Basin geometry vs soil layering" Soil Dynamics and Earthquake Engineering 25 (2005) 529–538.

88. Silva W.J., "Site geometry and global characteristic , state of the art report," Proceedings of workshop on dynamic soil properties and site characterization, National Science Foundation and Electric Power Research Institute ,Palo Alto, California, Berkeley, August 1988.

89. Silva, W.J., and Lee, K. (1987). “WES RASCAL code for synthesizing earthquake ground motions,” in State of the Art for Assessing Earthquake Hazards in the United States, Report 24, U.S. Army Engineers Waterway Experiment Station, Misc. Paper S-73-1.

90. Sitar, N., and Clough, G.W. (1983). “Seismic response of steep slopes in cemented soils,” J. Geotech. Engrg. 109(2).

91. Spudich, P., Lee, W. H., White, R. A., Harlow, D. H., Rogers, J. A., Dodge, D. A. “Digital seismograms of selected aftershocks of the Northridge earthquake recorded by a dense seismic array on February 11, 1994 at Cedar Hill Nursery in Tarzana, California, “ USGS open-file report, 1994.

92. Steidl, J.H. (2000). “Site response in southern California for probabilistic seismic hazard analysis,” Bull. Seism. Soc. Am., 90, S149-S169.

93. Stewart P.J., Chiou S., J, Bray J.D., Graves R.W. ,Somerville P.G., Abrahamson N.A.,’’ Ground motion evaluation procedures for performance-based design,’’ PEER Report 2001/09 (2001).

94. Stewart, J.P., and Sholtis, S.E. (1999). Topographic effects on seismic ground motions above and below a cut slope in sand, Report to U.S. Geological Survey, University of California, Los Angeles.

95. Sun, J. I., Golesorkhi, R. and Seed, H. B. (1988) "Dynamic Moduli and Damping Ratios for Cohesive Soils," Report No. UCB/EERC-88/15, Earthquake Engineering Research Center, University of California, Berkeley, 42p.

96. Toriumi, I., OHBA, S. and MURAI, N. (1984), “Earthquake Motion Characteristics of Osaka Plain,” Proc. of the 8th world conference on Earthquake Engineering, 2, 761-768.

97. Trifunac, M.D. (1973). “Scattering of SH waves by a semi cylindrical canyon,” Earthquake Engrg. Struct. Dyn., 1(3), 267-281.

98. Tucker, B.E., King, J.I., Hatzfeld, D., and Nersesov, I.L. (1984). “Observations of hard-rock site effects,” Bull. Seism. Soc. Am., 74, 121-136.

99. USGS Response to an Urban Earthquake - Northridge '94 http://pubs.usgs.gov/of/1996/ofr-96-0263

100. Wong HL and Trifunac MD. "Scattering of plane SH-wave by a semielliptical canyon,"Journal of Earthquake Engineering and Soil Dynamics 3,1974, pg. 157–169.

101. Wong HL. "Effect of surface topography on the diffraction of P, SV and Rayleigh waves," Bulletin of the Seismological Society of America, vol. 72, 1982, pg. 1167–1183.

102. Vahdani S and Wikstrom S. "Response of the Tarzana strong motion site during the Northridge earthquake," Soil Dynamics and Earthquake Engineering, vol. 22, 2002, pg. 837-848.

103. Vidale, J.E., and Helmberger, D.V. (1988). “Elastic finite difference modeling of the 1971 San Fernando, California earthquake,” Bull. Seism. Soc. Am., 78, 122-141.

104. Vucetic, M. and Dobry, R. (1991) "Effect of Soil Plasticity on Cyclic Response," Journal of the Geotechnical Engineering Division, ASCE, Vol. 111, No. 1, January, pp. 89-107.

105. Yegian, M.K., Ghahraman, V.G., and Gazetas, G., ‘’1988 Armenia Earthquake, II: Damage Statistics Versus Geologic and Soil Profiles,’’ Journal of Geotechnical Engineering, Vol. 120, pp.21-45, January, 1994.

106. Zen K., Umehara Y., Hamada K., Laboratory test sand in-situ seismic survey on vibratory shear modulus of clayey soils with different plasticities, Proc. 5th Japan Earthquake Engineering Symp.,Tokyo,1978,721–728.

APPENDIX A

SAMPLE INPUT DATA FOR QUAD4M

```
Model 1 Sinusoidal EQ S_032
UNITS (E for English, S for SI):                                    ***
(A1)            ***
E
       DRF        PRM     ROCKVP     ROCKVS    ROCKRHO              ***
(5F10.0)        ***
         1      0.65
 NELM NDPT NSLP                                                     ***
(3I5)           ***
 5112 5141    0
KGMAX KGEQ N1EQ N2EQ N3EQ NUMB   KV KSAV                           ***
(8I5)           ***
 2000 2000    1    1 2000    5    1    1
      DTEQ    EQMUL1    EQMUL2    UGMAX1    UGMAX2 HDRX HDRY NPLX
NPLY   PRINPUT *** (5F10.0,4I5,F10.0) ***
      0.01         1         1                        1    1    8
8      0.32
EARTHQUAKE INPUT FILE NAME(S) & FORMAT(S) (* for FREE FORMAT)  ***
(A)             ***
S_032.acc
*
 SOUT AOUT KOUT                                                     ***
(3I5)           ***
    1    1    1
STRESS OUTPUT FORMAT (M or C), FILE PREFIX, AND SUFFIX:         ***
(A)             ***
COMBINED
M1_S032
Q4S
ACCELERATION OUTPUT FORMAT (M or C), FILE PREFIX, AND SUFFIX:  ***
(A)             ***
COMBINED
M1_S032
Q4A
SEISMIC COEFF OUTPUT FORMAT (M or C), FILE PREFIX, AND SUFFIX: ***
(A)             ***
COMBINED
M1_S032
Q4K
SYSTEM STATE OUTPUT FILE:                                       ***
(A)
M1_S032.Q4R
    N  NP1  NP2  NP3  NP4 TYPE      DENS        PO       GMX
G        XL LSTR  *** (6I5,5F10.0,I5) ***
```

```
    1    1    5    6    2    1       124      0.45       658
438      0.15
    2    2    6    7    3    1       124      0.45       904
603      0.15
    3    3    7    8    4    1       124      0.45      1090
727      0.15
    4    4    8    9    9    1       124      0.45      1244
829      0.15
    5    5   13   14    6    1       124      0.45       658
438      0.15
    6    6   14   15    7    1       124      0.45       904
603      0.15
    7    7   15   16    8    1       124      0.45      1090
727      0.15
    8    8   16   17    9    1       124      0.45      1244
829      0.15
    9    9   17   18   10    1       124      0.45      1379
919      0.15
   10   10   18   19   11    1       124      0.45      1499
999      0.15
    .    .    .    .    .    .         .         .         .
.         .
    .    .    .    .    .    .         .         .         .
.         .
    .    .    .    .    .    .         .         .         .
.         .
 5110 5089 5138 5139 5090    1       124      0.45      3749
2499      0.15
 5111 5090 5139 5140 5091    1       124      0.45      3826
2551      0.15
 5112 5091 5140 5141 5092    1       124      0.45      3902
2601      0.15
    N      XORD      YORD   BC  OUT      X2IH      X1IH       XIH
X2IV      X1IV       XIV   *** (I5,2F10.0,2I5,6F10.0) ***
    1       0.0       0.0    3    1
    2      -2.1      -8.2    3
    3      -4.1     -16.4    3
    4      -6.2     -24.6    3
    5      -8.2       0.0         1
    6      -8.2      -8.2
    7      -8.2     -16.4
    8      -8.2     -24.6
    9      -8.2     -32.8    3
   10     -10.3     -41.0    3
    .         .         .    .    .
    .         .         .    .    .
    .         .         .    .    .
 5139   -1738.8    -360.9    2
 5140   -1738.8    -377.3    2
 5141   -1738.8    -393.7    3
```

CIRRICULUM VITAE

PERSONAL INFORMATION

Surname, Name	: CILIZ, Serap
Nationality	: Turkish (TC)
Date and Place of Birth	: 1 August 1975, Eskişehir
Marital Status	: Married
Phone	: +90 312 296 24 10
Fax	: +90 312 296 29 99
email	: sciliz@mitasengineering.com

EDUCATION

Degree	Institution	Year of Graduation
Ph.D.	METU Civil Engineering	2007
MS	METU Civil Engineering	2000
BS	METU Civil Engineering	1997
High School	Sivrihisar High School	1992

WORK EXPERIENCE

Year	Place	Enrollment
10.2001 – Present	Mitaş Engineering Inc.	Senior Design Engineer
09.2000 – 10.2001	Türkiye İş Bank A.Ş.	Software Specialist
12.1998 – 09.2000	METU - Civil Engineering	Research Assistant
08.1997 – 12.1998	Mitaş Inc.	Design Engineer

FOREIGN LANGUAGES

Advanced English, Basic French

PUBLICATIONS

1. BAKIR, B.S., OZKAN, M.Y. and CILIZ, S., “Effects of Basin Edge on The Distribution of Damage in 1995 Dinar, Turkey Earthquake”, Journal of Soil Dynamics and Earthquake Engineering. Vol: 22 (2002), pp. 335-345, Elsevier.
2. CILIZ, S., ÖZKAN, M.Y., ÇETİN, K.Ö., “Effect of Basin Edge Slope on the Dynamic Response of Soil Deposits”; 4th International Conference on Earthquake Geotechnical Engineering (4ICEGE), Greece 2007; (Accepted paper, will be published June, 2007)